Mechanochemistry of Disulfide Bonds in Proteins

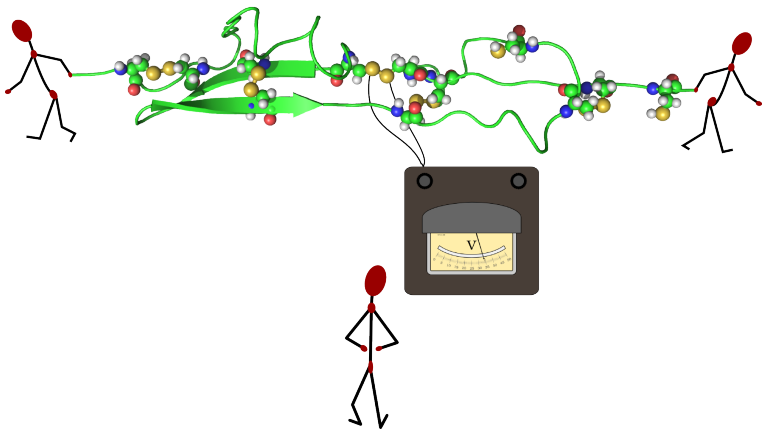

Ilona Beatrice Baldus

Heidelberger Institut für Theoretische Studien

HITS

Ruprecht-Karls-Universität Heidelberg

A thesis submitted for the degree of

Dr. rer. nat.

25 January, 2013

INAUGURAL - DISSERTATION

zur

Erlangung der Doktorwürde

der

Naturwissenschaftlich-Mathematischen

Gesamtfakultät

der

Ruprecht-Karls-Universität

Heidelberg

vorgelegt von

Diplom-Chemikerin Ilona Beatrice Baldus

aus Hamburg

Tag der mündlichen Prüfung: 25.1.2013

Mechanochemistry of disulfide bonds in proteins

Gutachter: Prof. Dr. Peter Comba
Prof. Dr. Rebecca Wade

To my family

Ist es der Sinn, der alles wirkt und schafft?

Es sollte stehn: Im Anfang war die Kraft!

Faust - Der Tragödie erster Teil

Johann Wolfgang von Goethe

Acknowledgements

This work was encouraged and supported by a number of people whom I would like to acknowledge at this point. First of all, I would like to express my gratitude to Dr. Frauke Gräter for the challenging task and her steady support, both scientifically and personally. Frauke's door was always open for discussion and she always found a way to encourage me when needed. I thank her for the freedom I had working on this task and bringing in my own ideas. My special thanks also goes to Prof. Dr. Peter Comba for taking over the role of my primary referee, for his steady interest, and support throughout the entire time of my PhD. It was very nice to be part of your group. Thanks to you both, Frauke and Peter, for encouraging my ambition for the popular science.

Many thanks to Bodo, Bogdan, Bronka, Carsten, Christian and Wolfram for all the helpful suggestions especially at the beginning of this thesis. Thanks to Camilo for your support and explanations these last months. I am grateful to Tobias Dick for drawing my attention to oxidoreductases. Thanks to my intern students, Olivia Waring and Leonie Martin, for your passionate participation in the tasks I gave you. Special thanks to Bronka and Camilo for carefully reading through the manuscript of this thesis.

Thanks to everybody at HITS, especially the Molecular Biomechanics group for scientific and less scientific discussions, and to Klaus Tschira, Andreas Reuter, and Bärbel Mack-Reuter for making this institute such a lovely working place. I warmly remember sunny coffee breaks in the beautiful HITS garden, especially with Bronka, Bogdan or the Astropysics group, a lovely time in Shanghai - especially thanks to Carsten, Fenny, Scott, Senbo, Wolfram and Yang Hui, and fantastic ski seminars with the Comba group.

I am grateful to all my friends and family for your support over all the years of my studies. Finally, I sincerely thank my husband Fabian for his kind encouragement, for trusting in me at any time, and for living every dream with me.

Abstract

Mechanical force alters a protein's stability not only due to its ability to unfold the biomolecule. As soon as a disulfide bond cross-linking the protein is exposed to force, its reduction rate is altered. Our first aim was quantifying the direct effect of force onto the chemical reactivity of sulphur-sulphur bonds in contrast to indirect, e.g. steric or mechanistic, influences. To this end, we evaluated the dependency of a disulfide bond's redox potential on a pulling force applied along the system. Our hybrid quantum and molecular mechanics simulations of cystine as a model system take conformational dynamics and explicit solvation into account and show that redox potentials increase over the whole range of forces probed here (30 - 3320 pN), and thus even in the absence of a significant disulfide bond elongation (< 500 pN). Instead, at low forces, dihedrals and angles as the softer degrees of freedom are stretched and contribute to the destabilization of the oxidized state. We find physiological forces to be likely to tune the disulfide's redox potentials to an extent similar to the tuning within proteins by point mutations.

Next, we asked how internal strain resulting from the protein structure tunes redox potentials using free energy calculations, more precisely non-equilibrium Molecular Mechanics transformations and the Crooks Gaussian Intersection method. We added a residue to the CHARMM force field that models a disulfide bond in the reference state and that can be transformed into a thiol in the product state. To our knowledge, this is the first approach to open a covalent bond by means of free energy transformation. We tested our method on *E. coli* and *S. aureus* thioredoxin, and could partly reproduce relative redox potentials of the wild-type and some mutants. We discuss promising routes to improve the accuracy of these challenging calculations.

Finally, we investigated the impact on force-induced unfolding by a special type of disulfide bond, a vicinal disulfide that links two adjacent cysteines. Our model system here is the von Willebrand factor (vWF) A2 domain. We observe similar stabilities in equilibrium for both the native system and its analogue with the disulfide bond broken and also similar collective motions. Application of an external force, however, induces a difference: Unfolding of the vWF A2 domain with the vicinal disulfide bond present leads to higher rupture forces than when it is missing. This indicates that the vicinal disulfide bond prevents the domain from unintentional unfolding.

Zusammenfassung

Mechanische Kraft kann ein Protein destabilisieren und entfalten. Kraft hat außerdem einen direkten Einfluss auf einzelne chemische Bindungen im Protein. Wird eine Disulfidbrücke, die eine Quervernetzung des Biomoleküls darstellt, einer Kraft ausgesetzt, verändert sich ihre Reduktionsrate. Unser erstes Ziel bestand darin, den direkten Effekt von Kraft auf die chemische Reaktivität der Schwefel-Schwefel-Bindung zu quantifizieren und ihn somit von indirekter Krafteinwirkung, wie sie durch Sterik und Mechanik des Proteins entsteht, abzusetzen. Wir haben untersucht, wie das Redoxpotentials einer Disulfidbindung in unserem Testsystem durch Zugkraft verändert wird. Hybride quantum- und klassische mechanische Simulationen von unserem Modellsystem Cystin berücksichtigen Konformationsdynamik in einem expliziten Lösungsmittel. Wir konnten zeigen, dass Redoxpotentiale über den gesamten untersuchten Kraftbereich (30 - 3320 pN) ansteigen. Dieser Energieanstieg konnte bereits in einem Kraftbereich beobachtet werden, in dem die Länge der Disulfidbindung von der Kraft unberührt bleibt (<500 pN). Stattdessen werden unter diesen kleinen Kräfte Dihedrale und Winkel, also die weichen Freiheitgrade, gedehnt und tragen so zur Destabilisierung des oxidierten Zustands bei. Kräfte, die unter physiologischen Bedingungen auftreten, haben also das Potential, das Redoxpotential einer Disulfidbindung um einen ähnlichen Betrag zu verändern wie Punktmutationen in Proteinen.

Als nächstes gingen wir der Frage nach, wie interne Spannung innerhalb eines Proteins Redoxpotentiale verändert. Hierzu bedienten wir uns der Methode der Freien Energie-Rechnungen, im Speziellen der nicht-Equilibrium Molekülmechanik-Transformationen und der Crooks Gaussian Intersection Methode. Wir erweiterten das CHARMM Kraftfeld um ein Residuum, dass

die Disulfidbindung im Referenzsystem modelliert und in zwei Thiole umgewandelt werden kann, um das Zielsystem darzustellen. Nach unserem Wissen ist dies der erste Ansatz, eine kovalente Bindung im Kontext einer Freien Energie Umwandlung zu öffnen. Wir nutzten *E. coli* und *S. aureus* Thioredoxin als Testsysteme für unsere Methode. Relative Redoxpotentiale der Wildtypen und einiger Mutationen konnten zum Teil reproduziert werden. Wir diskutieren vielversprechende Möglichkeiten, wie die herausfordernden Rechnungen verbessert werden könnten.

Am Ende der Arbeit untersuchen wir den Einfluss von kraftgestützter Entfaltung einer speziellen Disulfidbindung, der vicinalen Disulfidbindung, die zwei benachbarte Cysteine verbrückt. Als Modellsystem diente uns hier die A2 Domäne des von Willebrand Faktors (vWF). Wir verglichen die Domäne unter nativen Bedingungen mit einer Domäne ohne Schwefel-Schwefel-Brücke. Beide zeigen ähnliche Stabilitäten sowie hnliche kollektive Bewegung ihrer Hauptkomponenten. Ein Unterschied besteht jedoch unter Krafteinwirkung: Öffnen der Disulfidbindung senkt die Kraft die zur Entfaltung und zum Abreißen der α-Helix, in welche die vicinale Disulfidbindung eingebettet ist, aufgebracht werden muss. Dies deutet darauf hin, dass die vicinale Disulfidbindung die Domäne vor ungewollter Entfaltung schützt.

Contents

List of Figures

List of Tables

LIST OF ABBREVIATIONS

AFM	atomic force microscopy
a.u.	atomic unit
Å	Ångström
ΔA	free energy
CFT	Crooks' Fluctuation Theorem
CGI	Crooks Gaussian Intersection
Ch.	Chapter
CYD	residue used for transformation in free energy calculations
CYD^-	residue used as mono-protonated intermediate in free energy calculations
CYS	cysteine
CYS2	disulfide bonded cysteine
d_{CN}	distance between C and N terminal atoms
DNA	desoxyribonucleic acid
d_{SS}	sulphur-sulphur distance
DTT	dithiothreitol
E. coli	Escherichia coli
F	mechanical force
F_c	Faraday's constant
FEC	free energy calculation
FGTI	*fast growth* thermodynamic integration
fs	femtosecond
ΔG	reaction free energy
GFP	green fluorescent protein
GSH	glutathione (reduced form)
GSSG	glutathione (oxidized form)
h	Planck constant
$\hbar$	reduced Planck constant
$\mathcal{H}$	Hamiltonian
HOMO	highest occupied molecular orbital
k_B	Boltzmann constant
kJ	kilojoule
l	liter
λ	coupling parameter for free energy transitions
LUMO	lowest unoccupied molecular orbital
MD	Molecular Dynamics
MM	Molecular Mechanics
mV	millivolt
nm	nanometer

NBO	Natural Bond Analysis
P	probability
ox	oxidized state
pN	piconewton
ps	picosecond
QM	Quantum Mechanics
QM/MM	hybrid Quantum / Molecular Mechanics
red	reduced state
RNA	ribonucleic acid
S. aureus	Staphylococcus aureus
Sec.	Section
s.e.m	standard error of the mean
T	temperature
τ	transformation time
TI	thermodynamic integration
tip3p	transferable intermolecular potential 3P (3 point model)
tip4p	transferable intermolecular potential 4P (4 point model)
Trx	thioredoxine
TS	transition state
vs	virtual site
V	potential energy
vWF	von Willebrand factor
W	work
ξ	reaction coordinate

LIST OF ABBREVIATIONS

1

Introduction

Most fundamental processes in living organisms involve chemical reactions, i.e. a change in covalent bonding. Within the extensive catalogue of biochemical reactions, redox reactions represent a crucial class, being involved in processes such as respiration, cell proliferation, or energy metabolism (1, 2). A very specific, yet important kind of redox reaction involves the cleavage and closure of disulfide bonds. It controls the activity and interaction of proteins with other biomolecules (2).

1.1 Disulfide Bonds in Proteins

Proteins are the molecular building blocks of life. Their components are the amino acids that are attached to each other to form one long chain, which in turn is assembled into a highly organized structure. Proteins act as molecular motors, transport metabolites or ions, or catalyze essential reactions. Within a protein, disulfide bonds represent the most common link between amino acids apart from the peptide bond. They stabilize the protein and regulate its interaction with other proteins or DNA (2, 3). For example, if a reducing agent needs to be transported in an unreactive form, formation of a disulfide bond will prevent its reactivity. Formation and cleavage of disulfide bonds thus work as a switch for protein activity. Consequently, the process and control of opening and closing disulfide bonds are of particular interest and are the focus of this work.

Three possible mechanisms for the cleavage of disulfide bonds have been identified (4), namely the hydrolysis by either alkaline or acid-based activation and thiol / disulfide exchange. The latter, which is the most common mechanism (5), is typically

catalyzed by an oxidoreductase, a protein found in every living creature (6). The net oxidation of thiols leads to the formation of a disulfide bond as follows.

$$2\,R-SH \rightleftharpoons R-SS-R+2\,e^{-}+2\,H^{+} \tag{1.1}$$

The net reduction, resulting in the cleavage of the disulfide bond, requires a reducing agent such as $NADPH/H^{+}$:

$$R-SS-R+NADPH/H^{+} \rightleftharpoons NADP^{+}+2\,RSH \tag{1.2}$$

In a thiol / disulfide exchange, reducing equivalents are transfered between two thiol disulfide pairs (Eq. 1.3). The enzyme's thiol, ESH, attacks the substrate disulfide bond, forming a mixed disulfide intermediate. Then, a second enzyme thiol, undergoing intermolecular thiol / disulfide exchange, binds to the mixed disulfide, releasing the cleaved substrate. An oxidized enzyme remains.

$$\begin{aligned} ESH+R-SS-R &\rightleftharpoons E-SS-R+RSH \\ ESH+E-SS-R &\rightleftharpoons E-SS-E+RSH \end{aligned} \tag{1.3}$$

While some proteins are active only in the reduced form, other enzymes require a closed disulfide bond to operate (7). For example, reducing agents such as glutathione require an open state. Proteins like Ero1 or protein disulfide isomerase on the contrary are only active if the disulfide bond is closed, as their task is to oxidize thiols to disulfides (8). The reactivity of a disulfide bond determines its function, a question of interest in Chapters 3 and 4.

Disulfide bonds provide a protein with additional stability by cross-links, thereby constraining some degrees of freedom. Hence, such a link decreases the entropy of the unfolded state (3). Until recently, disulfide bonds were classified into catalytic or stabilizing sulphur-sulphur bonds. Then, Schmidt *et al.* put forward another kind of bond, the allosteric disulfide bond (9). Allosteric disulfide bonds mediate conformational changes of the protein upon cleavage, thereby controlling its function (10). Often, they link adjacent strands in an antiparallel β-sheet.

Another interesting kind of disulfide bond is the rare motif of vicinal disulfide bonds (11). Studies have shown that nicotinic acetylcholine requires this disulfide bond between the two adjacent cysteines to bind its receptor (12), and also methanol

dehydrogenase is only active with a closed disulfide bond (13). In this light, a vicinal disulfide bond found in the A2 domain of the von Willebrand factor (vWF) has been proposed to act as a redox activated conformational switch (14, 15), the role of which is examined in Chapter 5. The vWF is a large multimeric protein found in blood plasma. It is essential for normal hemostasis where it mediates the adhesion of platelets to the sub-endothelial connective tissue (16, 17). To be able to adhere blood platelets, the vWF needs to undergo unfolding, a procedure tightly controlled by mechanical force (16). The role of the vicinal disulfide in the von Willebrand A2 domain has been discussed to enhance its thermal stability and also to act as a high energy barrier, preventing the protein from spontaneous unfolding (14, 15). The high reactivity of allosteric and vicinal disulfide bonds could be due to an internal strain present in the unfavored configuration the disulfide bond is forced into by the protein environment. A pressing question in this regard is, if disulfide bond reactivity can be altered by mechanical force. This is a major focus of this thesis.

1.2 Mechanochemistry

A chemical bond like a sulphur-sulphur bond can be subjected to a mechanical force by internal strain as potentially present in specific configurations or by an external pulling force present e.g. during mechanical unfolding of a protein. We here ask if a force has an impact on the bond itself and on its propensity to undergo cleavage. Mechanochemistry describes the interplay between such a mechanical and chemical phenomenon (18).

From industrial processes in the rubber industry, it is known that a mechanical force can break covalent bonds in polymers, leaving behind two radicals, that do not necessarily recombine (19). More recent studies have revealed that mechanical force derived from ultrasound can alter pericyclic reactions in an unexpected way (20). Pericyclic reactions follow the Woodward-Hoffmann rules (21). Depending on whether they are induced by thermal or light energy, the ring opens con- or disrotatorically, respectively as shown in Figure 1.1 a and b. Hickenboth *et al.* could show that pulling the ring apart by a mechanical force opens a third reaction path: The opening takes place such that the pulled ends of the molecule always move away from each other. As a consequence, independently of the educt, the reaction always yields the *E,E*-isomer.

Thus, the *cis*-isomer opens disrotatorically whereas the *trans*-isomer opens conrotatorically (Fig. 1.1 c). In a similar way, even click reactions, which typically have a large thermodynamic stability, could be reversed by means of mechanical force (22).

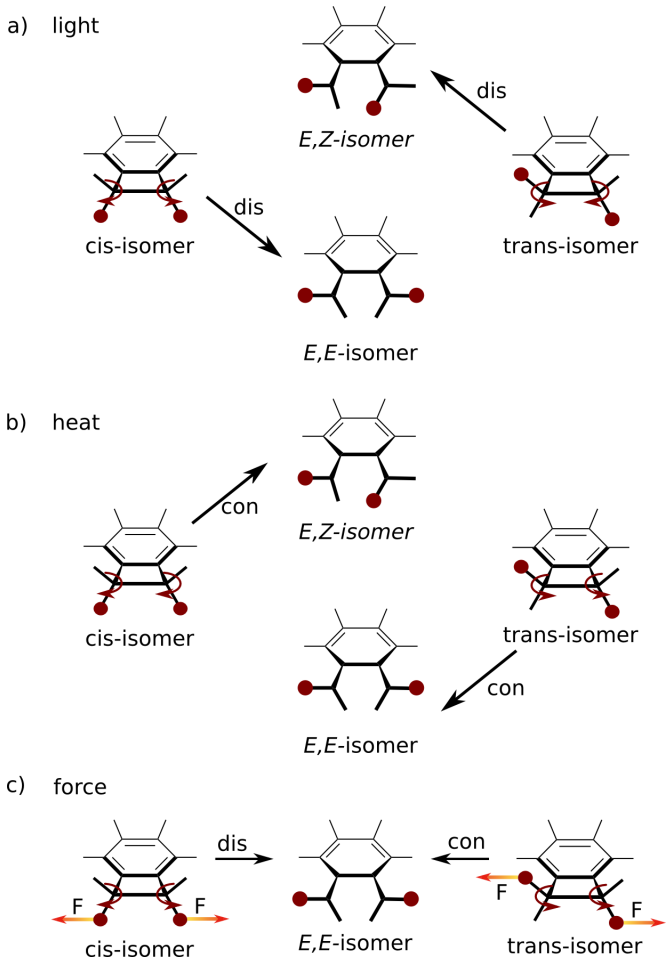

Figure 1.1: **Pericyclic reactions triggered by different energy sources** - While light and thermal energy trigger pericyclic reactions following the Woodward-Hoffmann rules, mechanical force enhances ring opening along a different pathway, namely along the pulling direction.

What is to be expected from a mechanical force acting on bonds in biological systems? To answer this question, Wiita *et al.* applied mechanical force to a protein substrate that contains a disulfide bond (23). Here, mechanical force was applied by means of single molecule force spectroscopy. A single protein was stretched using an atomic force microscope in force-clamp mode. The protein was unfolded, till the point

where the disulfide bond hindered further unfolding. Then, it was reduced by either *E. coli* or human thioredoxin (Trx, compare Figure 1.2). Overall, forces lead to an increase in reduction rate. At low forces, acceleration of the reduction by human Trx is larger than by *E. coli* Trx. At high forces, the opposite was found. Wiita *et al.* concluded that two different reduction mechanisms were responsible for this finding.

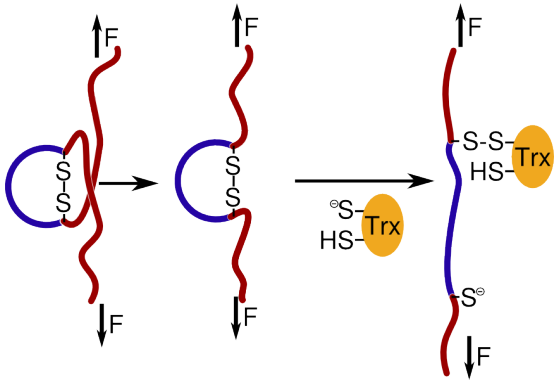

Figure 1.2: **Unfolding of a protein, followed by disulfide reduction** - A protein is unfolded by an external force until the disulfide bond hinders further unraveling. Reduction of the disulfide bond using thioredoxin takes place with the mechanical stretching force still present. Wiita *et al.* measured the dependency of reduction kinetics on the external pulling applied (23).

A similar experimental setup using DTT as a reducing agent shows an exponential increase in reaction rate depending on the applied force (24). Kucharsky *et al.* analyzed that question by using a series of macrocycles containing differently strained disulfide or carbon-carbon bonds and estimated the force in the scissile bond. In contrary to Wiita *et al.*, they claimed that mechanical force increases reactivity solely indirectly by steric effects. More specifically, force deforms the molecule such that the reducing agent can more readily access the disulfide bond (25). Wiita *et al.* expect that different factors strongly influence a disulfide's tendency to be cleaved. Parameters such as pH, temperature, electrostatics and reducing agent play a crucial role (24). To understand the impact of force alone we analyse in this thesis how an external pulling force alters the reactivity of a cystine's disulfide bond.

1.2.1 The Bell and the Dudko Model

How does force influence chemical reactions? Bell was the first one to ask this question. Based on a theoretical framework, he introduced a model to esimate the strength and the life time, τ, of specific bonds (26). His model allows predicting how chemical bonds can be broken via mechanical force instead of chemical reactions. He expects the life time of a bond to depend on the reciprocal of the natural frequency of the oscillation of atoms in solids, τ_0 and exponentially on the bond energy E_0, and the force F acting on the bond, following

$$\tau = \tau_0 e^{(E_0 - \gamma F)/k_B T}, \tag{1.4}$$

where γ is an empirical parameter, k_B is the Boltzmann constant, and T the temperature. Equation 1.4 was transformed into Equation 1.5 and became known as Bell's formula,

$$k(F) = k_0 e^{(F\Delta x^{\ddagger})/k_B T}. \tag{1.5}$$

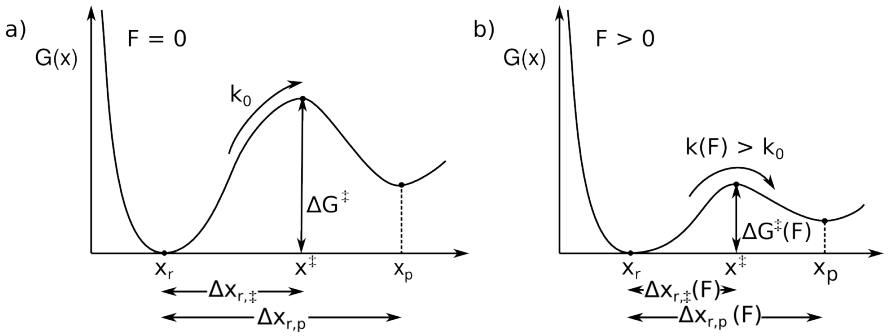

Figure 1.3: **Single-well free energy surface** - a) Intrinsic free energy with a minimum at x_r, and transition state at $x^{\ddagger}$ with a barrier height of $\Delta G^{\ddagger}$. The product is found at x_p. b) Free energy surface under a force larger than zero. The free energy barrier $\Delta G^{\ddagger}(F)$ is decreased with increasing external force F, resulting in a combined free energy surface $G(x) = G_0(x) - Fx$.

Here, $k(F)$ is the force-dependent reaction rate, k_0 is the intrinsic rate coefficient at zero force and $\Delta x^{\ddagger}$ the distance between free energy minimum x_r, and the transition state, $x^{\ddagger}$. Knowing $k(F)$ allows to determine k_0 and $\Delta x^{\ddagger}$. For the first time, Bell suggested that chemical bonds can not only be broken via chemical reactions but also through mechanical force.

According to Bell, the loading rate acting on the bond determines its unbinding force. Under the pulling force F, the molecule moves along a combined free energy surface $G(x) = G_0(x) - Fx$ along the pulling direction x. The bare free energy surface $G_0(x)$ is assumed to have a single well at $x_r = 0$ and a barrier of height $\Delta G^{\ddagger}$ at $x = x^{\ddagger}$ (Fig. 1.3). An external pulling force lowers not only the free energy barrier but also accelerates the reaction rate. This advance was later extended by Walton *et al.* They put forward the idea that also the stiffness of the transducer has a strong impact on the energy landscape (27). Their findings offer an explanation to contradictory observations from different mechanochemical experiments.

The Bell model assumes the barrier of the reaction to only be decreased by force, but not shifted. A refined theory to predict bond rupture has been introduced by Dudko *et al.* (28) to account for the shift of the transition state at $x^{\ddagger}$ towards the reactant upon force application. They surmise the average bond rupture to depend on the pulling velocity v, following $\langle F \rangle \sim (\ln v)^{2/3}$, whereas Hummer and Szabo at the same time suggested the following dependency: $\langle F \rangle \sim (\ln v)^{1/2}$ (29). In a joined work, Dudko, Hummer and Szabo later suggested a formalism fulfilling both exigencies:

$$k(F) = k_0 \left(1 - \frac{\nu F x^{\ddagger}}{\Delta G^{\ddagger}}\right)^{1/\nu - 1} e^{\Delta G^{\ddagger}[1-(1-\nu F x^{\ddagger}/\Delta G^{\ddagger})^{1/\nu}]}, \tag{1.6}$$

where $\nu = 2/3$ and $1/2$ corresponds to a linear-cubic and cusp free energy surface both of which are approximations. A linear-cubic energy surface is expected for very high forces.

In a recent study, Li *et al.* could show that a pulling force not only speeds up the reaction rate but also shifts the transition state (30). The higher the force, the shorter the disulfide bond in the protein at the transition state. These simulations provide molecular evidence for the Dudko-Hummer model.

1.3 Redox Potentials

Redox reactions play a key role in biology. They regulate processes as diverse as energy metabolism, respiration, photosynthesis, gene expression, signal transduction, and protein folding (31). The mitochondrial respiratory chain for example is well understood and revealed that redox events are tightly controlled by proteins or enzymes (32). Redox reactions affecting the amino acids in a protein can only change the redox state

of cysteines and methionines. Oxidation / reduction processes taking place between cysteine / cystine couples are very common in living systems. Enzymes such as Trx or peptides like glutathione (GSH) control such redox reactions. GSH is responsible for oxidative stress defense, redox regulation, signal transduction, and protein folding. Trx is a cofactor to ribonucleotide reductase. The latter catalyzes the reaction from RNA to DNA, and thus is essential for the DNA biosynthesis (7). Both, Trx and GSH reduce protein disulfide bonds. Though both undergo thiol / disulfide exchange, they act under different conditions due to their different redox potentials. They can be regarded as analogues to the NADH / NAD^+ and NADPH / $NADP^+$ couples, that take part in different redox cycles (2). Thus, they show selective interactions for different proteins and reactions.

Though redox reactions are widespread among biological reactions, many of them are still poorly understood and require further investigation. Therefore, reducing agents such as Trx or GSH are popular tools to study the effect of reduction of disulfide bonds in proteins. Such studies help understanding the stability of allergenes (33) or the shear-induced thiol / disulfide exchange in the vWF itself (34).

Determining redox potentials of proteins experimentally is elaborate. In principle, redox potentials can be calculated from the concentration of the reducing agent during titration (35). However, though redox potentials can be measured experimentally quite precisely, measured redox potentials are known to vary depending on the (proteineous) redox partner and experimental conditions. Also, tuning a redox potential by protein mutagenesis is resource intensive, as the effects of a single mutant on a disulfide bond's stability depend on a number of factors. More precisely, the structure of the protein, the pKa value of the disulfide, the strain on the bond and the protein's electrostatic environment but also the reduction partner have a large impact on the redox potential. These measurands are accessable from computational models. Thus, having a fast and simple way to calculate redox potentials from MD simulations would be desirable. We chose Trx as a model system. The active site contains a $CXXC$-motif that is conserved in all Trx-like proteins, and was shown to be essential for its activity (6). Mutations of the C-terminal amino acid of the XX dipeptide have shown that this sequence has a strong impact on the redox potential (6, 36). Given their importance, it is eligible to establish techniques that offer easy access to redox potentials and the factors that

influence them. It would allow a rational design of protein mutants with tailored redox potentials. Computer simulations are thus a valuable tool also in this regard (37).

1.3.1 Calculating Redox Potentials

A number of methods have been introduced over the last decades that provide ways to calculate redox potentials. The spectrum ranges from density function theory to calculate not only the redox potential but also the electronic structure of metal ions to pure Molecular Mechanics (MM) approaches. Calculations of individual metal ions or metal complexes typically use pure quantum mechanical (QM) descriptions (37, 38, 39). For taking the effect of a protein surrounding into account, a hybrid quantum mechanical / molecular mechanical (QM / MM) approach has been proven useful (40) but also mere classical descriptions have been demonstrated to successfully predict redox properties of enzymes which contain a reactive metal center that changes its redox state (41, 42, 43). We here followed two alternative approaches and will discuss their strengths and bottlenecks. We first used QM / MM calculations to investigate the impact of mechanical force on redox potentials (Ch. 3), and secondly calculated redox potentials of protein disulfide bonds, using classical molecular mechanics (Ch. 4).

1.4 Aims of this Project

We here asked how mechanical force tunes redox potentials on a molecular scale. We were interested in both, forces deriving from an external stretching, and forces induced by internal strain, in particular in their impact on disulfide bonds in proteins. We applied an external pulling force to protein disulfides and estimated the redox potential, using QM / MM calculations. In order to exclude electrostatic effects by the chemical surrounding, the study was started using an isolated cystine, the response to stress of which was later compared to the effects on stress observed for titin. Next, we asked how internal strain resulting from the protein structure tunes redox potentials as compared to different electrostatic environments. How do point mutations and thus the chemical and electrostatic environment of a bond tune its redox potential? A protein intensely investigated with respect to redox potentials and point mutations is thioredoxin. Therefore, we chose it as a model system and calculated redox potentials, using free energy calculations on the MM level of theory. Finally, we asked how the

internal strain in vicinal disulfide bonds can impact protein function. These bonds represent a rare motif in proteins and have been predicted to play an important role for protein stability. This motif is found in the von Willebrand factor A2 domain, which was subject of our investigations. We compared its stabilities towards mechanical force with and without the vicinal disulfide bonds. This thesis reveals a significant impact of mechanochemical effects on redox systems, resulting in changes of redox potential as large as they derive from different chemical surroundings.

2

Methods and Theory

This chapter outlines the theoretical framework of this thesis and the methods applied. We employed Molecular Mechanics (MM) to energetically describe the proteins investigated in this thesis (Section 2.1 and Ch. 3 to 5). An MM description allows the calculation of dynamic trajectories of proteins at reasonable computational expense and was the major workhorse of this thesis. We combined MM with a quantum mechanical description of the reactive center of the molecules for studying cystine reduction under mechanical force (Sec. 2.2 and Ch. 3). Free energy calculations (Sec. 2.3) were employed to predict redox potentials in thioredoxin (Ch. 4). Details on the particular simulation setup will be given in each chapter.

2.1 Molecular Mechanics

An accurate theoretical description of the dynamics of any molecule is given by the time-dependent Schrödinger equation,

$$\mathcal{H}\Psi = i\hbar \frac{\partial \Psi}{\partial t}, \tag{2.1}$$

where $\mathcal{H}$ describes the Hamiltonian, i.e. the sum of the kinetic and potential energy operators, Ψ the wave function, and $\hbar = h/2\pi$, with h being Planck's constant. In practice, computational resources limit the actual usage of Equation 2.1 and numerical approximations thereof to a few atoms. A number of approximations are made to describe larger molecules such as proteins that are built from several hundreds to thousands of atoms. In this thesis, simulation systems comprise e.g. $\sim 18,000$ protein

and water atoms for simulations of *E. coli* thioredoxin. At current state, Molecular Dynamics (MD) simulations at the Molecular Mechanics (MM) level of theory is the most common technique to reproduce the structure, dynamics, and energetics of proteins. This method is based on two major approximations. The first one is the use of a force field: molecules are described by a "ball and spring model", where the balls represent the nuclei, and bonds are described by springs. Electrons are not directly considered but indirectly by fitting the force field parameters according to molecular behavior. This approach follows the Born-Oppenheimer approximation. Since electrons are of much less weight than the nuclei, they move much faster. Therefore, it can be assumed that they immediately follow the nuclei's motion. There are two major groups of interactions between atoms in a force field, bonded and non-bonded interactions. Bonded interactions, i.e. bonds, angles and dihedrals are described by potentials. Non-bonded interactions comprise electrostatics and van-der-Waals terms.

The potential energy V of the system is given by the sum of bonded and non-bonded energies:

$$\begin{aligned} V(R) &= V_{\text{bonds}} + V_{\text{angles}} + V_{\text{dih}} + V_{\text{Coul}} + V_{\text{LJ}} \\ &= \sum_{\text{bonds}} k_b(b - b_0)^2 + \sum_{\text{angles}} k_\theta(\theta - \theta_0)^2 + \sum_{\text{dihedrals}} k_\phi(1 + \cos(n\phi - \delta)) \\ &+ \sum_{\text{i}} \sum_{\text{j>i}} 4\varepsilon_{ij} \left[\left(\frac{\sigma_{ij}}{r_{ij}} \right)^{12} - \left(\frac{\sigma_{ij}}{r_{ij}} \right)^{6} \right] + \frac{q_i q_j}{4\pi r_{ij}}, \end{aligned} \tag{2.2}$$

where k_b, b and b_0 and k_θ, θ and θ_0 are the force constant, the time-dependent values and the equilibrium values of the bonds and the angles, respectively. The third term describes the torsional angle, or dihedral. k_ϕ is the dihedral force constant, n is the multiplicity of the function, ϕ is the dihedral angle, and δ is the phase shift. The final two terms describe the Lennard-Jones and the Coulombic interactions, respectively. ε_{ij} and σ_{ij} are the depth and the width of the Lennard-Jones potential for a pair of atoms i and j. r_{ij} is the distance between the atoms, and q_i and q_j are their partial charges.

Some force fields, such as the CHARMM force field (44), additionally use a correction term for the vibration of angles, which are then referred to as Urey-Bradley angle vibrations. Also, "improper" dihedrals are not always described as suggested in Equation 2.2. Instead of modeling them as a torsion, they are sometimes treated as out-of-plane bending angles and written as harmonic functions, which depend on the distance of the plane the atom under consideration is bending out from (44, 45).

The second approximation is that the dynamics of the atoms are described by classical mechanics, following Newton's equation of motion (Eq. 2.3 to 2.5),

$$F_i = m_i a_i. \tag{2.3}$$

Equation 2.3 states that the force F_i acting on the atom i is the product of its mass m_i and its acceleration a_i. It can be written in terms of coordinates as

$$F_i = m_i \frac{d^2 r_i}{dt^2}, \tag{2.4}$$

where r specifies the coordinates of the atom, and t is the time. MD simulations proceed in finite time steps, which should be smaller than the time scale of the fastest motion in the simulation system. In the case of proteins considederd here, these are bond vibrations including hydrogen atoms, which were constrained, allowing 2 fs time steps. Forces are directly related to the potential energy given in Equation 2.2 with

$$F_i = -\frac{\partial V}{\partial r_i}. \tag{2.5}$$

For a comprehensive description of MD, we refer to relavant text books (45, 46).

2.1.1 Principle Component Analysis

A protein at ambient conditions typically shows large anharmonic motions, which are likely to be involved in the protein's function. However, within the many uncoupled thermal fluctuations, large correlated motions connected to the function might be difficult or even impossible to detect by visual observation of the trajectory. Principle component analysis (PCA) has been shown to be a useful method to detect relevant degrees of freedom from the trajectory of MD simulations of biomolecules. It is a statistical technique to find patterns in data of high dimensions. From the configurational space, PCA filters few collective essential degrees of freedom comprising positional fluctuations (47). These essential motions are called principle components. Comparing such principle components for similar proteins, e.g. for a protein and a mutant or for two different redox states of one protein, as we will demonstrate in Section 5.2, provides a straight-forward way to reveal differences from the trajectories.

To determine the principle components of a trajectory, the covariance matrix of all or a subset of atoms within the biomolecule is calculated and diagonalized. The following definition is based on the original paper by Amadei *at al.* (47). For a biomolecule of

N atoms, the vector $\mathbf{x} = (x_1, x_2, x_3, ..., x_{3N})$ describes the coordinates of these atoms. The covariance matrix is given by

$$C = \langle (\mathbf{x} - \langle \mathbf{x} \rangle)(\mathbf{x} - \langle \mathbf{x} \rangle)^T \rangle, \tag{2.6}$$

where $\langle\rangle$ denotes the ensemble average. The symmetrical covariance matrix C can be diagonalized by an orthogonal coordinate transformation T into the diagonal matrix Λ. Its diagonal elements are the eigenvalues λ_i.

$$C = T\Lambda T^T \quad \text{or} \quad \Lambda = T^T C T. \tag{2.7}$$

The i^{th} column of the transformation matrix T corresponds to the normalized eigenvector and thus to the principle component μ_i of C and its eigenvalue λ_i. The eigenvalue is the mean square positional fluctuation along the eigenvector and thus specifies its contribution to the total fluctuation. Mostly, only a few eigenvectors describe the major contributions of the fluctuations and therefore the essential degrees of freedom. Projecting a trajectory $\mathbf{x}(t)$ on an eigenvector μ_i yields

$$p_i(t) = \mu_i \cdot (\mathbf{x}(t) - \langle \mathbf{x} \rangle), \quad p_i(t) \in \mathbb{R} \tag{2.8}$$

For a PCA, the conformational ensemble sampled in the trajectory is usually projected on two or three eigenvectors to compare it with other emsemble in the same reduced essential subspace. Additionally, projecting the principle components back in the Cartesian space can be used to visualize atomic displacements associated with a given eigenvector:

$$x_i'(t) = p_i \mu_i + \langle \mathbf{x} \rangle. \tag{2.9}$$

2.2 Hybrid Quantum / Molecular Mechanics

A Molecular Mechanics description of a molecule is a useful approximate for its quantum mechanical nature, but in some cases involves restrictions not adequate for the problem under investigation. One of the restrictions of MM is that no bonds can be broken or reformed due to the harmonic approximation of chemical bonds (Eq. 2.2). In this thesis, we aimed at describing disulfide cleavage under mechanical force (Ch. 3). To this end, we used a hybrid description of quantum and molecular mechanics (QM / MM).

We described our reaction center, the disulfide bond and its adjacent atoms by quantum mechanics. The rest of the system was treated by molecular mechanics, thereby combining the advantages of a precise description of the reaction center with the high computational efficiency of an MM description.

In the GROMACS software package (48), the QM system is embedded into the MM system either through mechanical or electronic embedding. Through mechanical embedding, only the configuration of the protein influences the motion of the QM subsystem. This method is also referred to as QM + MM (37). The potential energy of the system, E_{pot}, is then determined by

$$E_{\text{pot}} = E_{\text{MM}}(\text{all}) + E_{\text{QM}}(\text{QM region}) - E_{\text{MM}}(\text{QM region}). \tag{2.10}$$

The potential energy is calculated for the entire system by the MM code and for the QM system by the QM code. For not adding the energy of the QM region twice, the MM energy of the QM region is substracted (Eq. 2.10). Electronic embedding includes the electrostatics of the MM atoms in close vicinity to the QM region (49). The Hamiltonian for the QM system embedded into the MM system, $\mathcal{H}^{\text{QM/MM}}$, is given by

$$\mathcal{H}^{\text{QM/MM}} = \mathcal{H}_e^{\text{QM}} - \sum_i^n \sum_J^M \frac{e^2 Q_J}{4\pi\epsilon_0 r_{iJ}} + \sum_A^N \sum_J^M \frac{e^2 Z_A Q_J}{e\pi\epsilon_0 R_{AJ}}, \tag{2.11}$$

where e and Z_A are the electronic and nuclear charge numbers of QM system, repectively, Q_J is the charge number of the MM system, r_{iJ} and R_{AJ} are the distances between the MM atoms and the electrons and nuclei of the QM system, respectively, and ϵ_0 is the electric field constant. The first term is the Hamiltonian of the isolated QM system. The two sums compute the electrostatics between the n electrons and the N nuclei of the QM system and the M charged MM atoms, respectively. All bonded interactions between QM and MM system are treated by MM.

2.2.1 Natural Bond Orbitals

Quantum mechanical calculations including QM / MM methods provide results on the molecular orbitals of the system. However, the wave functions describing the molecular orbitals do not fit into the Lewis picture where two atoms share a bond and lone pair electrons are localized. Natural Bond Orbital (NBO) analysis aims at approximating

the Lewis picture. To this end, wave functions are optimally transformed into a localized form, resulting in effective valence electron configurations for each atom (Natural Atomic Orbitals, NAO) or bond (NBO) (50, 51). These configurations allow drawing conclusions on the reactivity of certain bonds. We have applied NBO in Section 3.3.3 to get insight in the impact of mechanical force on the electronic configuration of the disulfide bond.

2.3 Free Energy Calculations

Free Energy calculations are a widely used method to estimate energetic differences between different states of proteins, such as protein-ligand binding, drug partioning across cell membranes (52), or redox potentials (41, 42). Various approaches have been developed of which the next section summarizes the most common ones. They can be classified into methods sampling at equilibrium (Sec. 2.3.1 to 2.3.3) or at non-equilibrium (Sec. 2.3.4). We here used the latter, namely the Crooks Gaussian Intersection (CGI) method, to calculate free energy differences between thioredoxin reduced and oxidized states (Ch. 4).

2.3.1 Perturbation Theory

A simple way to calculate free energies is given by the perturbation theory (52). The approach starts from an initial state, also referred to as the unperturbed, reference state. This state is known. Then there is a state of interest, also called target state, that can be reached through perturbation of the reference problem. The reference state is described by a Hamiltonian, $\mathcal{H}_0(x, p_x)$, which is a function of $3N$ Cartesian coordinates x and their conjugated momenta p_x. The Hamiltonian of the target state can be determined by

$$\mathcal{H}_1(x, p_x) = \mathcal{H}_0(x, p_x) + \Delta\mathcal{H}(x, p_x). \tag{2.12}$$

The difference in Helmholtz Free Energy, ΔA, is given by

$$\Delta A = -k_B T \ln \frac{Q_1}{Q_0}, \tag{2.13}$$

with

$$Q = \frac{1}{h^{3N} N!} \iint \exp\left[(-k_B T)^{-1} \mathcal{H}\right] \mathrm{dx}\, \mathrm{dp_x}. \tag{2.14}$$

h is Planck's constant. Equation 2.13 can be written as

$$\Delta A = -k_B T \ln \langle \exp \left[-k_B T \Delta \mathcal{H}(x, p_x) \right] \rangle_0. \tag{2.15}$$

ΔA between the states 0 and 1 can be estimated by sampling only the equilibrium configuration of the reference state. Thus, only one state is used to evaluate the Helmholtz Free Energy by an instantaneous convertion of the initial to the final state. Equation 2.16 gives access to the potential energy difference, ΔV, between the reference and the final state,

$$\Delta A = -k_B T \ln \langle \exp \left(-k_B T \, \Delta V \right) \rangle_0. \tag{2.16}$$

This method has been demonstrated to work for minor changes such as the impact of point mutations in DNA on its binding to netropsin (53), hydration free energy of small solutes such as an argon atom or a methanol molecule, or protein-ligand binding and host-guest chemistry (52).

2.3.2 Free Energy from Probability Densities

Another approach aims at sampling the entire phase space from the initital state 0 to the target state 1, which can be understood as two minima in the free energy landscape along a reaction coordinate ξ (compare Figure 2.1). This could be the distance between two molecules, a torsion angle or the change of atomic charges. The lower the energy, the more often the state is sampled. Thus, the free energy is related to the probability density function $P(\xi)$ of the reaction coordinate ξ through

$$A(\xi) = -k_B T \ln P(\xi). \tag{2.17}$$

In a probability density calculation, the free energy is determined from the number of visits of each state under the given conditions along the trajectory (52). The probability density of the sampled states can then be transferred to conditions different from those used for the original simulation and thus is a straight forward approach to calculate free energies.

On the downside, an energy difference of a few $k_B T$ reduces the probability $P(\xi)$ considerably, resulting in rare sampling of configurations with a large $A(\xi)$. Therefore, especially around the transition state, TS, few points are sampled. A rare sampling of the TS leads to large statistical errors. Increasing the simulation time to the point

where statistics of the TS become satisfying is not always feasible. Also in the present thesis, MD time scales are too short to see spontaneous visits of both the open and the closed sulphur-sulphur bond. Estimating a correct ΔG from differences in $P(\xi)$ is thus statistically problematic. A method sampling a larger phase space more easily is therefore needed.

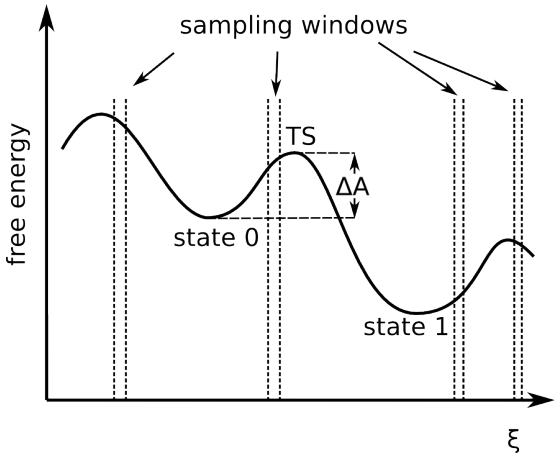

Figure 2.1: **Thermodynamic Integration - sampling** - The interval of interest is split into subintervals. Thereby, the energy differences within each window is reduced. Biasing the sampling to the restricted region within a window results in a more uniform sampling, as compared to the "brute-force" sampling described in Section 2.3.2. ΔA is the free energy barrier.

2.3.3 Thermodynamic Integration

Thermodynamic Integration (TI) uses a coupling parameter, λ, to describe the transition from the initial to the final state. It calculates the derivatives of the free energy with respect to the order parameter along the transition path (52). Each state along the transition is defined by the Hamiltonian $\mathcal{H}_\lambda$, which is a linear combination of the Hamiltonians $\mathcal{H}_0$ and $\mathcal{H}_1$, that in turn represent the starting state 0 and the final state 1, respectively:

$$\mathcal{H}_\lambda = (1-\lambda)\mathcal{H}_0 + \lambda\mathcal{H}_1 \tag{2.18}$$

As discussed in Section 2.3.2, sampling problems around the transition state can occur as the probability of sampling a given structure depends on its energy. A powerful method to circumvent this problem is the so-called stratification: The interval between

the initial and final state is split along the reaction coordinate ξ into subintervals. A biasing potential such as umbrella-sampling is used in each window. Thereby, a uniform sampling can be reached within each window, decreasing the statistical error. A number of other methods has been designed, such as *Slow Growth* thermodynamic integration. Here, the structure in state 0 is being changed into state 1 continuously and infinitely slowly by switching the coupling parameter λ from 0 to 1.

The work needed to perform the change along the reaction coordinate ξ corresponds to the change in free energy. This method requires the system to stay close to equilibrium. For a sufficiently smooth switching, the change in free energy can be written as

$$A(\xi_1) - A(\xi_0) = \int_{\xi_0}^{\xi_1} \frac{dA}{d\xi}\, d\xi, \tag{2.19}$$

which is equivalent to

$$\frac{dA}{d\xi} = \left\langle \frac{\delta \mathcal{H}}{\delta \xi} \right\rangle_{\xi}. \tag{2.20}$$

The subscript ξ indicates that $\mathrm{dA}/\mathrm{d}\xi$ is calculated for a fixed interval, i.e. at a given point on the reaction coordinate ξ (see Figure 2.1).

A similar method uses discrete numbers of intermediate points λ along the transition path that are held fixed over the course of the simulation (54). This method requires that sampling of each intermediate at a given λ occurs sufficiently close to equilibrium.

2.3.4 Non-equilibrium Transformations

In Sections 2.3.1 and 2.3.3, we have seen that free energies can be determined by a wide range of approaches. The perturbation theory uses an ensemble of energies each derived from a transformation in only one step, while TI requires infinitely slow transformations from state 0 to 1. These two concepts can be considered as the limiting cases of the more general formalism where the transformation takes place at finite rate (52).

For transformations at a finite rate, i.e. at non-equilibrium, the Jarzynski equation offers a way to estimate the equilibrium free energy as given in the following equation (55),

$$\langle e^{-W(\tau)/k_B T} \rangle = e^{-\Delta A/k_B T}, \tag{2.21}$$

where ΔA is the Helmholtz free energy. The work over the switching process of length τ is given by $W(\tau) = \int_0^1 \frac{\delta \mathcal{H}_\lambda}{\delta \lambda}\, \mathrm{d}\lambda$. A coupling parameter λ switches the system from state 0 to 1 (compare Eq. 2.18).

Powerful relations can be derived if forward and backward transformations are combined. The path direction may be returned, as the free energy is a state function. The work W^r accumulated on the reversed path, $\lambda^r(t) = \lambda(\tau - t)$ is given by

$$W^r(\tau) = \int_0^\tau \left. \frac{\delta \mathcal{H}[z(t);\lambda]}{\delta \lambda} \right|_{\lambda=\lambda^r(t)} \dot{\lambda}^r(t) \mathrm{dt}, \tag{2.22}$$

where t is the time and $z(t)$ the time-dependent trajectory. This leads to the following relation, originally derived by Crooks:

$$\langle e^{-W^r(\tau)/k_B T} \rangle = e^{-[A(0)-A(1)]/k_B T} \equiv e^{\Delta A/k_B T}. \tag{2.23}$$

With the second law of thermodynamics, that states that the work $W(\tau)$ performed during non-equilibrium simulations is on average larger than or equal to the free energy difference between the states, it follows

$$\langle W(\tau) \rangle \geq \Delta A. \tag{2.24}$$

In combination with Eq.2.21, this leads to an upper and lower bound for the free energy difference according to

$$-\langle W^r(\tau) \rangle \leq \Delta A \leq \langle W(\tau) \rangle. \tag{2.25}$$

As shown by Crooks (56, 57), the distribution of work values for forward and backward paths satisfies Equation 2.26, which is today known as the Crooks' Fluctuation Theorem (CFT).

$$\frac{P_f(W)}{P_r(-W)} = e^{k_B T(W - \Delta A)} \tag{2.26}$$

In combination with the Gaussian approximation from Equation 2.27 it allows calculating the mechanical work W of a switching process of length τ in a highly parallelizable and accurate way (58). The CFT links the work done on a system during a non-equilibrium transformation to the free energy difference between the final and the initial state. For a set of switching trajectories, the free energy, ΔA, is described by the distributions of work performed on forward and backward transformations, P_f and P_r.

The average of work distributions from a trajectory ensemble is given by the probability distribution $P(W)$ and can be approximated by a Gaussian function (58)

$$P_{f,r}(W) \sim \frac{1}{\sigma_{f,r}\sqrt{2\pi}} \exp\left[-\frac{(W - W_{f,r})^2}{2\,\sigma_{f,r}^2} \right], \tag{2.27}$$

where $W_{f,r}$ and $\sigma_{f,r}$ are the means and the standard deviations of the work distributions, respectively. The indices f and r refer to the forward ($\lambda = 0 \rightarrow 1$) and backward ($\lambda = 1 \rightarrow 0$) transformation. This yields

$$\begin{aligned} \Delta A_f &= W_f - \frac{1}{2} k_B \sigma_f \qquad \text{and} \\ \Delta A_r &= W_r - \frac{1}{2} k_B \sigma_r \end{aligned} \tag{2.28}$$

with a statistical accuracy of

$$\bar{\sigma}^2_{f,r} = \frac{\sigma^2_{f,r}}{N} + \frac{(-k_B T)^2 \sigma^4_{f,r}}{2\,(N-1)}. \tag{2.29}$$

2.3.4.1 Crooks Gaussian Intersection Method

A straight-forward and highly parallelizable method uses Crooks' Fluctuation Theorem to estimate free energies. It is called Crooks Gaussian Intersection (CGI). CFT (Eq. 2.26) causes that the change in free energy, ΔA, is equivalent to the work W for which $P_f(W) = P_r(-W)$. That corresponds to the intersection point of the forward and backward work distributions (Fig. 2.2). Estimating this intersection point by the use of a Gaussian approximation has been shown advantegeous (58).

Thus, the following equation can be used to estimate the free energy:

$$\Delta A_{CGI} = \frac{\frac{W_f}{\sigma_f^2} - \frac{-W_r}{\sigma_r^2} \pm \sqrt{\frac{1}{\sigma_f^2 \sigma_r^2}(W_f + W_r)^2 + 2(\frac{1}{\sigma_f^2} - \frac{1}{\sigma_r^2}) \ln \frac{\sigma_r}{\sigma_f}}}{\frac{1}{\sigma_f^2} - \frac{1}{\sigma_r^2}}, \tag{2.30}$$

where W_f and W_r, and σ_f and σ_r are the mean values and standard deviations of the work for the forward and backward transformation, respectively. For work distributions with $\sigma_f \neq \sigma_r$, Equation 2.30 results in two intersection points, even though ΔA is uniquely defined. Only $\sigma_f = \sigma_r$ yields a unique solution that is equal to

$$\Delta A_{CGI} = \frac{W_f - W_r}{2}. \tag{2.31}$$

Typically, if two results are obtained, one is close to the mean value of the two distributions, the other one can be found in the tail region of the work distributions. In general, the intersection point closer to the mean is the appropriate estimate of ΔA.

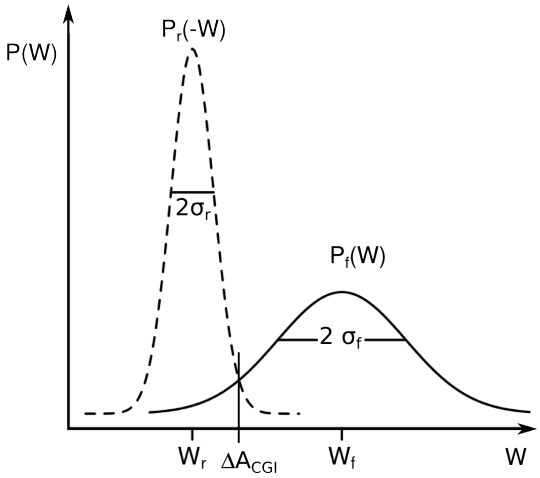

Figure 2.2: **Crooks Gaussian Intersection** - CGI estimates the free energy from the intersection point of forward and backward work distributions, which are assumed to be Gaussian.

2.3.5 The Thermodynamic Cycle

Instead of calculating the free energy of interest directly by one of the free energy calculation methods described above, it is often beneficial or the only feasible way to decompose the transition from state 0 to state 1 into several steps, i.e. reactions along a thermodynamic cycle. In particular, redox potentials, the focus of this work, are typically obtained from free energy changes along several steps. For example, the oxidation of azurin takes place when the pH changes from acidic to basic. Bosch *et al.* used the following thermodynamic cycle and yielded accurate relative redox potentials (41).

$$\begin{array}{ccc} \text{azurin}(\text{ox}, \text{pH}\,9) + \text{e}^- & \xrightarrow{\Delta A^{\text{redox}}_{\text{basic}}} & \text{azurin}(\text{red}, \text{pH}\,9) \\ \Big\downarrow \Delta \text{A}^{\text{H}^+}_{\text{ox}} & & \Big\downarrow \Delta \text{A}^{\text{H}^+}_{\text{red}} \\ \text{azurin}(\text{ox}, \text{pH}\,5) + \text{e}^- & \xrightarrow{\Delta A^{\text{redox}}_{\text{acidic}}} & \text{azurin}(\text{red}, \text{pH}\,5) \end{array} \tag{2.32}$$

This approach follows Hess' law: The change of energy is independent of the reaction path. The reduction potential ΔA^{redox}, can be described by

$$\begin{aligned} \Delta A^{\text{redox}} &= \Delta A^{\text{redox}}_{\text{basic}} + \Delta A^{\text{H}^+}_{\text{red}} \\ &= \Delta A^{\text{redox}}_{\text{acidic}} + \Delta A^{\text{H}^+}_{\text{ox}}, \end{aligned} \tag{2.33}$$

where $\Delta A^{\text{redox}}_{\text{acidic}}$ and $\Delta A^{\text{redox}}_{\text{basic}}$ are the redox free energies at pH 5 and pH 9, respectively, and $\Delta A^{\text{H}^+}_{\text{ox}}$ and $\Delta A^{\text{H}^+}_{\text{red}}$ are the free energies of deprotonation of the oxidized and reduced states, respectively.

2.3.6 Applications

MD-based free energy calculations have been applied to a broad range of biological and chemical systems. Among others, they have been used to determine solvation free energies (58), thermodynamic stabilities of proteins relative to their mutants (59), or to estimate the binding affinity between DNA and proteins (54). Thermodynamic Integration has been proven useful to calculate relative redox potentials of metalloproteins in which the central ion or a flavin core is reduced, resulting in a protonated radical (41, 42).

In all previous cases we are aware of, free energy calculations have not been applied so far to cases for which a chemical bond undergoes cleavage. Redox reactions involving flavins or metal ions primarily feature changes in partial charges or protonation states.

We here added an additional challenge, and used MD free energy calculations to reduce a disulfide bond that not only undergoes cleavage, but also comes along with large conformational changes of the reaction site, as will be detailed in Chapter 4. During the redox reaction exchanging a disulfide bond against two thiols, originally bonded interactions need to be switched into non-bonded interactions, for which we have developped a scheme within the CGI method described in Section 2.3.4.

3

Redox Potentials from Hybrid Simulations

3.1 Mechanochemistry of Disulfide Bonds

Similar to thermal or light energy, mechanical force can change chemical reactivity. Some recent examples have been discussed in Section 1.2. An example for this kind of mechanochemistry that we focused on here is the force-dependency of disulfide bond reduction. Generally, a pulling force accelerates the reduction of a disulfide by a chemical reducing agent (24, 60), according to the Bell or the Dudko-Hummer model described in Section 1.2.1. Divergence from this simple enhancement of reactivity by mechanical work has also been observed. Namely, the reduction of a protein disulfide bond with thioredoxin (Trx) was found to decelerate at low forces ($< 200\,\mathrm{pN}$) (23), and redox reactions by metal ions as reducing agents were found to be largely insensitive to forces (61). Hydroxide anions, in turn, show a decrease in susceptibility towards the mechanical force at large forces ($> 500\,\mathrm{pN}$) (62). Hence, the acceleration of disulfide bond reduction strongly depends on the reducing agent. The observed differences between reducing agents were ascribed to changes in the overall reaction mechanism (23, 61, 62).

To reconcile these findings, we here asked the fundamental question if mechanical force alters the redox potential of a disulfide bond. A redox potential measures the chemical stability of the bond and as such is independent from the reducing agent, reaction mechanism, or steric hindrance. Also, in the particular case of mechanical force, we can directly infer changes in the reactivity of the disulfide bond from the shift

in redox potential by mechanical force, as kinetics and thermodynamics are directly related. The reason is that, within the assumption that mechanical force tilts the energy landscape along the reaction coordinate x by $F \cdot x$ (compare Eq. 1.4 (26)), the shifts in the product and transition state free energy with respect to the reactant free energy are linearly proportional. Therefore, a stabilization of the product with respect to the reactant by mechanical force also involves an acceleration of the reaction by lowering the activation energy. Thus, within the framework of the Bell model, the redox potential is directly related to the relative reactivity of a bond and allows the validation of our calculations by experimental measurements of force-dependent reaction rates.

Previous theoretical studies have given detailed insight into the reduction and cleavage of disulfide bonds in the absence of mechanical force (63, 64, 65). In addition, Rickard et al. could show that the electron affinity of partly optimized structures rises when elongating the disulfide bond (66). Also, Iozzi et al. (67) recently presented a study showing that forces in the range of 100 to 400 pN promote reduction of a disulfide bond. The conclusions presented in these studies all result from restrained optimizations performed *in vacuo*.

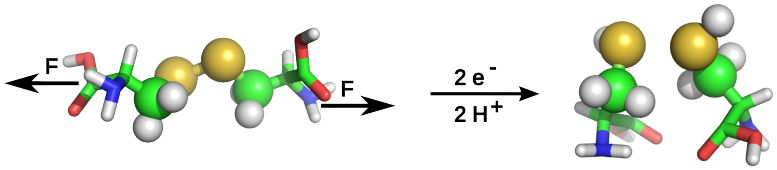

Figure 3.1: **Reduction scheme** - Scheme of cystine reduction by addition of two hydrogens (and two electrons) under a constant mechanical force acting on the terminal atoms, C and N, respectively, as indicated. QM atoms are shown as spheres.

The relevant experiments to compare to, however, are performed in water at ambient conditions. For direct comparison, we here aimed at mimicking the force spectroscopy experiments (24, 60, 61, 62) as closely as possible. We subjected the disulfide bond containing molecule to a constant pulling force, that is applied on the terminal N and C atom, respectively (Fig. 3.1). As a a simplified case, we used cystine as a model system. Our Molecular Dynamics (MD) simulations, the general concept of which is described in Chapter 2.1, take free dynamics and solvation into account. We solvated our protein model system in explicit water and simulated at room temperature and

1 bar. This is of particular importance, since experiments have shown a strong impact of solvent on the disulfide mechanochemistry (60). We applied hybrid quantum and molecular mechanical (QM / MM) calculations to this problem to allow bond opening. For details on QM / MM, see Section 2.2. We indeed found a strong increase in redox potential, i.e. a higher reactivity, with pulling force. Unexpectedly, elongation of the disulfide bond itself sets in later than the destabilization of the system. Low forces (up to $\sim 500\,\mathrm{pN}$) stretch the angles and dihedrals enclosing the disulfide bond rather than the bond itself. Still, a change in redox potential was observed within this range of small forces. Obviously, chemical destabilization of the system arises from any minor change in the conformation in the vicinity of the reaction center.

3.2 Calculating Redox Potentials

The redox potential can be calculated from the reaction free energy, ΔG, i.e. the difference between the free energy of the disulfide-bonded oxidized state, G_{ox}, and the reduced state, G_{red}, that results from the addition of each two hydrogens and electrons (Fig. 3.1). The relative change in redox potential due to the mechanical force F, $\Delta E^0_{\mathrm{redox}}(F)$, then is given by the difference between the reaction free energies at force F, $\Delta G(F)$, and at zero force, $\Delta G(F=0)$, following Nernst's equation,

$$\Delta E^0_{\mathrm{redox}}(F) = \frac{\Delta G(F) - \Delta G(F=0)}{F_{\mathrm{c}}}, \tag{3.1}$$

where F_{c} is the Faraday constant.

Full disulfide bond reduction includes the addition of two electrons and two protons, and results in a product with two thiols, i.e. with a broken sulphur-sulphur bond (Fig. 3.1). Such an open state is force-independent, as the pulling force, acting on two individual molecules in opposite directions, does not cause a restoring force anymore. Therefore, G_{red} is force-independent. In principle, for estimating the redox potential of a disulfide bond, other product states can be considered alternatively, namely a radical anion resulting from the addition of one electron, and a mono-protonated state. However, also for those reaction intermediates, we find spontaneous opening of the sulphur-sulphur bond at ambient conditions, even in the absence of force (see Section 3.3.2). Thus, the force-independent reduced state cancels out in Equation 3.1, and

we calculated the force-dependent redox potential, $\Delta E^0_{\text{redox}}(F)$, directly from the energy difference between the oxidized state at force F, $G(F)$ and zero force, $G(F = 0)$. As another consequence of the force-independent product state, the redox potential calculations are also unaffacted from any assumption of the protonation state of the product.

We approximated the free energy by the electronic energy of the quantum mechanically treated region (Fig. 3.1), E_{QM}. Due to the electronic embedding into the classically treated environment, E_{QM} includes the electrostatic interaction with the solvent and the rest of the cystine (see also Section 2.2).

It is a time average obtained from picosecond scale MD simulations, thereby capturing the thermal fluctuations of the system. We note that choosing the full QM / MM energy, which also include the interaction energy within the MM system, was unfeasible. The high fluctuations of the inter-water non-bonded interaction (in the 1000 kJ/mol range) impeded a reliable estimation of time-averaged energies (see Fig. 3.2).

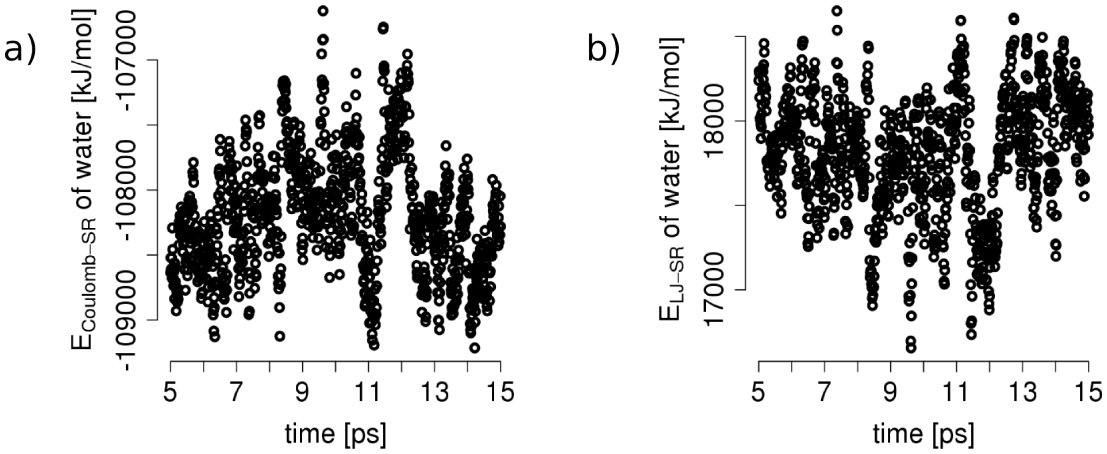

Figure 3.2: **Short-range interactions of water** - a) Coulomb and b) Lennard-Jones interactions between water molecules fluctuate significantly, prohibiting reliable time averages of full QM / MM energies.

On the other hand, more efficient quantum mechanical methods, such as semi-empirical functionals, would allow longer time scales but very likely would not be accurate enough for treating the sulphur-sulphur bond opening.

Using Equation 3.1, we obtained $\Delta E^0_{\text{redox}}(F)$ for forces up to $F = 3320\,\text{pN}$ from QM / MM MD simulations totaling more than 2.0 ns of simulation time.

3.2.1 Simulation Setup

All Molecular Dynamics (MD) simulations were carried out using the GROMACS 4.0.5 package (48). For the hybrid QM / MM calculations we used GROMACS 4.0.5 interfaced with Gaussian03 (68, 69).

A cystine, created with the Molecular Operating Environment software (MOE 2008.10; Chemical Computing Group, Quebec, Canada), was solvated in a box of explicit water of TIP4P (70). The box was large enough to allow a 1.5 nm distance in x and y directions. We used a larger length of 8 nm in z-direction, along which the molecule will be subjected to a pulling force (see below), in order to prevent interactions with itself in periodic boundary conditions. A salt concentration of 0.1 mol/l was chosen, resulting in 2370 water molecules and four ions of each sodium and chloride. Cystine was chosen as a simple model system for disulfides in proteins. The disulfide bond, the adjacent methylene groups and two link atoms were treated with QM, and the remainder with MM, as shown in Figure 3.1.

3.2.2 Simulation Details

For all production runs, the following procedure was used: First, the system was energy minimized with a pure molecular mechanical description, using the steepest descent algorithm. We used the OPLS-AA force field (71) for all MM simulations and minimizations. Next, we performed a pure MM MD simulation, where the system was heated to 300 K, using the Berendsen thermostat (72) over 20 ps at a time step of 2 fs. The time step of temperature coupling was chosen as 0.1 ps and the pressure was kept at 1 bar via isotropic coupling with the Parrinello Rahman barostat (73), with a time constant of 1.0 ps. Thus, we here work with an NpT ensemble. Due to the small size of the system it is important to couple the entire system to the temperature reservoir to prohibit large energy fluctuations of the cystine. The Lincs constraint (74) was used on all bonds. Non-bonded interactions were calculated within a cut-off of 1 nm. Electrostatic interactions beyond 1 nm were treated with Particle-Mesh Ewald (75) with a grid spacing of 0.12 nm.

The next step was a 10 ns MD simulation for equilibration, here using the Nosé-Hoover thermostat (76, 77) with a coupling constant of 0.4 ps for temperature coupling. Forces and velocities were taken from the heating simulation.

From the equilibration, 10 configurations were chosen between 2 and 10 ns for subsequent QM / MM simulations without force. First, a QM / MM energy minimization was performed, using the steepest descent algorithm. An interface between GROMACS 4.0.5 (48) and Gaussian 03 (68) was used for these simulations, with the QM system electronically embedded into the MM-system (69). The QM system was treated with MP2/6-31+G* (78) as suggested by Bergès et al. (79) and included 10 atoms: the two sulphur atoms, both CH_2 groups and the link atoms between C_α and C_β.

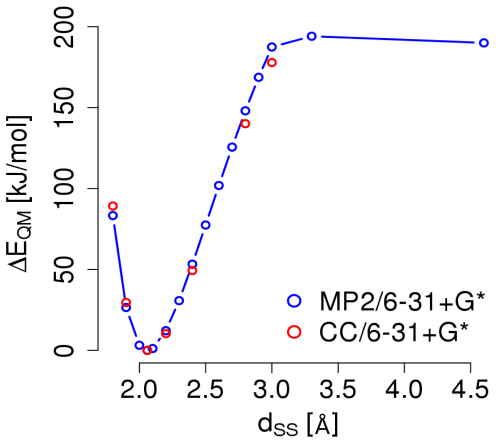

Figure 3.3: **Potential energy of the QM system depending on the disulfide bond length** - The energy of the QM treated system as a function of sulphur-sulphur bond length was obtained from restrained optimizations of cystine with pure QM, using MP2/6-31+G* *in vacuo*. The bond length was elongated stepwise, then optimization was performed, while freezing the position of both disulfide atoms. As expected, the dissociation of the disulfide is described by a Morse-like potential. QM / MM calculations using the MP2/6-31+G* level of theory is a widely used method, which, however requires validation for the disulfide system used here. To validate that the method is appropriate, we calculated the single point energies for the disulfide bond elongation, using coupled cluster (CC), and conclude that using MP2 is of sufficient accuracy. For better comparison, we set both minimum energy values to zero. See Table 3.1 for details.

In restraint optimizations of the entire cystine *in vacuo*, the MP2/6-31+G* method produces a Morse-potential for disulfide bond elongation in close agreement with the results of a Coupled Cluster level of theory (see Figure 3.3), and thus can be expected

to yield reliable energies for the redox potential calculations carried out here.

For all QM / MM calculations, the MM region was treated as described above. Lincs constraints (74) were only applied to bonds involving hydrogen, and the time step was changed to 0.5 fs. The Berendsen thermostat and barostat (72) were applied. Other simulation parameters were the same as for pure MM MD simulations. As conformations are sampled at 300 K, we did not use any zero point energy or thermal corrections. The electronical embedding took solvation effects into account.

d_{SS} [nm]	E_{elec} MP2/6-31+G* [kJ/mol]	CC/6-31+G* [kJ/mol]
1.80	-3779832	-3780049
1.90	-3779889	-3780108
2.00	-3779912	
2.06	-3779916	-3780138
2.10	-3779914	
2.20	-3779903	-3780128
2.30	-3779885	
2.40	-3779862	-3780089
2.50	-3779838	
2.60	-3779814	
2.70	-3779790	
2.80	-3779767	-3779998
2.90	-3779747	
3.00	-3779728	-3779960
3.30	-3779721	
4.60	-3779725	

Table 3.1: Absolute electronic energies, E_{elec}, of optimized cystine at a given sulphur-sulphur distance. Energies were optained from restrained optimization: The sulphur-sulphur bond length, d_{SS}, was elongated stepwise, while freezing the positions of the sulphur atoms. Compare Figure 3.3.

10 simulations, each 20 ps in length, were performed without applying any force. For evaluation of these zero-force simulations, only data for $t > 10$ ps was used. Simulations at forces up to 498 pN were performed starting from a randomly chosen set of coordinates and velocities of the zero-force QM / MM simulations. For any force larger than 498 pN, the structure and velocities were read in from the MD simulation at the

next-smaller force. Thereby, we did not introduce large errors into the simulation by suddenly applying a large force to a structure equilibrated at zero force. We applied the constant force onto the terminal N and C atoms in z-direction, i.e. in the longest dimension of our simulation box. To check for convergence, we performed additional simulations at F =166, 332 and 498 pN, which started from structures sampled at 830 pN instead of 0 pN. We did not observe any significant differences between these force-quench and force-jump protocols in terms of geometries and energies after 5 ps, and concluded that the 15 ps time scale was sufficient for full relaxation to the respective force. Overall, we performed 15 simulations each at F = 30, 50, 100, 166, 332, 498 and 830 pN and 5 simulations at F = 664, 1162, 1660, 2490 and 3320 pN, each lasting 15 ps, resulting in an overall simulation time of more than 2 ns.

3.3 Results

3.3.1 The QM / MM Setup

The reduction of a disulfide bond consists of several steps. Full reduction leads to two thiols, as shown in Figure 3.1. However, the first reduction step is the addition of a single electron. We first investigated this additional step of redox reaction in detail, and modeled an isolated cystine in water. We compared its average energy to the energy of its radical anion, sampling exactly the same configurations as the oxidized cystine. Next, we sampled the structure of the radical anion and thereafter calculated the energy of these sampled structures at the electronic state of the oxidized cystine. Finally, we compared the energies of the equilibrated oxidized and radical structures to the energies of the states differing by one electron. Table 3.2 summarizes the energy values obtained from these calculations. Enforcing an electron into the structure of a closed disulfide bond or taking it away from the radical structure both lead to an increase in quantum energy.

One important parameter that strongly influences the outcome of a QM / MM calculation is the way the QM part is implemented into the MM part. Two different methods are here available: mechanical or electronic embedding. For mechanical embedding, the QM part is only mechanically enforced to fit in the surrounding MM part. Electronical embedding additionally takes the charges of the protein and surrounding water molecules into account, thereby stabilizing the addition of a single electron to

Comparison	ΔE^{a}_{QM}	ΔE^{a}_{pot}	ΔE^{b}_{QM}	ΔE^{b}_{pot}
$(ox + e^{-})$ - ox	216 ± 66	1837 ± 2122	240 ± 2	241 ± 1776
red - ox	-588 ± 98	-62 ± 1900	33 ± 2	-296 ± 188
$(red - e^{-})$ - red	715 ± 109	2652 ± 2706	171 ± 2	180 ± 1987

Table 3.2: Difference in energy between a cystine and a cystine radical

a: electronic embedding
b: mechanical embedding
Errors represent the sum of the errors of the mean of both states.

a disulfide bond. The increase in energy upon adding or removing an electron was independent from the embedding scheme. This holds for both the energy of the QM subsystem, which we here refer to as the quantum energy E_{QM}, and the potential energy E_{pot} of the entire system. Such an increase is not surprising, as the cystine is reduced or oxidized but reorganization is prevented. In case of electronic embedding, E_{pot} is influenced by the charges surrounding the system. We find a significant difference between the treatment of the quantum region for the energy difference between the equilibrated structures of reduced and oxidized species: Only E_{QM} using mechanical embedding shows a higher energy for the reduced species. In all other cases, the radical anion is surrounded by water that can stabilize the charge. E_{QM} resulting from mechanical embedding shows the smallest fluctuations, but the lack of stabilization by the water in mechanical embedding makes a wrong assumption. Therefore, we henceforth work with electronic embedding.

As demonstrated by E_{QM} derived from mechanical embedding and also evident when comparing E_{QM} to E_{pot}, including the water in the energy calculations increases the energy fluctuations. One approach to decrease water fluctuation would be to use implicit solvent which, however, is known to be a rather poor approximation of solvent effects on proteins or peptides. Instead, we compared the energy fluctuations of potential and kinetic energies and of the temperature for both protein and water seperately. We found that due to the small system size, overall fluctuations could be minimized by using temperature coupling on the entire system rather than on cystine and water seperately.

To analyze if the chosen QM system was large enough, we set up a system with a larger QM box, containing 20 QM atoms, for comparison. It is the next larger

QM system possible, if one allows QM / MM boundaries only at single bonds, thereby minimizing boundary affects on electronic conjugations. Figure 3.4 shows the test system, a cystine with capped termini. Calculation times did not allow further analysis of the larger QM box. While the system with the smaller QM region (compare Fig. 3.1) allowed the calculation of 10 000 steps per day, the large QM system only yielded 135 - 220 steps per day, which is insufficient for comparison of structures and energies.

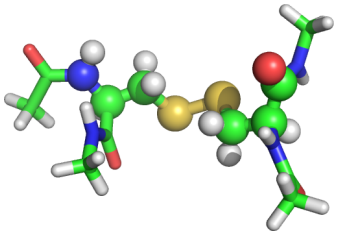

Figure 3.4: **Larger QM system** - To estimate size effects of the QM system, we set up a larger system for comparison. QM / MM calculations of this enlarged system yielded no more than 135 steps per day.

Thus, we used another comparison to confirm that the QM region was well chosen. From the final snapshot of five independent trajectories at each force we performed a pure QM single point calculation, using Gaussian03. We qualitatively find the same results as from QM / MM pulling simulations as will be detailed in Section 3.3.3. Another important aspect to determine a sufficiently large QM region are the lowest unoccupied (LUMO) and the highest occupied molecular orbitals (HOMO). The opening process of a disulfide bond includes the formation of another disulfide bond to one of the sulphur atoms. Therefore, the HOMO is going to react. Figure 3.5 shows the HOMO of cystine for single point calculations for structures equilibrated at different forces. The HOMO mainly concentrates on the disulfide bond and the adjacent C_β-atoms. The higher the forces, the smaller the HOMO as the HOMO is increasingly destabilized. We note that the LUMO was calculated to be located on one of the oxygen atoms, an artifact which we suppose to be due to the relatively restricted size of the QM system, which the MM part, however, can partly compensate for.

We have seen that QM and QM / MM calculations qualitatively lead to similar results. QM calculations, both restrained optimizations and single point calculations are computationally less demanding than QM / MM MD calculations. However, structural optimizations involve sampling problems, which QM / MM dynamics in explicit

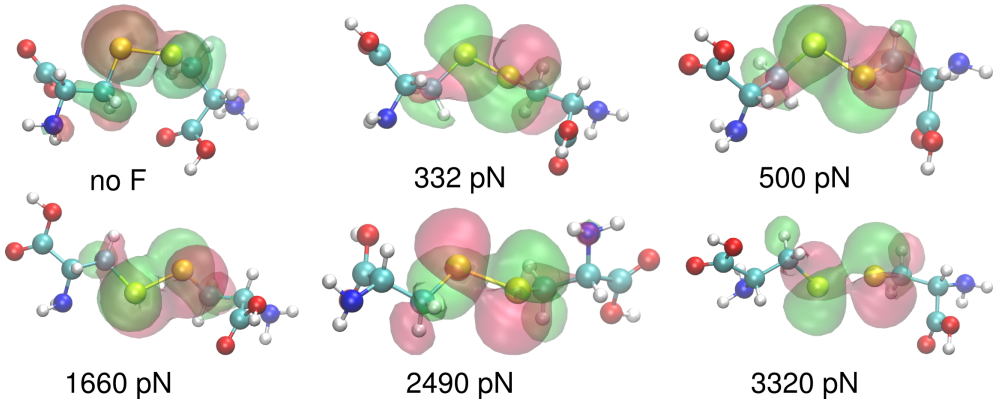

Figure 3.5: **HOMO of cystine** - We performed single point QM calculations on cystine configurations derived from QM / MM equilibrations at the given forces. The HOMO is mainly concentrated on the disulfide bond and the adjacent C_β-atoms for all forces applied, as expected. These findings confirm that the size of the QM region is reasonable.

water can prevent. Additional QM calculations further clarified this backdraw of QM optimizations.

We performed QM optimizations of the QM region at different levels of theory for the oxidized state (normal disulfide bond) and the radical anion of dimethyldisulfide in implicit water. Then, we performed a rigid scan along the sulphur-sulphur bond distance at both redox states. Finally, for the MP2 level of theory, we used restrained optimization for further comparison. Figure 3.6 shows the Morse potentials of the disulfide bond at different levels of theory.

Both, the energies of the oxidized and radical structure converged at UHF, UB3LYP and MP2 level of theory, in contrast to the CASSCF reduced state (Fig. 3.6 d). All scans show that the energy of the reduced state is lower than of the oxidized state, as we have also observed from QM / MM calculations using electronical embedding. To estimate the impact of the reorganization free energy, we next performed restrained optimizations, at the MP2 level of theory using the 6-31+G* basis set in implicit water. We allowed the methyl groups to structurally reorganize freely at each disulfide bond length (Fig 3.7 a). At high sulphur-sulphur distance, they start moving towards each other apparently because of beneficial dispersion interactions. This behavior is the opposite of what is to be expected from a pulling force and an artifact from the distance scans, even though this is a routinely applied technique.

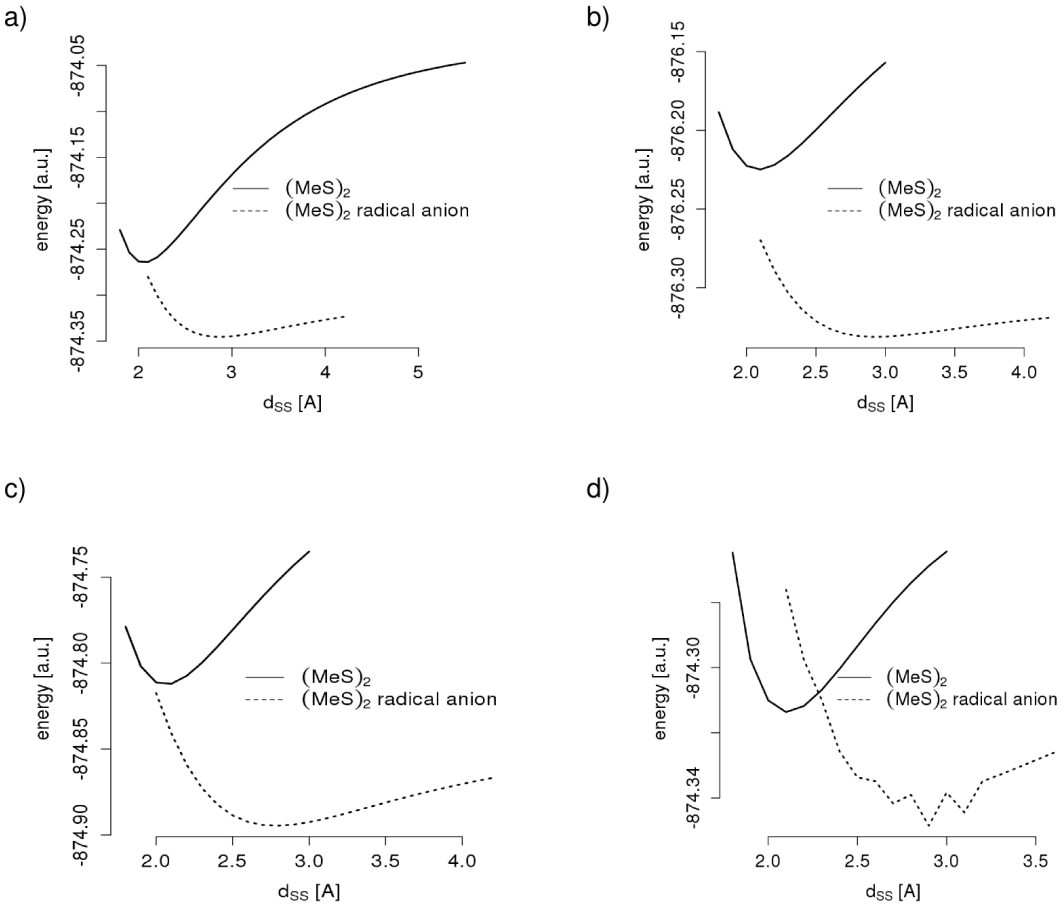

Figure 3.6: **Energy of cystine for a range of disulfide bond lengths** - We used pure QM calculations to perform rigid scans, elongating the disulfide bond length of dimethyldisulfide $(MeS)_2$ and the corresponding radical anion. We used the following levels of theory: a) UHF, b) UB3LYP, c) MP2, d) CASSCF(6,6) and CASSCF(3,3) for the oxidized and reduced states, respectively. All data points were calculated using the 6-31+g(d,p) basis set and implicit water.

We also considered the option of a spin-cross over. Restrained optimization of the triplet state shows that this is not to be expected for sulphur-sulphur distances shorter than 3.5 Å. To better immitate an external pulling force, we performed another scan of restrained optimization, where we fixed the distance between the Methyl-C atoms and allowed the sulphur atoms to organize freely (Fig. 3.7 b).

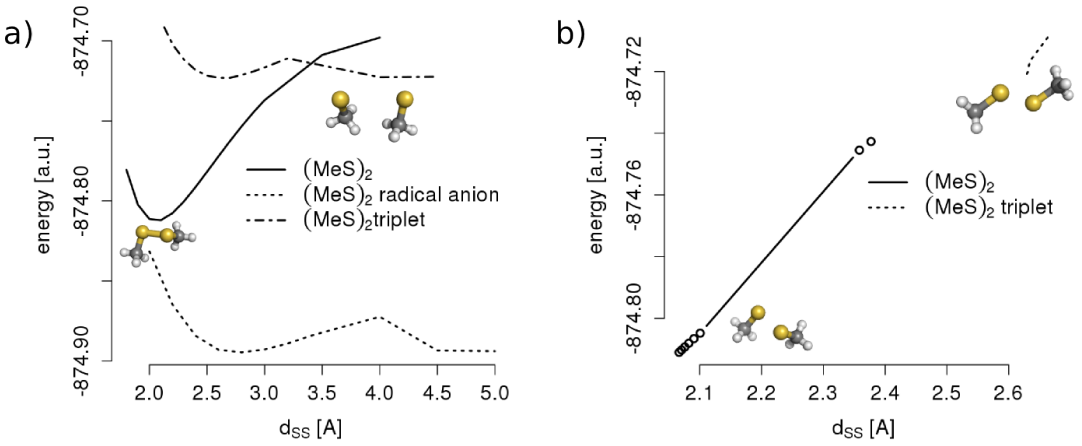

Figure 3.7: **Stretching the molecule by restrained optimizations** - a)Allowing the methyl groups to reorganize during a restrained elongation of the sulphur-sulphur bond leads to clustering of the methyl groups, a behavior contradictory of what is to be expected from mechanical pulling forces. b) Restrained optimizations with a growing yet fixed carbon-carbon distance leads to a jump in sulphur-sulphur bond length and also a linear increase in energy with distance, again different from external pulling.

We elongated the C-C distance in steps of 0.1 Å. Up to C-C distances of 3.0 Å, this leads to minor changes in the sulphur-sulphur distance of less than 0.1 Å, as we will later also see for QM / MM calculations (compare Sec. 3.3.4). Instead, enlarging the C-C distance from 3.0 to 3.5 Å results in a jump of 0.3 Å in disulfide bond length. We find a linear increase in energy with the disulfide bond length, an effect opposed to what QM / MM calculations show (compare Fig. 3.11). The triplet state at the same carbon-carbon distance results in a completely different range of disulfide bond lengths, and no overlap was found. In other words, the triplet state is energetically unfavored and should dissociate spontaneously. Overall, the QM optimizations yield unrealistic structures or energies, which we mainly attribute to that lack of solvent and thermal

fluctuations.

Does QM / MM represent the charges on the sulphur atoms in an adequate way? Adding a charge to the cystine QM / MM system leads to a negative charge, mainly located and equally distributed over both sulphur atoms. In contrast, a pure QM calculation of cystine allows only 6 % of the negative charge to distribute over the disulfide groups, while 94 % are located on the more electronegative COOH groups. Thus, the QM / MM description again represents the charge densities in a disulfide bond more realistcally, in contrast to QM calculations.

The following conclusions have been drawn from these calculations. First, we have seen that the energy difference between the oxidized structure itself and the same conformations with an electron enforced into it neglects the reorganization energy. We assume the latter to play an important role in the redox potential and therefore in the following allow structures to relax in MD simulations. Secondly, testing of the QM subsystem has shown that it is chosen sufficiently large. Thirdly, and most importantly, rigid scans even if performed in implicit solvent are not optimally reproducing the experimental conditions of external single molecule pulling in water and at room temperature. While the reactant state, the disulfide bonded state, is clearly defined and computationally easily accessible, the redox potential calculations also require a proper definition of the reduced state. The latter is experimentally and theoretically much debated. This is the topic of the next section.

3.3.2 Defining the Reduced State

A redox potential measures the energy difference between the reduced and oxidized state. We here are interested in the change of redox potential upon force application. Applying a range of mechanical forces to the oxidized state to calculate its force-dependent energy is straightforward, as the disulfide bond can withstand forces up to 3320 pN on the picosecond time scale. The question arises if the reduced state can withstand mechanical forces, or opens the sulphur-sulphur bond. In the latter case, its energy would be force-independent. Simple electron addition to a disulfide bond, the primary reaction mostly chosen to study redox reactions quantum mechanically (63, 64, 65), results in a radical anion, which was previously found to maintain a chemical bond between the sulphur atoms in QM calculations of minimized structures *in vacuo* (66).

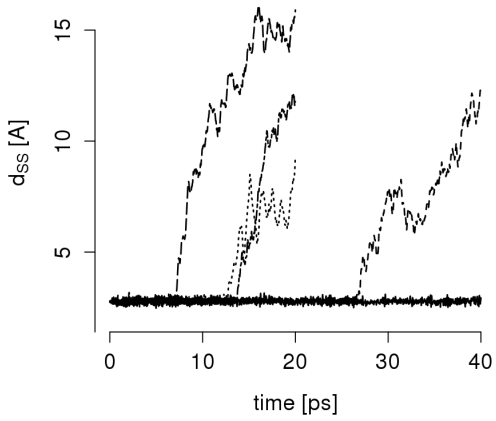

Figure 3.8: **Dynamics of the reduced disulfide radical anion** - The radical anion of cystine opens in four out of five independent trajectories at $F = 0$ and at $T = 300\,\mathrm{K}$, resulting in a thiolate anion and a thiyl radical. As we find the open state to be the equilibrium state, it is independent of force. Thus, its energy can be accounted for as a constant and the relative changes of the redox potential by force are independent from the energy of the reduced state.

As a first step of estimating the force-dependent stability of the reduced state, we performed QM / MM calculations of the radical anion at ambient conditions, in explicit solvent, and in the absence of force. These simulations were set up in a way equivalent to simulations of the oxidized state: The same configurations from the pure classical MD simulations that were used for QM / MM minimization in the oxidized state were chosen and minimized with one additional electron in the QM region (charge -1, multiplicity 2). Then, five independent QM / MM simulations were started, at the same conditions used for the oxidized state, again with a charge of -1 and a multiplicity of 2. We observed a dissociation of the disulfide bond within the first 40 ps for four out of five simulations of the reduced state (Fig. 3.8).

As the radical introduces a negative charge and periodic boundary conditions were used throughout all simulations, instabilities might arise from the net charge in the simulation system. We therefore added a sodium cation to our calculations. Even though energy fluctuations decreased, no increase in stability was achieved (Fig. 3.9). Thus, in contrast to previous findings for the same system at 0 K *in vacuo*, the open state is the equilibrium state of the radical anion in water at ambient conditions, even in the absence of force.

The protonated radical, resulting from the addition of one electron and one proton, can be considered as another feasible product state of the reduction reaction. Previous estimates for the pKa of a disulfide radical anion range from 6 to 10 (80, 81),

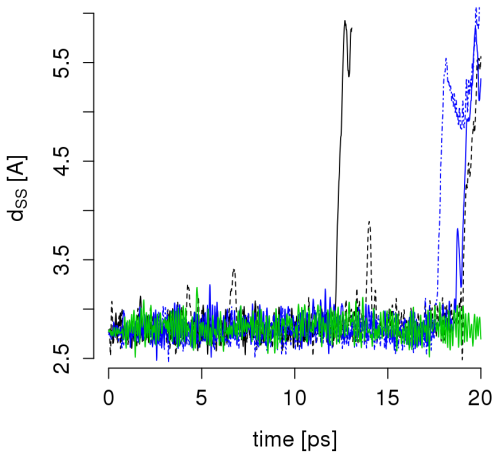

Figure 3.9: **Dynamics of the reduced disulfide radical anion with an additional Na^+-ion** - Adding an electron to the system introduces a negative charge that is not cancelled out. We could show that neutralizing the charge with a sodium ion did not increase the stability of the system. The distance between the two sulphur ions still increases till the bond breaks, in four out of five simulations over 20 ps.

and strongly depend on the chemical surrounding. This is similarly the case for fully reduced cysteine residues; while proteins predominantly contain protonated cysteines, the catalytic cysteine in thioredoxins, for example, has been clearly shown to be deprotonated (82). We used a number of methods to check whether the protonated reduced state as another possible product state was closed, and thus force-dependent. QM optimizations showed a closed state only for semi-empirical methods (AM1 and PM3), whereas further refinement (UB3LYP, UMP2) showed that the bond dissociated upon optimization. This was further confirmed by a QM / MM energy minimization at the MP2/6-31+G* level of theory, which again lead to dissociation (Table 3.3). These findings suggest that the addition of a proton to the radical anion does also not stabilize the reduced state any further, as we observe spontaneous bond lengthening in both QM and QM / MM optimizations for this uncharged radical species.

Obviously, the doubly protonated reduced state, that consists of two molecules of cystein, does not feature a bond between the sulphur atoms, and as a consequence its energy is independent of force. In summary, we considered three different products as possible reduced state: The doubly protonated reduced state, as shown in Figure 3.1, the protonated radical and the radical anion. We found all three possible product states to open at ambient conditions, and thus being independent of force. We conclude that irrespective of its precise nature and protonation, the product state is force-independent, and it is fair to estimate force-altered redox potentials solely on the basis of the oxidized state. Thus, in the following, we only consider the closed, oxidized

method	d_{SS} [Å]
AM1	1.99
PM3	1.95
UB3LYP/6-31+G*	3.19
UMP2/6-31+G*	3.93
QM / MM	3.25

Table 3.3: Optimization of the protonated radical, that is now neutral in charge, shows dissociation for any level of theory higher than PM3

state, the cystine molecule.

3.3.3 Force-dependent Redox Potentials of Cystine

We here investigated the impact of mechanical force on the redox potential of the disulfide bond in cystine solvated in water from MD simulations. To this end, we applied mechanical forces in the range of 0 to 3320 pN to the N- and C-termini of cystine. The changes in redox potential as a function of force are shown Figure 3.10 a. As expected, we observed an overall increase in redox potential with mechanical force. In other words, stretching forces acting on the molecule enhance the electron affinity of the disulfide bond by destabilizing the molecule. However, this pronounced increase in redox potential is only found for forces greater than 166 pN. Forces below 100 pN, instead, show the opposite trend. Surprisingly, they stabilize the system slightly and thus decrease the redox potential, as shown in the inset of Figure 3.10 a. Counter-intuitively, this involves a shortening of the disulfide bond at low force (see further below).

From single snapshots from the trajectories at different forces, we performed natural bond orbital (NBO) analysis. Methodological details are given in Section 2.2.1. Restrained optimizations with the coordinates of the N- and C-termini frozen, were performed with the 6-31+G* basis set on the MP2 level of theory, implemented in Gaussian09 (83). NBO analysis was then performed by the NBO 3.1 program (51). Figure 3.10 b shows the p-character of the two sulphur natural hybrid σ_{S1-S2} bond orbitals, which rises when force is increased. This observation confirms the finding that the HOMO concentrates more strongly on the disulfide bond as force rises (compare Fig. 3.5).

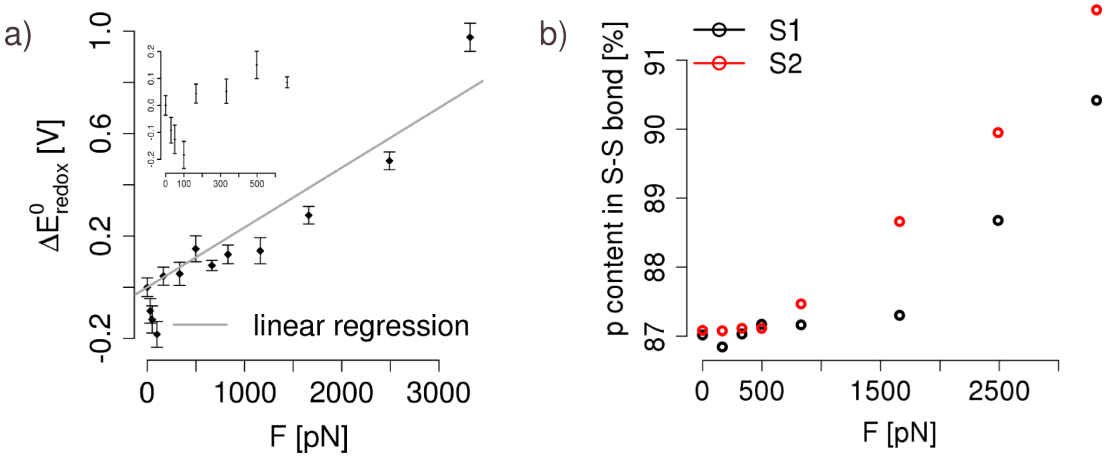

Figure 3.10: **Force fine-tunes redox potentials** - a) Mechanical force changes the redox potential towards higher reduction potentials. From our linear regression (solid line), we estimated the distance on the reaction coordinate between reactant and product, $\Delta x_{\mathrm{r,p}}$. The redox potential $\Delta E^0_{\mathrm{redox}}$ continuously increases with force, except for small forces (see main text). Error bars represent the s.e.m. obtained from the average values over each trajectory at a given force, b) p-content of the sulphur-sulphur bond.

Assuming force to tilt the energy landscape linearly by $F \cdot x$, one can obtain the distance between the reactant and product state along the reaction coordinate, $\Delta x_{\mathrm{r,p}}$. This is the basic assumption of the Bell model (26), which relates mechanical force to kinetic rates (Sec. 1.2.1). We here infer force-induced thermodynamic changes on the same basis. The free energy landscape is linearly tilted by force, following

$$G(F, x) = G(x, F = 0) \; - \; Fx). \tag{3.2}$$

Both, transition and product state are shifted linearly by force with respect to the educt state. Though often thought of as the superior model, the Dudko model cannot be used in this context. The Dudko model (Sec. 1.2.1) makes assumptions for the shape of the energy landscape to deduce a non-linear change in transition barrier, $\Delta G_{r,\ddagger} > 0$, and thereby rate upon force application. It hence cannot make predictions for the force-induced change in the overall reaction free energy, $\Delta G_{r,p} < 0$, between reactant and product state. Thus, we here follow the Bell model and estimate $\Delta x_{\mathrm{r,p}}$, the distance between reactant and product state (compare Fig. 1.3), from a linear fit to our force-dependent redox potential data to be 0.37 Å over the entire range of forces probed

Force range [pN]	$\Delta x_{\mathrm{r,p}}$ [Å]	$\Delta x_{\mathrm{r,\ddagger}}$ [Å]
0 - 830	0.25	
0 - 3320	0.37	
100 - 400		0.34[a]
100 - 400		0.23[b]

a: taken from reference (24)
b: taken from reference (60)

Table 3.4: Estimated $\Delta x_{\mathrm{r,p}}$ from linear regression and experimentally measured $\Delta x_{\mathrm{r,\ddagger}}$

here. Due to the non-linear dependency of $\Delta E^0_{\mathrm{redox}}$ on force (Fig. 3.10 a), we obtain a smaller $\Delta x_{\mathrm{r,p}}$ of 0.25 nm for forces up to 830 pN (Table 3.4).

How does our estimated $\Delta x_{\mathrm{r,p}}$ compare to experimental data? Force clamp experiments allow measuring the distance between the reactant and the transition state, $\Delta x_{\mathrm{r,\ddagger}}$. Such an experiment performed on a titin immunoglobulin domain yielded a $\Delta x_{\mathrm{r,\ddagger}}$ of 0.34 Å (24). Other thiol containing reducing agents resulted in $\Delta x_{\mathrm{r,\ddagger}}$ between 0.23 and 0.35 Å (23, 60) (compare Table 3.4). Overall, the experimental and calculated values for the distance of the reactant to the transition and product state, respectively, largely overlap, semi-quantitatively validating our results.

Force-dependent redox potential changes have not been measured, to our knowledge, to date. We here refer to distances measured along the reaction coordinate from the changes in reduction rates upon stretching. In a disulfide bond reduction by DTT, $\Delta x_{r,p} \sim 0.34$ Å (24). Values vary with the reducing agent, between 0.23 and 0.35 Å (60). From the force-dependent redox potential, we similarly inferred the distance, here between reaction and product state, to be $\Delta x_{r,p} \sim 0.25$ - 0.37 Å. Thus, our results overlap with the experimental results, or in other words, a similar force sensitivity is found, which can be interpreted by a transition state close in structure to the product state.

3.3.4 Structural Changes

The observed overall increase of the disulfide's electron affinity can involve the deformation of various degrees of freedom of the system in the vicinity of the bond. We next analyzed the structural features of cystine under a stretching force that are likely to cause the increase in redox potential and thus the enhanced tendency for sulphur-

sulphur bond scission. As expected, the destabilization of the system by the applied mechanical force, as measured by ΔE_{QM}, overall involves a lengthening of the disulfide bond (Fig. 3.11 a). Within the force range probed here, the bond elongates by up to 0.2 Å, which corresponds to roughly 10 % of the initial length, within the oxidized state. However, our QM / MM calculations show that at low forces smaller than 500 pN, the disulfide bond length does not increase steadily (black curve in Figure 3.11 b), even though the end-to-end length between the cystine's termini increases (blue curve). We find that low to intermediate forces up to 500 pN lengthen and destabilize the oxidized state significantly without considerably stretching the disulfide bond. Instead, unexpectedly, we even observe a slight shortening of the disulfide bond in the regime of small force application (from 0 pN to 30 pN).

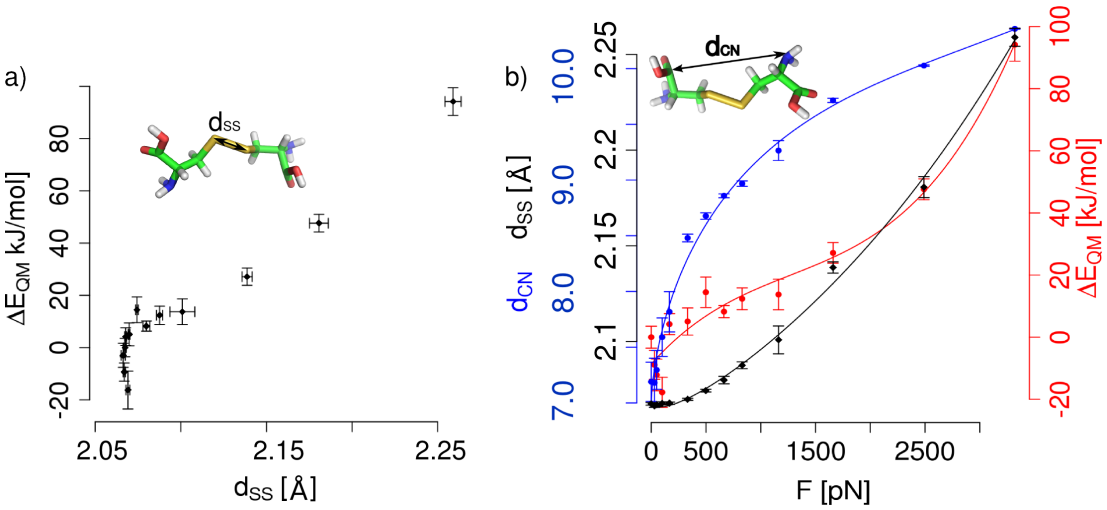

Figure 3.11: **Structural changes** - Mechanical force changes the redox potential of cystine by shifting the conformational equilibrium to larger bond lengths, angles and dihedrals. (a) Both the energy of cystine, $\Delta \mathrm{E_{QM}}$, and the elongation of the sulphur-sulphur bond, $\mathrm{d_{SS}}$, rise with mechanical force. However, at forces lower than 500 pN, the destabilization of the cystine does not involve any significant bond lengthening. (b) In addition to the lengthening of the sulphur-sulphur bond (black), force leads to a lengthening of the whole molecule, measured by the distance between the termini, $\mathrm{d_{CN}}$ (blue). Taken together, these changes in softer and stiffer degrees of freedom cause the energy ΔE_{QM} (red) to rise over the whole range of forces. In all figures, the energy and redox potential obtained at $F = 0\,\mathrm{pN}$ served as a reference. Lines serve as guides to the eye.

The lengthening of the disulfide bond is significant only at forces larger than 500 pN (Fig. 3.11 b), and thus can explain the observed rise in redox potential only partly. Apparently, other degrees of freedom that contribute to the stability and thereby to the redox potential of cystine are effected by mechanical force. Indeed, at forces below 500 pN, the overall length of the cystine molecule, measured by d_{CN}, increases (Fig. 3.11 b). This lengthening at low forces is caused by changes in the dihedrals and angles in proximity to the disulfide bond (Fig. 3.12). The dihedral angle enclosing the disulfide bond is the degree of freedom that starts changing first. Without any mechanical force applied externally, it samples angles around 80 °. Though flexible, as evidenced by the large error bars, the dihedral angle expands already upon application of the smallest force probed here, namely 30 pN, to around 115 °. At forces of 1160 pN and higher, the average dihedral angle is $\sim$ 170 °. As the maximum extension is already reached, forces larger than 1160 pN do not increase the dihedral angle any further. An analogous picture was found for the two CSS angles enclosing the disulfide bond. Increasing the force from zero to 1000 pN enlarges the angle from 103 to $\sim$ 105 °. For forces larger than 1160 pN - that is where dihedrals are already extended to be nearly planar - angles are continuously being stretched up to 114 °. In a simplistic view, we can infer a sequence of events upon stretching a disulfide bond from this analysis. This is to say, cystine elongates first by extending soft dihedrals all the way up to nearly 180 °, secondly by stretching angles, and lastly by elongating the comparably stiff sulphur-sulphur connection itself. The high force-sensitivity of angles and even more so for dihedrals implies that the extension of the overall cystine molecule at low forces (Fig. 3.12 b) can be primarily attributed to the stretching of dihedrals and angles, leaving the disulfide bond largely unchanged.

As already implied, fully releasing the force from 50 pN to 0 pN elongates the disulfide bond marginally by $\sim 10^{-3}$ Å (see Figure 3.11), thereby destabilizing the cystine and leading to a rise in $\Delta E^0_{\text{redox}}$, as shown in the inset in Figure 3.10 a. Apparently, low forces act on degrees of freedoms orthogonal to the disulfide bond length. This counter-intuitive behavior is likely to be cystine specific, since it was not observed for a larger protein (titin I27) (30).

To ensure that the bond shortening we observed is not an artifact of the QM / MM calculations, we performed pure QM optimizations on a cystine, where we enlarged the dihedral angle stepwise. The disulfide bond shows a minimum in bond length not in

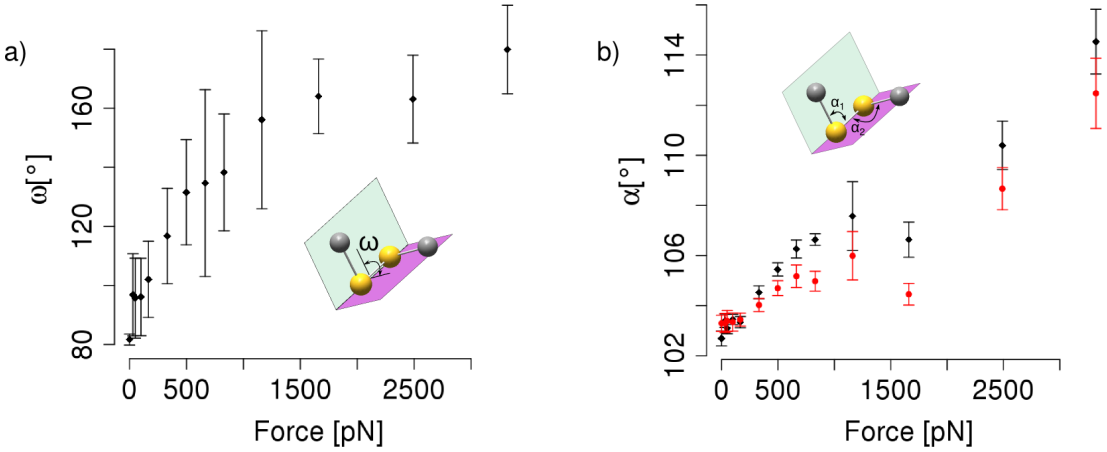

Figure 3.12: **Impact of force on the angles and dihedrals surrounding the disulfide bond** - Changes of softer degrees of freedom of cystine, i.e. angles and dihedrals, by mechanical force. a) Dihedral angles ω between the cystine side chain atoms C_β-S-S'-C_β' (see inset) increase already at forces as small as 50 pN, and open up to $\sim 170\,^\circ$. Other dihedrals show similar tendencies (not shown). b) Angles α_1 and α_2 between C_β-S-S' and S-S'-C_β', respectively, show changes over nearly the whole force range (from $F > 320$ pN).

the fully optimized structure, but at a torsion that is $10\,^\circ$ larger than the one found in the minimized structure (see Figure 3.13).

3.4 Discussion

We here employed Molecular Dynamics simulations of cystine at ambient conditions to assess the effect of mechanical force on disulfide reduction. By quantifying the redox potential, our study allows conclusions independent from the reducing agent and reduction mechanism. We find that a pulling force, even at forces as small as a few 100 pN, directly affects the redox potential, i.e. the chemistry of the disulfide bond. This major result of our study, the thermodynamic destabilization of the oxidized state by force, can be directly related to the force-altered kinetics of single molecule force experiments. As mentioned in the Methods section, the increase in redox potential entails a lowering in the activation barrier for reduction (compare Section 1.2.1, as the free energy landscape is steadily tilted by force according to the Bell or other refined models (see the linear fit to $\Delta E^0_{\mathrm{redox}}$ according to Bell in Figure 3.10 a) (26, 84). Our results

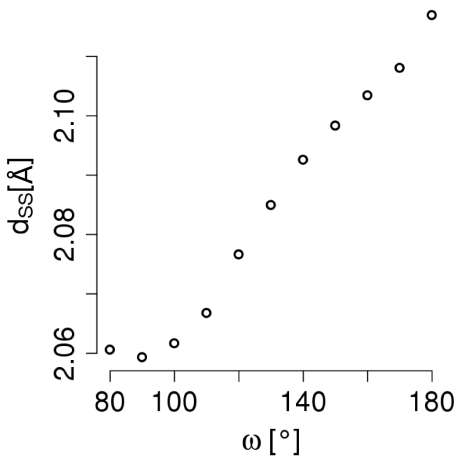

Figure 3.13: **Dihedrals surrounding the disulfide bond** - Restrained optimization of cystine with pure QM, using MP2/6-31+G* *in vacuo*. Here, the dihedral angle enclosing the disulfide bond was enlarged step wise and restrained, while the optimizations was performed. In accordance with our QM / MM calculations, the disulfide bond length shows a minimum for $\omega > \omega_{min}$.

thus can explain the enhanced reactivity observed in various recent force spectroscopy experiments and in calculations (23, 24, 30, 60, 61, 62). Other factors such as substrate accessibility or changes in the reaction mechanism can additionally alter the reaction rates. However, as we here show, mechanical force does destabilize the oxidized system directly, which is sufficient to explain the experimental rate enhancement by force. In this light, the mechanical insensitivity of disulfides in strained ring structures (25) is surprising and might possibly be caused by several compensating effects which are subject to further investigations.

Remarkably, lower and medium forces (between 50 and 830 pN) primarily affect the softer degrees of freedom, namely angles and dihedrals, while the disulfide bond remains unstreched or even becomes shortened. Only at high forces (beyond ~ 500 pN), stretching of the disulfide bond itself sets in. Both effects jointly lead to a steady destabilization of the system and thus an increase in redox potential throughout the whole range of forces (30 - 3320 pN) probed here. At 3320 pN, the maximum force investigated here, we found the disulfide bond to stretch by 0.2 Å and dihedrals to fully open (i.e. close to 180 °). We compared these findings for the isolated cystine to a cystine in a mutant of I27, a titin immunoglobulin domain, under different stretching

forces. Again, the disulfide bond shows a slow increase in bond length upon stretching, while angles and dihedrals enlarge already significantly in the low force regime (results not shown). Also, angles and dihedrals in titin expand up to 180 °, in a similar way as discussed for cystine, (compare reference (30)). Thus, our major findings are largely independent from the system comprising the sulphur-sulphur bond. The decrease in disulfide bond length, however, seems to be specific for cystine. How this shortening of disulfide bond length at low forces is related to catch-binding (24, 85), could not yet be understood and remains to be explored.

As opposed to our results, the COGEF study recently presented by Iozzi et al. (67) predicts the bond to stretch by 0.35 Å till the rupture point - which is found for ~ 3500 pN - but the dihedrals enlarge no more than up to 120 °. The major differences between the two approaches is that we take solvation and dynamic fluctuations at room temperature into account, whereas Iozzi's study was performed *in vacuo* using optimization, i.e. by comparing minimized structures. Apparently, these different conditions cause very different degrees of freedom to be affected by mechanical force. In other words, the dynamics at ambient conditions allow the structure to relax differently to the relaxation taking place at 0 K *in vacuo* as it is the case for the COGEF approach. We note that the different levels of theory used by Iozzi et al. (B3LYP) and us (MP2), is unlikely to give rise to the discrepancies, as they yield similar bond lengths, and only differ in their electron affinity for sulphur-sulphur systems (79).

How are the changes in redox potential upon force application related to previous experimental findings? We above have quantified the sensitivity of our redox system towards a mechanical force, in other words the extent to which the energy landscape is tilted by a given force, in terms of $\Delta x_{\mathrm{r,p}}$, the distance between reactant and product state along the reaction coordinate (Table 3.4). The force-sensitivity of the redox potential, measured by $\Delta x_{\mathrm{r,p}}$, is of a similar magnitude as the force dependency of the redox reactivity probed in experiments, in terms of $\Delta x_{\mathrm{r},\ddagger}$. We can conclude that our QM / MM calculations are in line with previous force spectroscopy experiments. They suggest that the whole redox reaction is as susceptible to the mechanical force as the transition barrier. The structural interpretation of Δx then implies the transition state to highly resemble the product state.

The above analysis of our force-dependent redox potential calculations is based on the simple assumption that force tilts the energy linearly along the reaction coordinate,

as originally proposed by Bell (26). However, other advanced non-linear models have been put forward and have proven useful (84) to interpret force-altered reaction rates probed experimentally. Devising a non-linear model for estimating force-depedent redox potentials for the disulfide bond, i.e. a Morse potential, might further improve the accuracy of our analysis, is, however, out of the scope of the present study.

How does the observed force-sensitivity of the disulfide bond redox potential compare to the variation in redox potential of this bond in different chemical environments? Our calculations estimated a force of $\sim 300\,\mathrm{pN}$ to increase the redox potential by $\sim 50\,\mathrm{mV}$, while an external force as high as $\sim 1000\,\mathrm{pN}$ increases the redox potential by $\sim 140\,\mathrm{mV}$. On average over the whole force range, we obtain from $\Delta x_{\mathrm{r,p}}$ a force-sensitivity of $0.23\,\mathrm{mV/pN}$. In living organisms, we usually find redox potentials in the range of 200 to 300 mV, i.e. variations $< 100\,\mathrm{mV}$. Figure 3.14 shows some examples of thioredoxin mutations and their redox potentials (86). A single point mutation changes the redox potential by no more than 32 mV. As another example, engineered disulfide bonded GFP mutants feature redox potentials differing by no more than 10 - 20 mV. Such an alteration of redox potential would require a pulling force of several tens of piconewtons.

As demonstrated by this comparison (Fig. 3.14), a change in redox potential can be similarly achieved by either a change in the biochemical neighborhood, e.g. a mutation, or a mechanical force in the 100 pN range. The question arises if a mechanical force of this magnitude is likely to act on a disulfide bond in the living cell. Titin immunoglobulin domains have been shown to unfold at forces in the range of 150 to 300 pN (88). Another example for a biological system experiencing mechanical force is the fibronectin / integrin cluster. Its bond strength is estimated to lie between 30 and 100 pN (89). In general, forces on a single molecule in living organisms are estimated to be a few piconewtons or a few tens piconewtons large (90) and thus are able to tune redox potentials significantly.

3.5 Conclusions

In conclusion, force can alter the redox biochemistry in the cell to an extent comparable to single point mutations in redox reactive proteins. We expect our approach, by including conformational sampling and explicit solvation, to reliably predict the correct

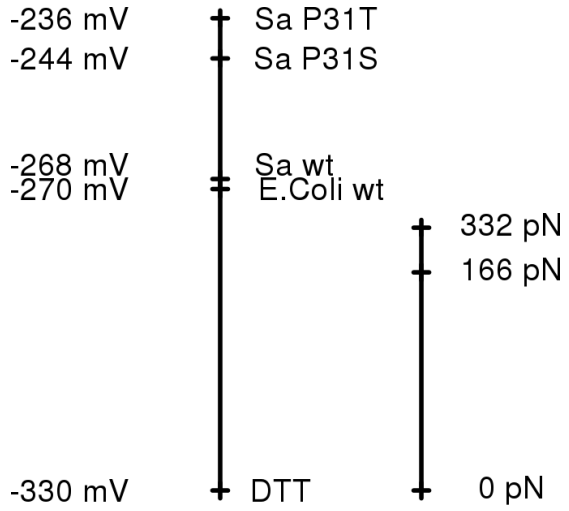

Figure 3.14: **How does force change the redox potential as compared to chemical environments?** - Redox potentials in biological systems in comparison to redox potentials induced by mechanical force. Left: measured redox potentials for chemical and biological reducing agents, namely DTT (87), *E. coli* thioredoxin (6), and (*S. aureus*) thioredoxin, including two mutants (86). Right: Shifts in redox potential for cystine from our QM / MM calculations, shown at the same scale. Force-altered redox potentials cover a similar range as those sampled within different molecules and mutants.

tendencies in $\Delta E^0_{\text{redox}}$ upon force application. A more thorough treatment based on free energy calculations (42, 91) (Ch. 4) and taking proton uptake into account might in future help to make quantitative estimates of force-altered redox potentials.

3.6 Outlook

Having succesfully calculated the redox potentials of cystine at different forces, we now want to use this method to estimate the redox potentials of larger systems and to further compare the impact of force to the impact of a chemical surrounding. To this end, we built oligomers with a cystine in the center and one glycine residue at three of the termini. The idea was to calculate a series of redox potentials with different oligomers where one of the residues (X) is being exchanged (see Figure 3.15).

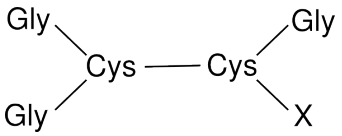

Figure 3.15: **Oligomer models** - A scan of oligomers in which X is by a number of differend (e.g. charged aminoacids would alow to systematically characterize the effect of the (electrostatic) environment on the sulphur-sulphur bond's redox potential.

From an MD equilibration, we could see that such an oligomer was much more confomationally flexible than expected so that conformational sampling might become a bottleneck. A protein containing a similar pattern is Trx. The motif common for the active site of all Trx and Trx-like proteins is the $CXXC$ loop, consisting of two cysteine residues C, enclosing two other amino acids X. It is thought of as a redox rheostat, its sequence determines the redox potential (6). We followed the protocol given in Section 3.2.2, and calculated redox potentials between the oxidized (disulfide bond is closed) and doubly protonated reduced state for different Trx mutants. In contrast to the force dependent redox potentials of cystine, here, the reduced state needs to be taken into account as it differs for different mutants. However, we find the reduced state to be easily deprotonated, thus unstable and difficult to sample in QM / MM simulations. In addition, the redox potential calculations presented here have the disadvantage to approximate the change in free energy during the redox reaction by the QM energy, a potential energy. Entropic effects are thus fully neglected. For these reasons, we next

devised an alternative approach, MM-based free energy calculations and applied it to Trx and its mutants (Ch. 4).

4

Free Energy Calculations

In Chapter 3, using hybrid quantum and classical mechanical calculations, we could show protein disulfide bonds to be destabilized by mechanical force, which results in a shift in redox potential, similar to shifts found when changing the chemical environment of the bond. In this chapter, we devise an approach to calculate any redox reaction free energy in order to compare disulfide bond stabilities in redox proteins.

4.1 Redox potentials from Free Energy Calculations

Differences in redox potential of proteins are the driving force of many vital biochemical reactions. A fundamental understanding of redox processes under physiological conditions opens up opportunities to get deeper insights into biochemical pathways. While redox potentials of proteins are in principle experimentally accessible, an alternative computational approach would allow to systematically screen and tune redox properties of proteins by mutagenesis, prior to the more elaborate experimental validation. We use free energy calculations (FEC) to calculate the redox potential of proteins that undergo thiol- / disulfide exchange.

To this end, we chose thioredoxin (Trx), a ubiquitous protein, as a model system to design and test our method. Trx shares a common motif with all Trx-like proteins, the *CXXC* motif, where *C* refers to cysteine and *X* to any other amino acid. It is thought of as a redox rheostat, as its sequence determines the redox potential (6). Trx is a thiol- / disulfide oxidoreductase, a family that occurs in all living organisms. As the name suggests, these oxidoreductases catalyze the oxidation of thiols to disulfides

and the backwards reaction but also disulfide isomerization. The *XX* dipeptide in the active site is known to control redox properties, and is thus expected to be very useful for the design of new thiol- / disulfide oxidoreductases with new redox potentials (92). Quan *et al.* have shown that the *CXXC* also changes the protein's ability to isomerize disulfides (6), a feature that could be approached with the method introduced here. Cleavage and isomerization behavior of disulfide bonds in proteins play a crucial role in their activity and are thus of great interest. This chapter introduces an approach to calculate the redox potentials of disulfide bonds in proteins when they undergo cleavage. The redox potential of a cystine in a protein corresponds to the free energy of opening that disulfide bond.

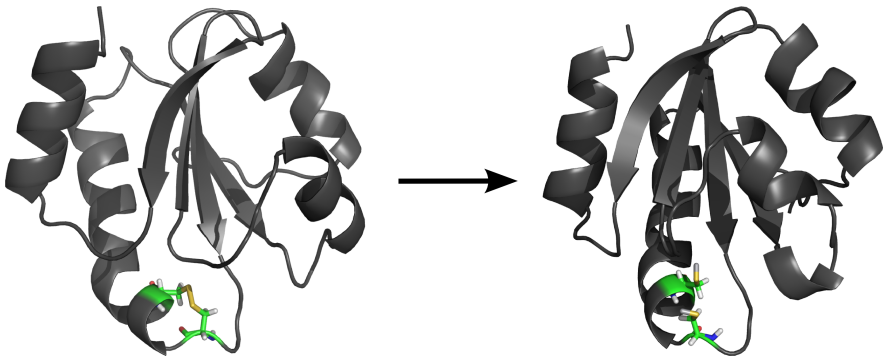

Figure 4.1: **Disulfide reduction in thioredoxin** - We use Trx of *E. coli* as a model system to calculate the redox potential of disulfide bonds. Left: oxidized Trx, right: reduced Trx. The cysteines of the active site are shown as sticks.

Since the redox free energy is a state function, it is independent of the reaction path. Therefore, we expect optimized geometries of the initial state, which in our case is the oxidized state, and of the final state (the reduced state) to provide the free energy through an arbitrary path. In our FEC, the parameter λ switches the system in an alchemical transformation from the oxidized to the reduced state (see Section 2.3). Thereby, the Hamiltonian of the disulfide bonded state is exchanged by that of the open state. When a bond shall be opened, not only the force constant of the bond itself has to be set to zero. Also, angles and dihedrals that enclose the bond disappear. Furthermore, whenever a bond exists, non-bonded interactions are excluded. Therefore, in order to open a bond, they need to be introduced again. This represents a challenge in the setup of the free energy calculations, which will be detailed in Section 4.2.1.

4.2 Setup of Thioredoxin Free Energy Calculations

4.2.1 Simulation Setup

All Molecular Dynamics (MD) simulations were carried out using the GROMACS 4.5.5 package (48). For the wild-type *E. coli* Trx, solution NMR structures of the oxidized and reduced form are available (pdb entry: 1XOA and XOB, respectively) (93). For the wild-type and its mutants, P31S and P31T, of *S. aureus* Trx, X-ray structures were available (pdb entries: 2O7K, 2O85, 2O87 (86), respectively. The *S. aureus* wild-type and its mutants were missing residues 1 to 3, which is why the mutations refer to residue 31 instead of residue 34. The *E. coli* mutants P34A, P34D and P34K were modeled through homology modeling from 1XOA, using the Molecular Operating Environment software (MOE 2008.10; Chemical Computing Group, Quebec, Canada).

The protein was solvated in a box of explicit water of TIP3P (70). The box was large enough to allow a 1.2 nm distance in all directions. A salt concentration of 0.1 mol/l was chosen to mimic physiological conditions, resulting in approximately 5500 water molecules and, depending on the mutant, 15 to 17 sodium and eleven chloride ions. Thereby, the system was neutralized. We added a dummy atom, named HUD, of the mass of a hydrogen atom and connected it to the sulphur atom of the cysteine residue. It will later be transformed into the proton of the open cysteine. The atoms that experience transformations of their Hamiltonian are the C_β, the S and the HUD atom. Each of them is additionally represented by another virtual site of mass zero (see Section 4.2.3 for details).

4.2.2 Simulation Details

First, the system was energy minimized using the steepest descent algorithm. We used the CHARMM27 force field to which we added an additional residue, we here refer to as CYD, see Section 4.2.3 for details. Next, the water was equilibrated while the motion of the heavy atoms of the protein was restrained with a potential of 1000 kJ/mol at 300 K for 100 ps. Then, we released the position restraints and equilibrated for 15 ns at $\lambda = 0$. The temperature was controlled using velocity rescaling (94), the time step for temperature coupling was chosen as 0.4 ps. Protein and solvent were seperately coupled to the thermostat. The pressure was kept at 1 bar, using isotropic pressure coupling via the Parrinello-Rahman barostat and a coupling constant of 1.0 ps. We started each

simulation with a random set of velocities. The Lincs constraint (95) was used on all bonds containing a hydrogen atom or the dummy that was to be transformed into a hydrogen. Hydrogen atoms are recognized by GROMACS due to their starting letter, H. Therefore we named the dummy atom HUD. Non-bonded interactions were calculated within a cut-off of 1.0 nm. Electrostatic interactions beyond 1.0 nm were treated with Particle-Mesh Ewald (75) with a grid spacing of 0.12 nm. We used a time step of 2 fs and periodic boundary conditions for all simulations.

From the 15 ns equilibration, we used 15 configurations, one every nanosecond, starting from 1 ns. From each of these 15 starting structures, we initiated 10 independent *Fast Growth* thermodynamic integration (FGTI) simulations with a different set of starting velocities, resulting in 150 independent transformation simulations. The transformation time τ was chosen as 500 ps, λ was changed with every simulation step, resulting in $\Delta\lambda = 4 \cdot 10^{-6}$ per step. Instead of using pressure coupling, we here work with a canonical ensemble, to yield a free energy from the transformation. Non-bonded interactions were calculated within a cut-off of 1.3 nm. Electrostatic interactions beyond 1.0 nm were treated with Particle-Mesh Ewald (96) with a grid spacing of 0.12 nm. All remaining parameters were the same as for the equilibration at $\lambda = 0$.

For each of the $\lambda_{0\to1}$ transformations, we also performed a backward simulation, $\lambda_{1\to0}$, starting from the final snapshot. The same parameters as for the forward transformation were used. Here, λ started at 1 and $\Delta\lambda = -4 \cdot 10^{-6}$. We further sampled the open state ($\lambda = 1$) for 15 ns, using the same parameters as for $\lambda = 0$.

4.2.3 Transformation Details

In addition to the standard topologies of free cysteine (CYS) and disulfide bonded cysteine (CYS2), we introduced an additional cysteine residue type, which is a copy of CYS2. We expanded it by one atom and three virtual sites (vs), and refer to it as CYD. The atom, a dummy of mass of 1.008 a.u. according to the hydrogen mass, is bonded to the sulphur. We named it HUD, as it will be transformed into the hydrogen atom. The three remaining virtual sites are located at the same positions as the C_β, S and the HUD, respectively. Virtual sites are constructed such that their position is determined by a bond from the original CYS2 residue. Figure 4.2 shows the atoms and virtual sites, including the transformed atoms and C_α. The upper level topology (with continous bonds) shows the atoms. They have full Lennard-Jones and Coulomb potential in the

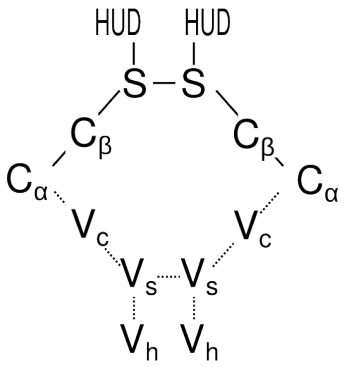

Figure 4.2: **Scheme of the CYD residue** - The residue CYD is a copy of the CYS2 residue, expanded by one atom, HUD - that will be transformed into a hydrogen - and three virtual sites, V_c, V_s and V_h, that are located in the same positions as C_β, S and HUD, respectively. Here, the virtual sites have not been superimposed onto their respective atoms for clarity.

$\lambda = 0$ state, as detailed below. The lower level (dotted bonds) shows the virtual sites that are in exactly the same position as the atoms on top of them. Their Coulombic potential is zero at $\lambda = 0$ and will be switched on in the course of the transformation. For the $\lambda = 1$ state, they serve to describe the Lennard-Jones potentials of atoms that are bonded in the initial state. A virtual site is not bonded, only its position is fixed to the atom it represents. Table 4.1 shows which virtual site is positioned by which atom.

virtual site	atom 1	atom 2	on top of
V_c	C_α	C_β	C_β
V_s	C_β	S	S
V_h	S	HUD	HUD

Table 4.1: Construction of the virtual sites. The position of each virtual site is controlled by two atoms, atom 1 and atom 2.

In the CHARMM27 force field used here, atoms connected by less than three bonds do not interact via non-bonded interactions. Thus, for a disulfide bond, the two sulphur atoms do not "see" each other's charges nor is there any Lennard-Jones potential between them. Once the bond is removed, these interactions are necessary to correctly simulate the open state. Within GROMACS, Lennard-Jones potentials can be controlled via a list (the so-called pair-list), and in this way can be switched on from zero in the oxidized state ($\lambda = 0$) to full Lennard-Jones interactions in the reduced state ($\lambda = 1$). However, any interaction added to the pair list will also introduce a Coulombic interaction between the atoms that is only dependent on the charge of the atom and thus

particle	$\lambda = 0$	$\lambda = 1$
C_β atom	-0.1	0
C_β virtual site	0	-0.11
S atom	-0.08	0
S virtual site	0	-0.23
HUD atom	0	0
HUD virtual site	0	0.16

Table 4.2: Partial charges of transformed particles to correctly take the Coulombic interactions of the oxidized ($\lambda = 0$) and reduced states ($\lambda = 1$) into account.

cannot be tuned through this list.

For example, transforming a Lennard-Jones potential of zero between two connected sulphur atoms ($\lambda = 0$) to a non-zero Lennard Jones potential of two sulphur atoms in cysteine thiols ($\lambda = 1$) also adds a non-zero Coulomb potential between the two sulphur atoms even at $\lambda = 0$. At this oxidized state, however, the two directely bonded atoms should not interact electrostatically. On the other hand, setting the charge of sulphur to zero for the $\lambda = 0$ state would also set all its other Coulomb interactions, for example those with the neighbored residue, to zero and thus would introduce errors, too.

How can one switch on non-bonded interactions between the cleaving residues without introducing errors into the closed structure? This is where the virtual sites come into play. We added a pair of one sulphur atom and one sulphur virtual site to the pair list. At $\lambda = 0$, the Lennard-Jones potential is zero, the charge is non-zero. At $\lambda = 1$, the Lennard-Jones potential is switched on, the charge is switched off. Instead, the charge of the virtual site on sulphur changes from zero (at $\lambda = 0$) to -0.23 (at $\lambda = 1$) (see Table 4.2). Charges derive from CYS and CYS2.

Virtual sites, however, involve another complexity to be aware of. The virtual sites on the sulphur atoms interact via short-range Coulomb interactions as they are not connected via bonds. Adding this interaction to the pair list would create an additional Coulomb interaction and thus introduce an error. Thus, by adding the pair $S_{atom} - S_{vs}$ to the pair list, no Coulomb potential is added for that pair.

We proceed equivalently for C_β and HUD. See Table 4.2 for details. By setting the charge of the sulphur atoms to zero, also the Coulomb interaction between the nitrogen atom in the backbone and the sulphur atom disappears. The nitrogen and the

sulphur atom are separated by three bonds (compare Figure 4.3), the kind of interaction typically controlled via the pair list. The interaction between the atoms is thus present, the Lennard-Jones potential available for both $\lambda = 0$ and $\lambda = 1$. Only the Coulomb interaction for the open state is missing. We therefore add the $N_{atom} - S_{vs}$ pair to the pair list, set the Lennard-Jones potential to zero for both closed and open state (it is already available) and thus have added the missing Coulomb interaction.

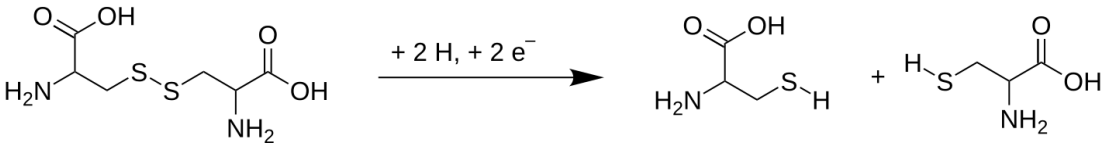

Figure 4.3: **Cystine reduction** - Scheme of the reduction of cystine to two cysteines.

Table 4.3 summarizes all interactions that were added to the pair list. We note that for some interactions such as the C_α-HS' interaction, between C_α of one cysteine and the HS atom of the other cysteine, the Lennard-Jones potential of the 1,4 interaction (in case of the closed state) is different to the one of the open state. The same exclusions were used for virtual sites as for the atoms that they represent.

We also tried to calculate the free energy by using snapshots from the open structure equilibrated at $\lambda = 1$. We find the energies of the backwards simulations to be largely shifted, thereby abrogating the overlap of the work distributions.

4.2.4 The Oxidized State

One of the main conditions for an FEC to be successful is the end points being correctly represented (52). We therefore tested our initial and target structure upon their quality to reproduce the oxidized and reduced state that they represent, respectively. For the initial state, we chose the oxidized state, for which $\lambda = 0$. Even though virtual sites have been introduced into the standard CHARMM27 force field (see Section 4.2.3) the disulfide bond is closed. No non-bonded interactions shall be found between the two sulphur atoms nor between either of the two sulphur atoms to either of the adjacent C_β-atoms. A simulation at $\lambda = 0$ should sample the same configurational space as a simulation of the oxidized species using the standard CHARMM topology. We here use the Trx of *E. coli*, for which NMR structures of both the oxidized and the reduced species are known, and compare the CYS-CYS bonded interactions, as these will be

particle 1	particle 2	$\lambda = 0$	$\lambda = 1$
C_α1	S2	1,4 potential	open state
C_α1	S$\underline{H}$1 dummy	off	on
C_β1	C_β2	1,4 potential	open state
$C_\beta\underline{H}$1 (two)	S2	1,4 potential	open state
$C_\beta\underline{H}$1 (two)	S$\underline{H}$1 dummy	off	on
C_β1	S2 dummy	off	on
S1	S2 dummy	off	on
$C_\beta\underline{H}$1 (two)	S$\underline{H}$2 dummy	off	on
S1	C_β dummy	off	on
S1	C_α2	1,4 potential	open state
C_α2	S$\underline{H}$2 dummy	off	on
S1	$C_\beta\underline{H}$2 (two)	1,4 potential	open state
C_β1	S$\underline{H}$2 dummy	off	on
S1	S$\underline{H}$2 dummy	off	on
C_β2	S$\underline{H}$2 dummy	off	on
S2	S$\underline{H}$1 dummy	off	on
S$\underline{H}$1 dummy	S$\underline{H}$2 dummy	off	on
$\underline{H}$N	C_β dummy	off	off
N	S dummy	off	off
C_β dummy	O	off	off
$C_\alpha\underline{H}$	S dummy	off	off
S dummy	C_{backbone}	off	off

Table 4.3: Lennard-Jones interactions between transformed atoms and the remaining residue. In some cases, GROMACS uses different potentials for non-bonded interactions separated by exactly three bonds, i.e. between the atoms 1 and 4, here referred to as 1,4 interaction, and short-range interactions between atoms separated by more than three bonds. To emphasize which value has been used, we here refer to the value of the latter as open state.

changed during the non-equilibrium transformation. They include the sulphur-sulphur bond length, the adjacent angles and dihedrals and also the non-bonded energy between the two cysteine residues.

We here show the distribution of all relevant structural parameters that define the bonded state and will be transformed upon bond opening. We compare the data from

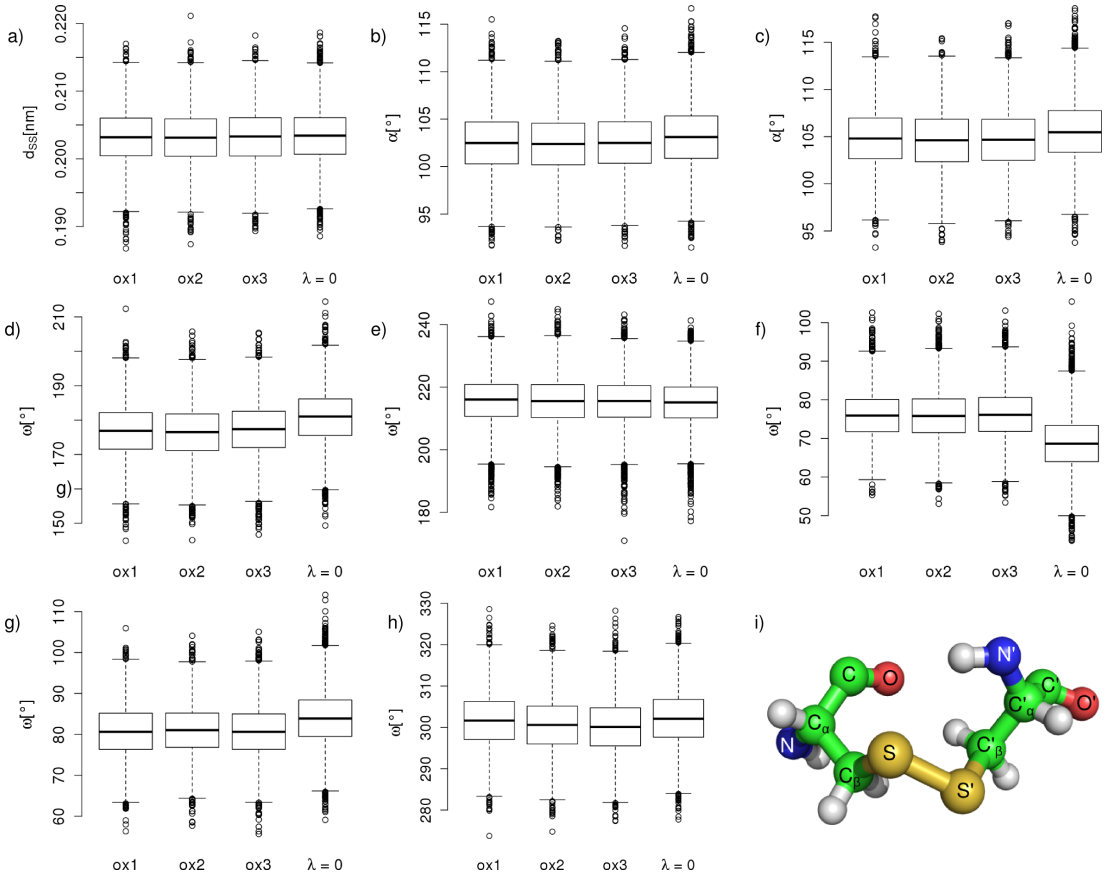

Figure 4.4: **Structural validation of the $\lambda = 0$ state** - We here compare the initial state ($\lambda = 0$) to the closed disulfide structure of *E. coli* Trx sampled by a standard topology (ox1, ox2 and ox3 from three independent MD simulations). We consider disulfide bond length, angles and dihedrals in the oxidized state. a) disulfide bond length, b) $C_\beta SS'$ angle, c) $SS'C_\beta'$ angle, d) dihedral along $NC_\alpha C_\beta S$, e) dihedral along $C_\alpha C_\beta SS'$, f) dihedral along $C_\beta SS'C_\beta'$, g) dihedral along $SS'C_\beta C_\alpha'$, h) dihedral along $S'C_\beta' C_\alpha' N'$, i) oxidized state with labels given in (a - h).

the $\lambda = 0$ state using a modified topology with virtual sites (Section 4.2.3) to the corresponding values of three independent simulations of the oxidized state which uses its default topology. We find a large overlap of the distributions for all parameters observed with the $\lambda = 0$ ensembles varying within the range sampled by the ox1, ox2 and ox3 simulations, which here serve as a reference. The disulfide bond length and the angles barely differ from the reference structures ox1 to ox3 (Figure 4.4 a-c). Among the dihedral angles, $C_\alpha C_\beta SS$' (Figure 4.4 e) is the only one uneffected by the introduction of virtual sites into the topology. The S'C_β'C_α'N' dihedral shows fluctuations from one simulation to another, with $\lambda = 0$ being in good agreement only with ox1 (Figure 4.4 h). The remaining mean values of the dihedrals differ by five to ten degrees. We suspect these differences to derive from the weight of the dummy atoms attached to the sulphur atoms that will be changed into a hydrogen in the course of the reduction. We conclude that the overall conformational space of the cystine in *E. coli* Trx is largely unaffected by our topological modifications to the topology of the oxidized state as required for the subsequent FECs.

Furthermore, a correctly parameterized $\lambda = 0$ state should provide the same energies between the two connected cysteine groups as the closed state described with the default topology. To test this, we calculated the non-bonded interactions between the two cystine groups in the $\lambda = 0$ state. From the $\lambda = 0$ trajectory, for comparison, we also calculated the energies that result when using the default closed structure topology. We note that to this end, it is necessary to rewrite the trajectory of the $\lambda = 0$ equilibration without any dummy atoms and to calculate interaction energies from it with closed structure parameters. We further checked the non-bonded interactions within each cysteine. For all Coulomb and Lennard-Jones interaction energies we obtain identical values (within the precision of the calculations) and conclude that our $\lambda = 0$ topology reliably describes the oxidized state.

4.2.5 The Reduced State

Reducing a disulfide bond results in two thiols, in our case in two cysteine residues. Two hydrogen atoms have been introduced in the course of the reduction (where dummies have served as placeholders in the oxidized state). The disulfide bond was taken away, i.e. the force constant of the disulfide bond and both adjacent $C_\beta SS$ angles have been transformed to zero and non-bonded interactions between the two cysteine residues are

now switched on. To evaluate the quality of the description of the $\lambda = 1$ state, we again compare our equilibration simulation to three independent simulations of the crystal structure, in this case of the reduced structure using the default topology without any virtual sites. We compare the sulphur-sulphur distance, the adjacent $C_\alpha C_\beta S$ angles (Figure 4.5 a - c) and the $NC_\alpha CN'$ dihedrals (e - h) along the backbone from one cysteine residue through the two linking residues to the second cysteine residue and also both NCCS-dihedrals (d and i). We find the $\lambda = 1$ state to well reproduce the reduced structure.

As for the oxidized state, we also compare the non-bonded energies between the two residues to the non-bonded energies they have when modeled with the default topology of the open structure. To this end, we again rewrite the trajectory of $\lambda = 1$ without any dummy atoms (compare Section 4.2.3 for details) and calculate the energies for every conformation within the trajectory according to the default topology created for the NMR structure. GROMACS calculates two terms of non-bonded interactions: 1,4-interactions for atoms that are separated by three bonds, and short-range interactions that are found at distances within a certain cut-off, and additionally are separated by more than three bonds. The sum of 1,4- and short-range interactions for both Coulomb and Lennard-Jones interactions in our $\lambda = 1$ state is the same as the energies resulting from the same trajectory using the default topology. Our comparisons also confirm the reduced state to be correctly parameterized at $\lambda = 1$ with the virtual site approach described in Section 4.2.3.

4.2.6 Thermodynamic Cycle

Keeping structural changes to a minimum in the course of a FEC ensures better results as the system is likely to be closer to equilibrium. Thus, in our first approach, we set up a thermodynamic cycle (compare Eq. 4.1 and Section 2.3.5) in order to allow the system to adjust more slowly and therefore more accurately to the transformation. As an intermediate, we introduced a structure with one protonated cysteine, and the other one remaining a negatively charged thiolate. Such a residue did not yet exist in our force field. Therefore we added the residue, hereafter called CYD^-. Charges for cystine and the cystine thiolate have been taken from ADF charge calculations by Swart *et al.* (97). We here calculated the charge differences and adjusted CYD^- accordingly

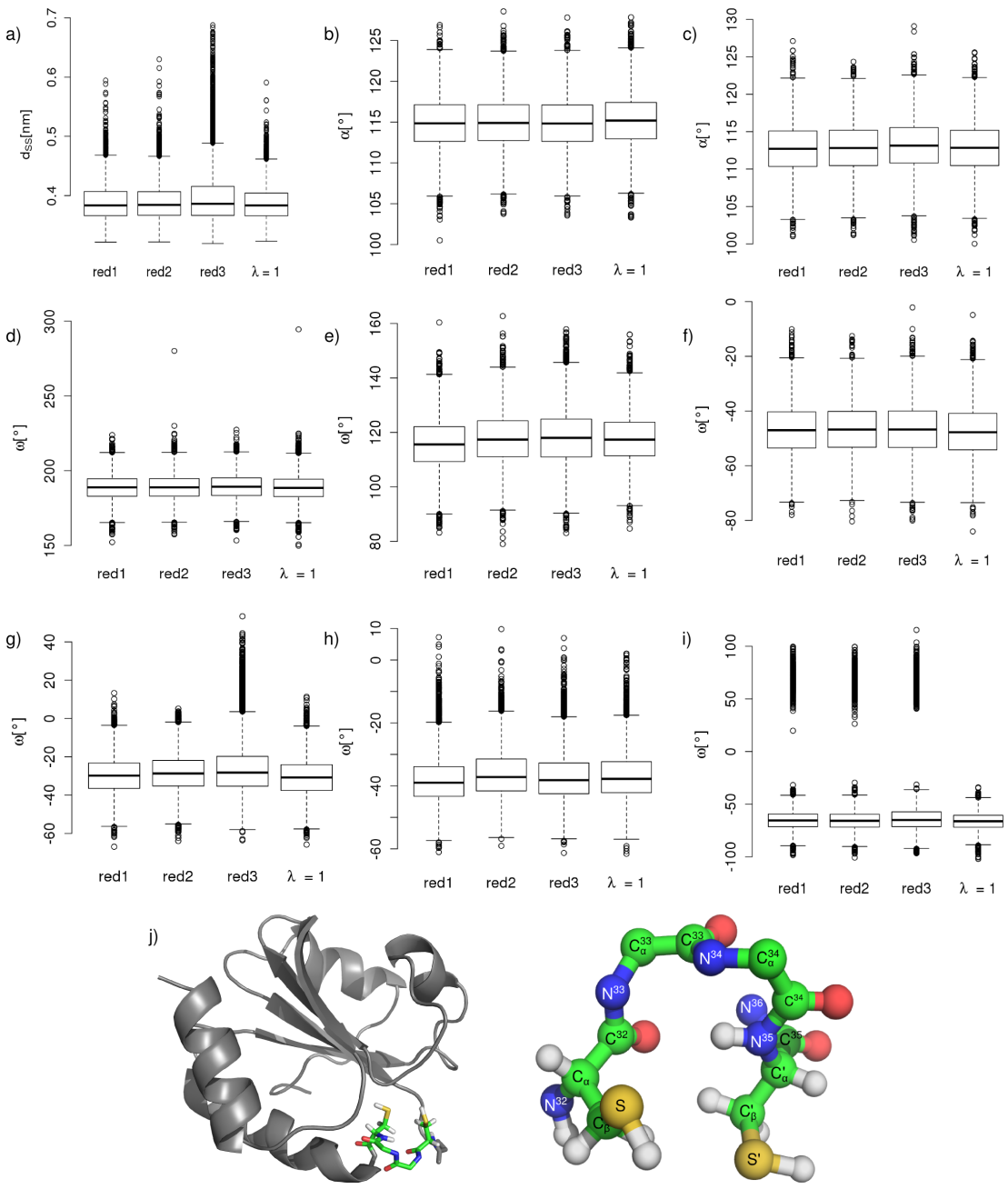

Figure 4.5: **Structural validation of the $\lambda = 1$ state** - We here compare the final state ($\lambda = 1$) to the open dithiol structure of *E. coli* Trx sampled by a standard topology (red1, red2 and red3 from three independent MD simulations.) We compare a) the distance between the two sulphur atoms that are now no longer bonded, and angles and dihedrals in their close vicinity. b) $C_\alpha C_\beta S$ angle, c) C_α'C_β'S' angle, d) dihedral along $N^{32}C_\alpha C_\beta S$, e) dihedral along the backbone $N^{32}C_\alpha C^{32}N^{33}$, f) dihedral along $N^{33}C_\alpha^{33}C^{33}N^{34}$, g) dihedral along $N^{34}C_\alpha^{34}C^{34}N^{35}$, h) dihedral along $N^{35}C_\alpha$'$C^{35}N^{36}$, i) dihedral $N^{35}C_\alpha$'C_β'S', j) reduced state with labels given in (a - h). The reactive site, *CPGC*, is shown with sidechains only for the two cysteines for clarity.

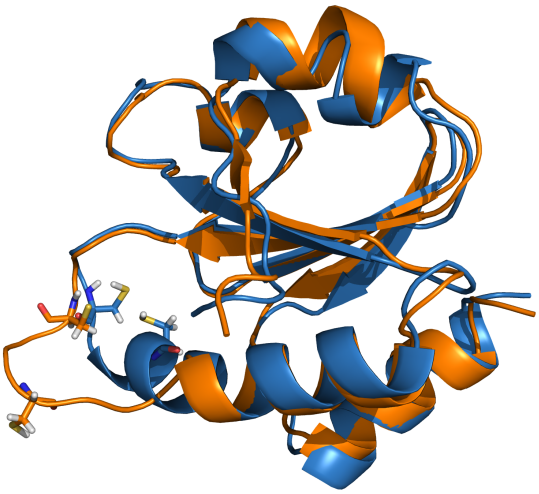

Figure 4.6: **Putative thiolate intermediate of reduced *E. coli* Trx as compared to the doubly protonated form** - We here compare the native, doubly protonated reduced structure (blue) to the structure of the reduced state with only one of the cysteines protonated (orange). The two residues between the cysteine residues are part of an α-helix, independently of the redox state of the cysteines. However, the helix unravels if one of the residues is a thiolate.

in our force field. To balance the appearing charge upon introducing CYD^-, we further added a dummy atom that we simultaneously transformed into a sodium cation.

$$\begin{array}{ccc} S-S & \xrightarrow{H^+ + 2e^- + Na^+} & S^- + S-H + Na^+ \\ \downarrow{\scriptstyle H^+ + 2e^- + Na^+} & & \downarrow{\scriptstyle H^+ - Na^+} \\ H-S+S^- + Na^+ & \xrightarrow{H^+ - Na^+} & HS + SH \end{array} \tag{4.1}$$

Here, we used the reduced state as the reference state and transformed it to the mono protonated state. We find the mono protonated state to be very unstable as compared to both the oxidized protein with the closed bond and the doubly protonated cysteine. We show the structure of the mono-protonated structure compared to the doubly protonated structure in Figure 4.6.

Both, for the oxidized and fully protonated state, the residues close the cysteines form an α-helix. Only for the anionic thiolate intermediate, this secondary structure is destroyed. We assume that the additional charge destabilizes the protein. Given the large distortion in the intermediate, we hereafter directly transform the disulfide bond into the doubly protonated state to keep structural changes as small as possible, thereby minimizing the space of free energy landscape that remains to be sampled.

4.2.7 Redox Potentials from Crooks Gaussian Intersection Method

The aim here is the calculation of redox potentials for *E. coli* and *S. aureus* Trx and some mutants. To this end, we prepared simulation systems and topologies which allow a transformation from the oxidized to their reduced states and back using FEC. This section describes the FEC. We chose a non-equilibrium CGI method as described in Section 2.3.4.1. To this end, we performed FGTI of each of the Trx wild-type and mutants for both the opening and closing process of the disulfide bond. The mechanical work of the switching process is obtained from $W = \int_0^1 \frac{\delta H(p,R,\lambda)}{\delta\lambda}\delta\lambda$. According to Jarzynski (98), the free energy ΔA is the work for which $\mathrm{P_f(W)} = \mathrm{P_r(-W)}$, i.e. the intersection point of the two work distributions. We calculated the latter from the distribution of forward and backward work, following Equation 2.30. In this way, we successfully calculated the redox potentials of three out of four mutants of *E. coli* and two out of three mutants for *S. aureus* Trx (see Figure 4.7 a and b, respectively). Though shifted in absolute numbers, we predict redox potentials for the three *E. coli* mutants which correlate strongly with measured values ($\mathrm{E_{redox}}$ in the range of -254 to -240 mV). A strong disagreement between experiment and our calculations is found for the wild-type (at an experimental value of -270 mV) for which a different reduction mechanism has been predicted (see Sec. 4.3 for further discussion).

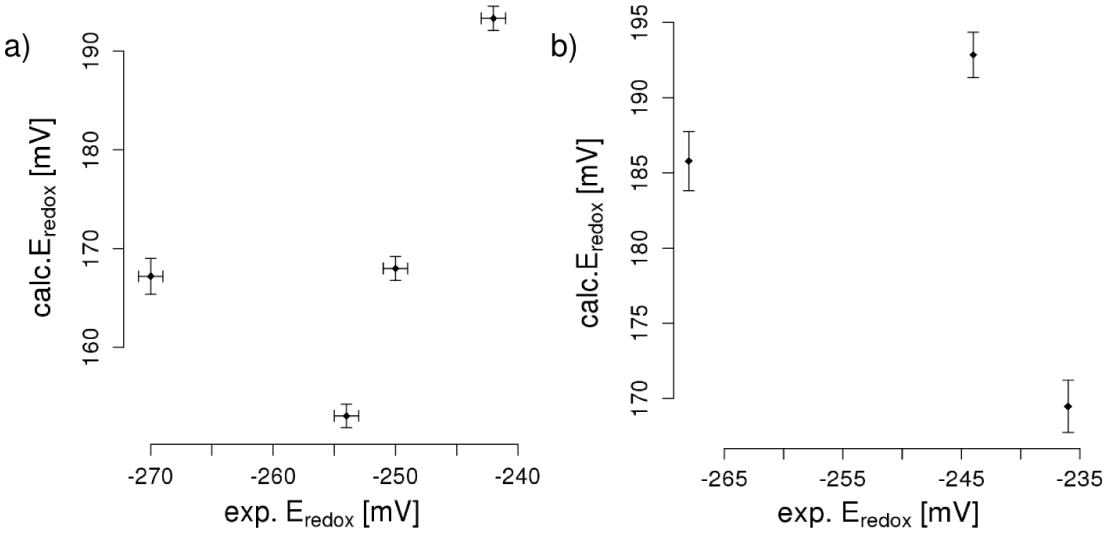

Figure 4.7: **Calculated versus experimental redox potentials** - We calculated the redox potentials for a) *E. coli* Trx wild-type and three of its mutants and for b) *S. aureus* Trx wild-type and two of its mutants. Error bars represent the s.e.m.

For *S. aureus* Trx, it is the P31T mutant (at an experimental redox potential of -236 mV) relative to the other two proteins (wild-type and P31S), for which we underestimate the redox potential. A reason for this might be the larger spread of backwards work distribution as compared to the other mutants, as further discussed in Section 4.3.

To obtain the results shown in Figure 4.7, we used 15 different input structures from each of which we started ten FGTIs from $\lambda = 0$ to 1 within 500 ps. The final structures were transformed backwards, from $\lambda = 1$ to 0. Figure 4.8 a shows sample energy curves for forward and backward simulations. Integration of $\frac{\delta\mathcal{H}}{\delta\lambda}$ yields the work (compare Sec. 2.3.4). Our data thus comprises 150 work values for each oxidation and reduction. From 15 subgroups of each data set, we calculated 15 intersection points, which we averaged. The standard error of the mean (s.e.m.) of these 15 intersection points represents the error.

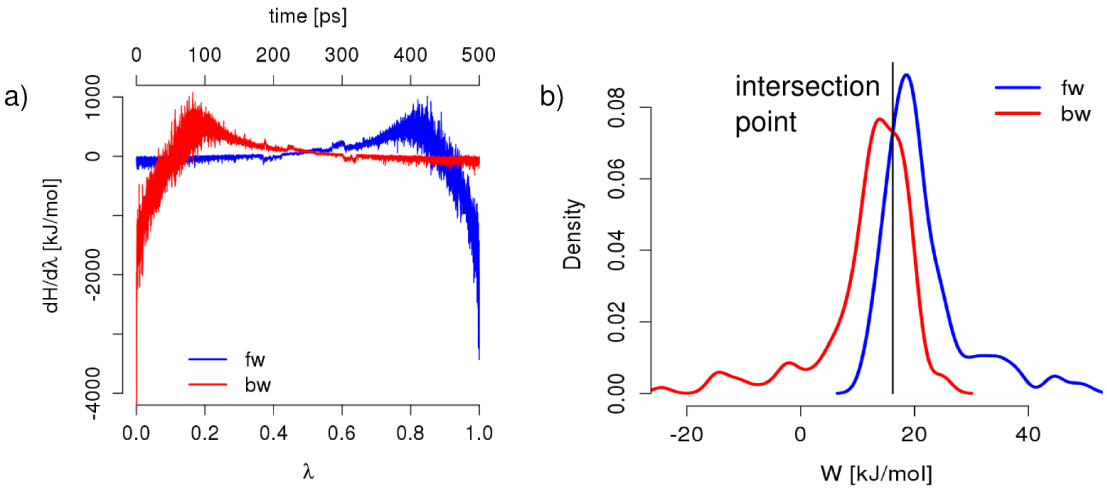

Figure 4.8: **Thermodynamic integration for reduction and oxidation transformation of wild-type *E. coli* Trx.** - a) Change of $d\mathcal{H}/d\lambda$ along the reaction coordinate λ for one forward (fw, reduction) and one backward (bw, oxidation) transformation within 500 ps, b) Work distribution obtained from 150 $d\mathcal{H}/d\lambda$ curves each for the forward and backward transformation.

4.2.8 Transformation Time

The transformation time and the number of samples play a crucial role in the accuracy of the redox potential calculated (58). We tested transformation times at $\tau = 80$, 200,

320 and 500 ps and sampling sizes from 50 to 150 samples for each forward and backward simulations. Figure 4.9 a shows the free energies obtained for forward and backward simulations at τ = 80, 200, 320 and 500 ps, respectively. The longer the simulation time, the larger the overlap of the interquartile range. The better the overlap of two simulations, the more accurate the calculated free energy, according to reference (58). In agreement to that, we find a large decrease in the error bars from τ = 80 ps to 500 ps. Additionally, from 200 to 500 ps the value of the calculated redox potential shows smaller changes and thus likely converges (Figure 4.9 b).

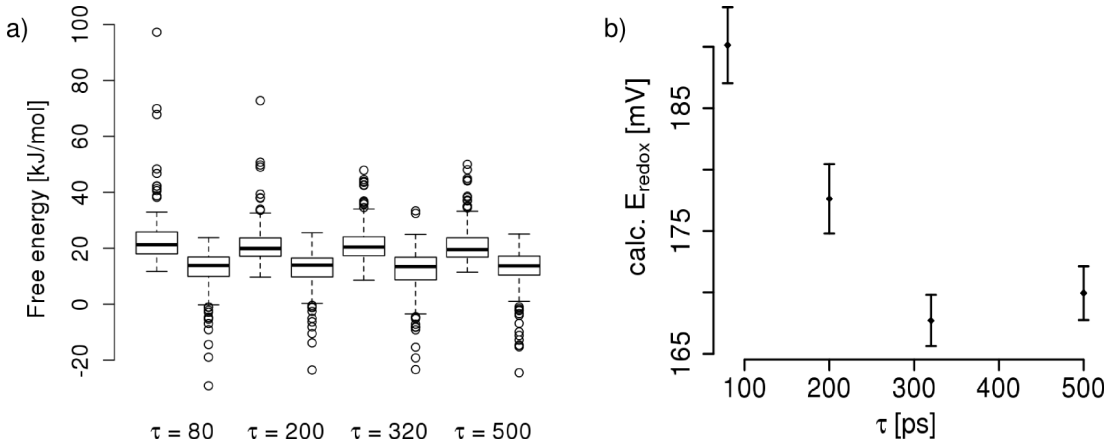

Figure 4.9: **Convergence of the calculated work value and the redox potential in dependence of** τ - a) Work distribution of the forward and backward transformation for τ = 80, 200, 320 and 500 ps, respectively. Longer transformation times lead to a larger overlap of forward and backward work distributions, b) resulting redox potentials for the transformation times shown in a). Error bars represent the s.e.m.

We also tested the influence of the size of our work data sets on the accuracy of our FEC by comparing standard deviations of subsets. We used subsets of the size of 50, 100 and 150 data points. We found a slight improvement of standard deviation between 50 and 100 data points, and no significant improvement from 100 to 150 data points, suggesting 100 data points, i.e. 100 TI runs to be sufficient. In the following, we show results from all 150 TI trajectories.

Another way to assess the quality of our calculations is the following. According to Crooks' fluctuation theorem (Eq. 2.26), the following equation should hold:

$$\ln \frac{P_f(W)}{P_r(-W)} = k_B T(W - \Delta A). \tag{4.2}$$

For a temperature of $T = 300\,\mathrm{K}$, $\beta = 1/k_B T = 0.4$. Equation 4.2 shows a linear dependency, which should be reproduced by a homogeneous data set. We use this condition to analyze our data and find a significant improvement with the transformation time τ. Figures 4.10 a - d show the according plots for $\tau = 80$, 200, 320 and 500 ps, respectively. The longer the transformation time, the better the linear fit. We further found the value of β to improve with τ, with an exception found for $\tau = 320\,\mathrm{ps}$.

β can be directly obtained from the slope of the graph. The intercept with the y-axis corresponds to $\beta \cdot \Delta F$. Our calculations underestimate β by $\sim 30\%$. If longer transformation times may improve this value and thereby the outcome of the calculated redox potentials remains to be elucidated.

4.3 Discussion, Summary and Outlook

We here calculated redox potentials from MD simulations through FECs. To the best of our knowledge, this is the first approach to open a covalent bond, using MM FECs. As a reference to the closed (λ =0) and the open (λ =1) state, we used three independent MD simulations of each the oxidized and reduced forms of Trx, respectively, that were derived from NMR structures. We compared the disulfide bond length, two angles and five dihedrals enclosing the disulfide bond. We find a large overlap for the interquartile range of all measurands, though the entire range is slightly shifted as compared to three independent simulations of the oxidized state for the angles and three of the dihedrals (compare Figure 4.4 b - d, f and g). This could derive from the mass of the dummy atom that exists to be transformed into a hydrogen. It is the standard procedure not to change masses in the course of FECs. Should the mass of the dummy atom be shown to be the source of the shifted angles and dihedrals, it would be recommendable to examine, if better results can be achieved by also changing the mass.

Comparison of the product state ($\lambda = 1$) to three independent simulations of the reduced structure showed no difference in average values nor in the distribution of the sulphur-sulphur distance, the angles nor the dihedrals. We find the direct transformation from the oxidized state to the doubly protonated fully reduced state to induce smaller structural changes than by usage of an intermediate state.

Using the CGI approach with FGTI, we were able to predict relative changes in redox potential for a subset of the mutants, suggesting an only limited accuracy due

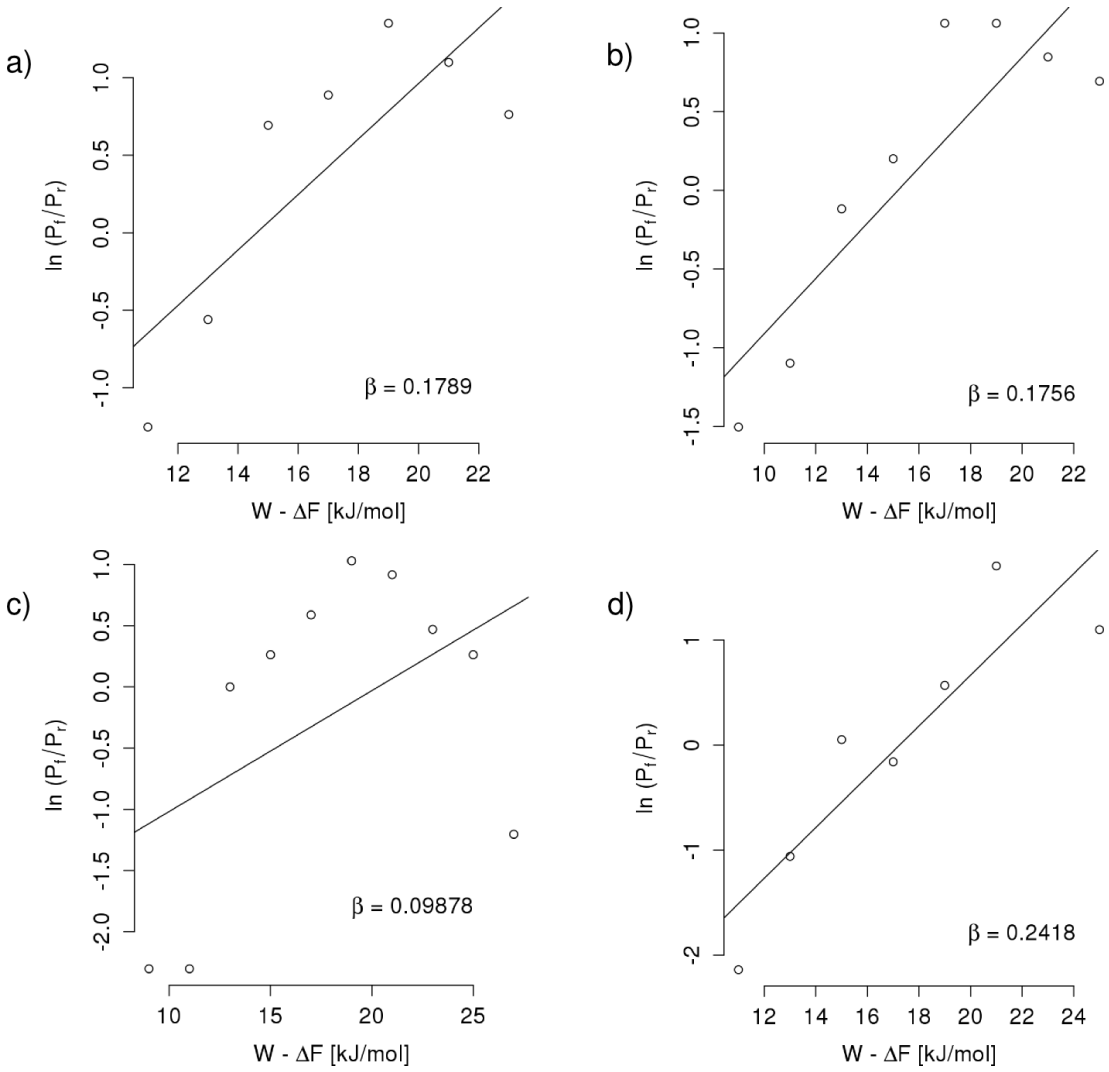

Figure 4.10: **Quantifying our data quality according to Crooks' Fluctuation Theorem** - For each energy distribution obtained with different transformation times, τ, we tested the probability density of free energies to satisfy CFT. a) $\tau = 80\,\text{ps}$, b) $\tau = 200\,\text{ps}$, c) $\tau = 320\,\text{ps}$, d) $\tau = 500\,\text{ps}$. β should equal $1/k_B\text{T} = 0.4$ and serves as a measure for the quality of the data.

to systematic or statistical errors. However, the order of magnitude in redox potentials covered in our simulations of $\sim 50\,\mathrm{mV}$ agrees well with the range probed experimentally ($\sim 30\,\mathrm{mV}$) for the seven proteins under investigation.

The electron rich indole ring of the proline in the wild-type is in close vicinity to the thiol. It has been discussed to possibly act as base, thereby assisting in deprotonating the thiol (86), and thus increasing its reducing power, which is reflected by its lower redox potential. This catalyzing effect is neglected by our approach, and another possible source of error.

Several tests indicate convergence of the transformation at $\tau = 500\,\mathrm{ps}$. Cross-valdation of the data is presented in Figure 4.10, however, did not yield correct values for $k_B T$. It is advisable to analyze, if longer transformation times lead to better agreement.

Overall, provided an improved accuracy by addressing these problems, this approach can be transferred to other bond breaking reactions, and thus can widen the field of MM FECs. A possible next step would be to apply the approach to other thiol-disulfide oxidoreductases such as DsbA. Just like Trx, the latter contains the *CXXC* motif as an active site, though redox potentials are in a completely different range. It would be desirable to reproduce and later also predict redox potentials for mutants containing more than a point mutation in the active site.

Further, such an approach could be used to study tensile disulfides, similar to what we have shown in Chapter 3 but for disulfides in different chemical surroundings.

5

Vicinal Disulfide Bond under Force

Investigations on redox potentials of disulfide bonds (Ch. 3 and 4) have shown that they are not only very sensitive to their chemical surroundings but also to mechanical force. Some cystines exist in unusual patterns which have been suggested to have a specific function, e.g. as regulators of the dynamic or mechanical reponse of a protein. The X-ray structure of the von Willebrand factor (vWF) A2 domain revealed a vicinal disulfide bond, a rare arrangement of two adjacent cysteine residues whose function has not been clarified yet. In this chapter, we focus on this vicinal disulfide bond and its potential to alter the vWF A2 function. We used Molecular Dynamics (MD) simulations to analyze the A2 domain's dynamics at ambient conditions and under a pulling force, with the vicinal cysteines forming either a disulfide bond or two thiols.

5.1 Vicinal Disulfide Bonds

The formation of a disulfide bond between two adjacent cysteine residues leads to a vicinal disulfide bond. Such disulfides are very rare motifs in proteins and functionally important where they occur (99). Their function has been shown to be manifold, ranging from controlling binding to protein activity (12, 13, 100) to redox-activated conformational switches (11). The X-ray structure of the vWF A2 domain revealed the existence of such a vicinal disulfide bond, but only speculative explanations have been reported to date (15, 16). The vWF is a multidomain protein that plays a central

role in hemostasis and thrombosis in the vascular system. The A2 domain is a shear-sensor domain that is involved in the process of hemostatically regulating the length of vWF (15). Unfolding of the domain by mechanical force controls cleavage of A2.

The vicinal disulfide bond occurs close to the C-terminus, between Cys^{1669} and Cys^{1670} at the C-terminus region which has been shown to be the first part that unfolds under external force (16). It induces a constrained turn of the backbone which is significantly different to the reduced nature of the cysteines (11). Together with the backbone of their residues, vicinal disulfides form a strained 8-membered ring. The peptide bond is constrained to an ω angle of $-152\,^\circ \pm 1$, in contrast to the ω angles in planar peptide bonds usually present in the backbone which occur at $180\,^\circ$ (*trans*) or at $0\,^\circ$ (*cis*) (15). This pronounced difference between the two redox states suggests the disulfide bond to act as redox switch, and to influence domain unfolding prior to the proteolysis by ADAMTS-13 (14, 16).

The vicinal cystine represents a rigid pattern that could provide resistance of the α6-helix against force, thereby influencing its unfolding behavior. Luken *et al.* observed that vWF A2 temperature induced unfolding requires significantly higher temperatures with the vicinal disulfide bond present as opposed to the open state (14). Here, we aim at understanding how the A2 domain unfolds under mechanical stress when the disulfide bond is reduced as opposed to the scenario of the closed bond, and thereby elucidate its function, by using MD simulations. Figure 5.1 shows the structure of the vWF A2 domain and the nomenclature of the structural elements that will be used from here onwards.

5.2 Von Willebrand Factor A2 Domain at Equilibrium

How does the presence of the vicinal disulfide bond induce differences in structure and dynamics of the vWF A2 domain? And do these differences lead to changes in the unfolding behavior? We started with a comparison of the oxidized and the reduced state of the domain under equilibrium conditions (when no external force is applied). Sampling over five independent trajectories for both, the oxidized and reduced state, each lasting 20 ns, revealed no significant changes in the global topology of the protein as seen in the number of hydrogen bonds (h-bonds) within the α6-helix and also between the α6-helix and the remaining part of the protein (Figure 5.1, Table 5.1). The root

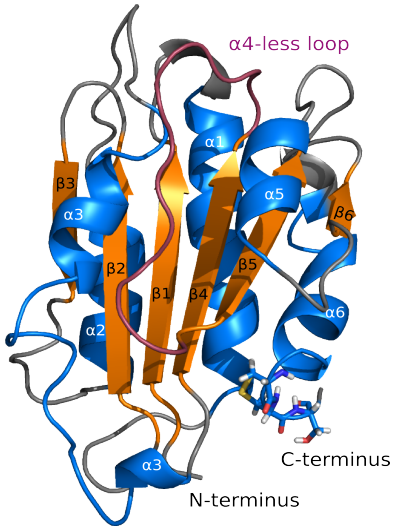

Figure 5.1: **Nomenclature of structural elements of the vWF A2 domain** - The von Willebrand factor A2 domain, derived by Zhang *et al.* (15), highlighting the vicinal disulfide bond (sticks) and the main secondary elements.

mean square deviation (RMSD) of the backbone atoms is marginally larger for the reduced state as compared to the oxidized state, the radius of gyration is identical for both redox states, thus not revealing any significant differences (Table 5.1). Thus, independent from the redox state, the vWF A2 domain is stable at ambient conditions.

Observation	oxidized	reduced
h-bonds within α6	7.54 ± 0.43	7.64 ± 0.49
h-bonds from α6 to the remaining domain	6.67 ± 0.06	6.24 ± 0.27
RMSD [nm]	0.14 ± 0.01	0.17 ± 0.004
radius of gyration [nm]	1.476 ± 0.001	1.482 ± 0.002

Table 5.1: Comparison of the stability of the oxidized and reduced state of the vWF A2 domain.

To detect local changes within the domain we carried out principle component analysis (PCA, see Section 2.1.1). The projection of the trajectories of the equilibrium simulations on the first eigenvector of the combined oxidized states show that the major contributions to the dynamics for both, the oxidized and reduced state, derive from the α6-helix with the vicinal disulfide, the α3-helix and the α4-less loop. Projecting the combined trajectories of all oxidized and reduced state simulations on the first two eigenvectors of the oxidized state shows similar collective motions for all but one of the oxidized trajectories (Figure 5.2). The remaining four equilibrium simulations show projections of the trajectories on the first two eigenvectors overlapping with all projec-

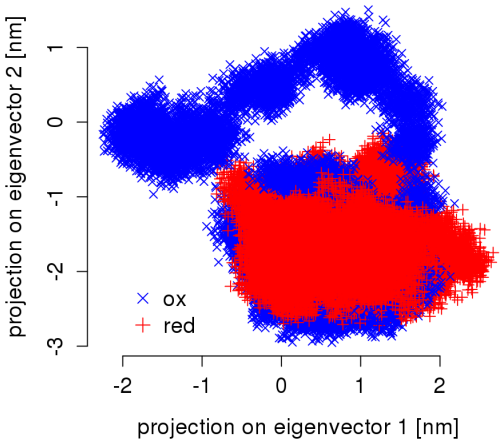

Figure 5.2: **Comparison of motion along eigenvectors** - Projection of the trajectories of the oxidized and reduced equilibrium simulations on the first two eigenvectors of the oxidized trajectory.

Eigenvector	%-age of motion
First	30 %
Second	11 %
Third	6 %
Fourth	4 %
Fifth	4 %

Table 5.2: Percentage of the first five eigenvectors of the overall motion.

tions of the reduced state. The outlier shows stronger motion of the three secondary structure elements mentioned above as compared to the other trajectories. The relevance of this exception to the stability against unfolding remains to be elucidated. The first two eigenvectors account for more than 40 % of the overall motion of the protein. The third and all following eigenvectors account for 6 % of the dynamics and less. The explicit values are listed in Table 5.2.

We conclude that the two redox states are equally stable and show only minor differences in their dynamics. To test if the two redox states respond differently to force, we next performed force-induced unfolding.

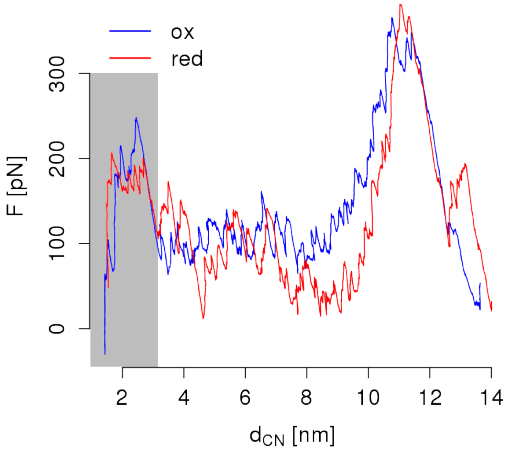

Figure 5.3: **Force profile for unfolding of the oxidized and reduced A2 domain** - The oxidized form ruptures at a slightly higher force than the reduced structure. We here show sliding averages over 200 frames in each point, for both d_{CN} and the force. The gray area indicates α6 unfolding.

5.3 Force probed unfolding of the A2 domain

Baldauf *et al.* have recently shown that the vWF A2 domain unfolds stepwise under pulling forces till the ADAMTS-13 cleavage site is exposed (16). A force acting on both the N- and C-terminus of the domain peels off the C-terminus step-wise, starting from the α6-helix that contains the vicinal disulfide bond we are interested in. We here performed force-probed MD simulations with the vicinal cysteines forming a disulfide bond in the first case and being reduced in the second case.

Figure 5.3 shows example force profiles for the oxidized (ox) and reduced (red) state in dependence on the end-to-end distance, d_{CN}. We find slightly higher rupture forces for the oxidized α6-helix detaching from the rest of the protein compared to the forces we observed for detaching the reduced α6-helix.

From five independent pulling simulations, we observe average rupture forces of 326 ± 6 and 301 ± 16 pN for the oxidized and reduced species, respectively. The oxidized α6-helix is stiffer, as predicted, thus detaches as a rigid body from the rest of the protein. The reduced structure allows the helix to peel off stepwise. Thus, slightly less force is needed. Figure 5.4 shows snapshots along the trajectory of the α-helix detaching from the rest of the protein. Starting at equal end-to-end distances, the oxidized and the reduced α6 helix induce different unfolding patterns. After 10 ns, when the end-to-end distance is at 3.42 ± 0.05 and 3.76 ± 0.07 nm for the oxidized and reduced state, respectively, the α6 helix remains fully folded and detaches as a rigid body, only if the disulfide bond is present. Without the disulfide bond the helix unravels step-wise. After

20 ns, the helix is entirely destroyed for the reduced case, while parts of it remain folded in the oxidized case. After 34 ns of pulling, the distance between N and C terminus was found at 9.29 ± 0.06 and 9.86 ± 0.26 with the disulfide open and closed, respectively. Thus, at equal pulling speed, the reduced species unfolds more easily.

We next asked how the vicinal disulfide bond influences the response to force of the isolated helix. To address this issue, we performed force-clamp simulations at constant forces, the results of which will be introduced in the next section.

5.3.1 Elongation of the A2 α6-helix

How does a vicinal disulfide bond change an α-helix' response to mechanical force? Berkemeier *et al.* recently reported on an α-helix linking two myomesin domains, that at low forces could unfold and refold again (101). The 24 residue long myomesin helix was stretched, using atomic force microscopy (AFM) and MD simulations. In a recent, more detailed study, Xiao *et al.* found a balance of un- and refolding of that same α-helix under constant forces of up to 15 pN (102). In analogy to these simulations, we performed force-clamp simulations of the isolated helix at 5, 10 and 20 and 30 pN and also compared it to the helix' dynamics at equilibrium conditions. We especially focussed on differences in presence and absence of the vicinal disulfide bond.

Without an external force, the isolated α6-helix has a strong tendency to coil, if the vicinal cysteines form a disulfide bond (Fig. 5.5). Apparently, the isolated helix is disturbed by the presence of the vicinal disulfide bond. However, the α6-helix is stabilized in the presence of the disulfide bond when packed onto the domain, as we did not observe this phenomenon for any of our equilibrium simulations (compare Section 5.2 and Fig. 5.1).

We analyzed the secondary structure for the helix in the oxidized (ox) and reduced (red) state under different forces. Even though we observed a coiling of the helix (Fig. 5.5 a), our analysis shows that the α6-helix remains intact around the central residues during our 5 ns simulation, for both redox states of the cysteines. The constant force pulling simulations were performed over 300 ns. For 5, 10, and 20 pN, we performed five independent simulations for each redox state. Here, we show representative secondary structure plots (103). Stretching at 30 pN has been modeled once for each redox state. At $F = 5$ pN large parts of the α-helix remain intact, though the oxidized state appears to be more stable. At 10 and 20 pN, the helix unfolds to a large

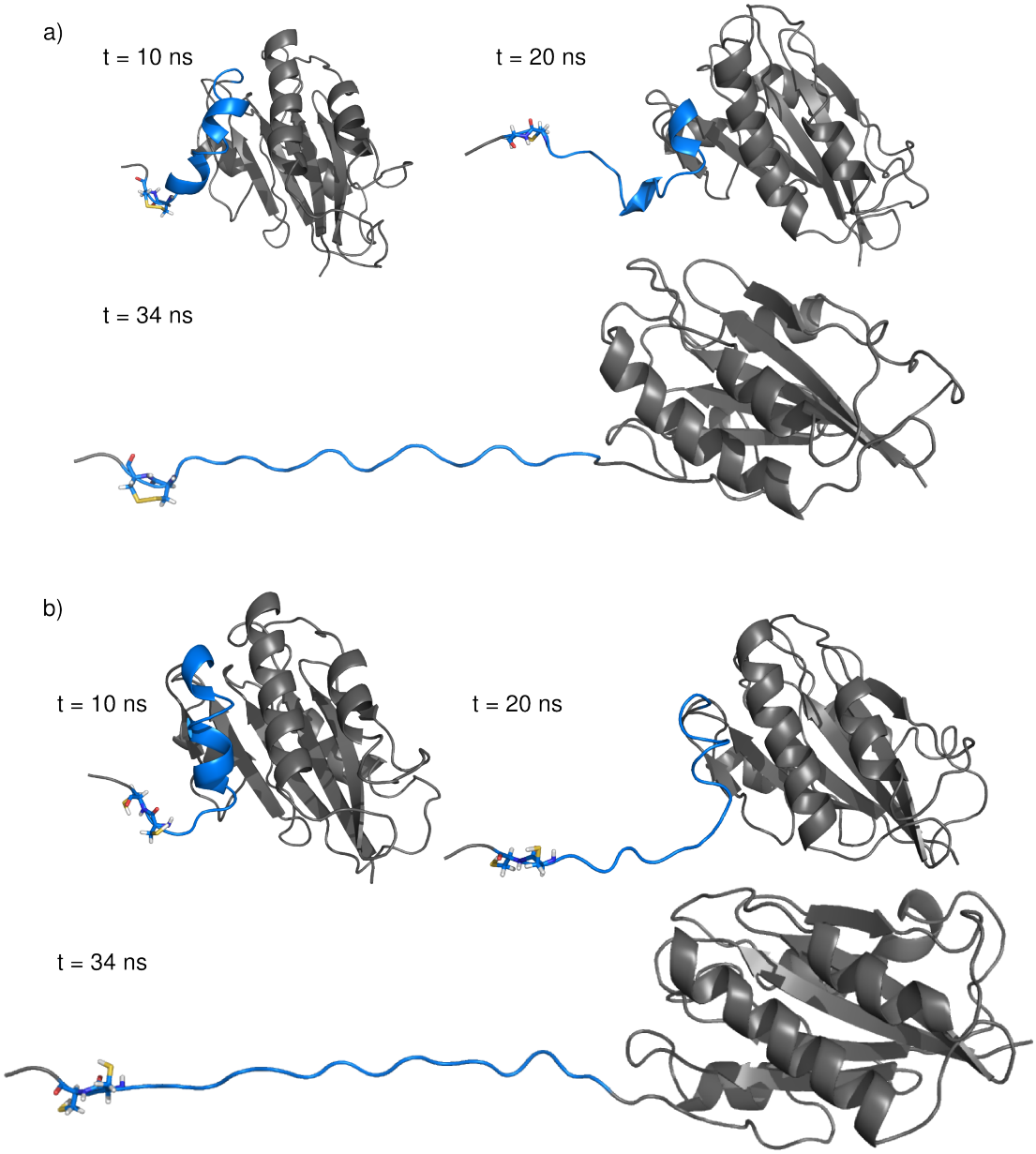

Figure 5.4: **Detaching of the α6-helix** - a) With the vicinal disulfide bond present, the α6-helix is pulled away from the protein core like a rigid body before starting to unravel, b) in absence of the vicinal disulfide bond, the helix detaches stepwise and unravels while detaching.

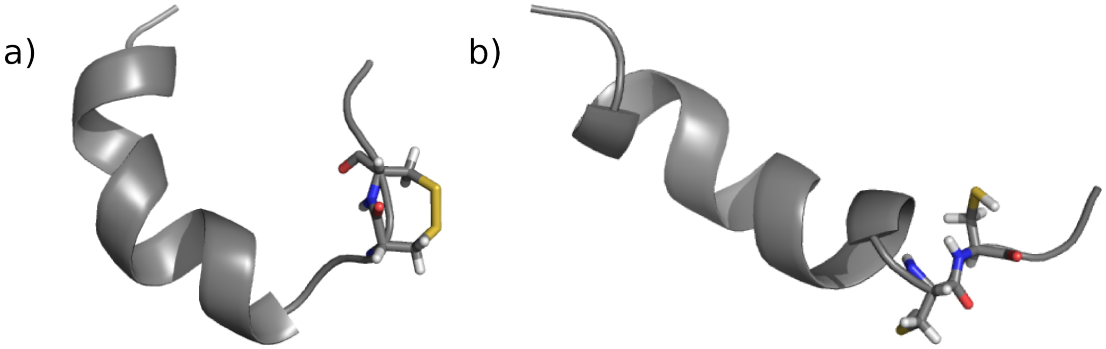

Figure 5.5: **α6-helix with and without vicinal disulfide bond** - a) With a vicinal disulfide bond present, the α6-helix shows a stronger tendency to coil at ambient conditions as compared to b) with the disulfide bond being open.

Force [pN]	d_{CN} (ox)	d_{CN} (red)
5	1.98 ± 0.13	2.11 ± 0.19
10	2.36 ± 0.11	3.22 ± 0.33
20	3.56 ± 0.20	3.55 ± 0.22
30	4.24	4.79

Table 5.3: α6-Helix stretching under low forces

extent and partly refolds. At 30 pN, no refolding could be observed, regardless of the redox state.

As a further measurement of unfolding and refolding, we measured the end-to-end distances of the α6-helix and counted in how many states it has been sampled. Packed in the protein, the 13 residue long helix has a length of approximately 2.2 nm. Under a small mechanical load, we find a similar average length. Table 5.3 shows all average helix lengths for $F = 5$, 10, 20 and 30 pN for the oxidized and reduced states. All data derive from the last 100 ns of the simulations, when the helix has equilibrated under force (Fig. 5.6). The average helix length, d_{CN}, grows quicker in absence of the disulfide bond than with the bond closed. One exception is found at 20 pN, where the oxidized and reduced state reveal identical average values for d_{CN}.

Comparison of the distributions of end-to-end distances at different forces reveals a more detailed picture (Fig. 5.7). At 5 pN, we observe two peaks for the helix with the vicinal disulfide bond (ox), while the length of the reduced helix shows a broad distribution. The larger peak of d_{CN} of the oxidized structure can be found at distances

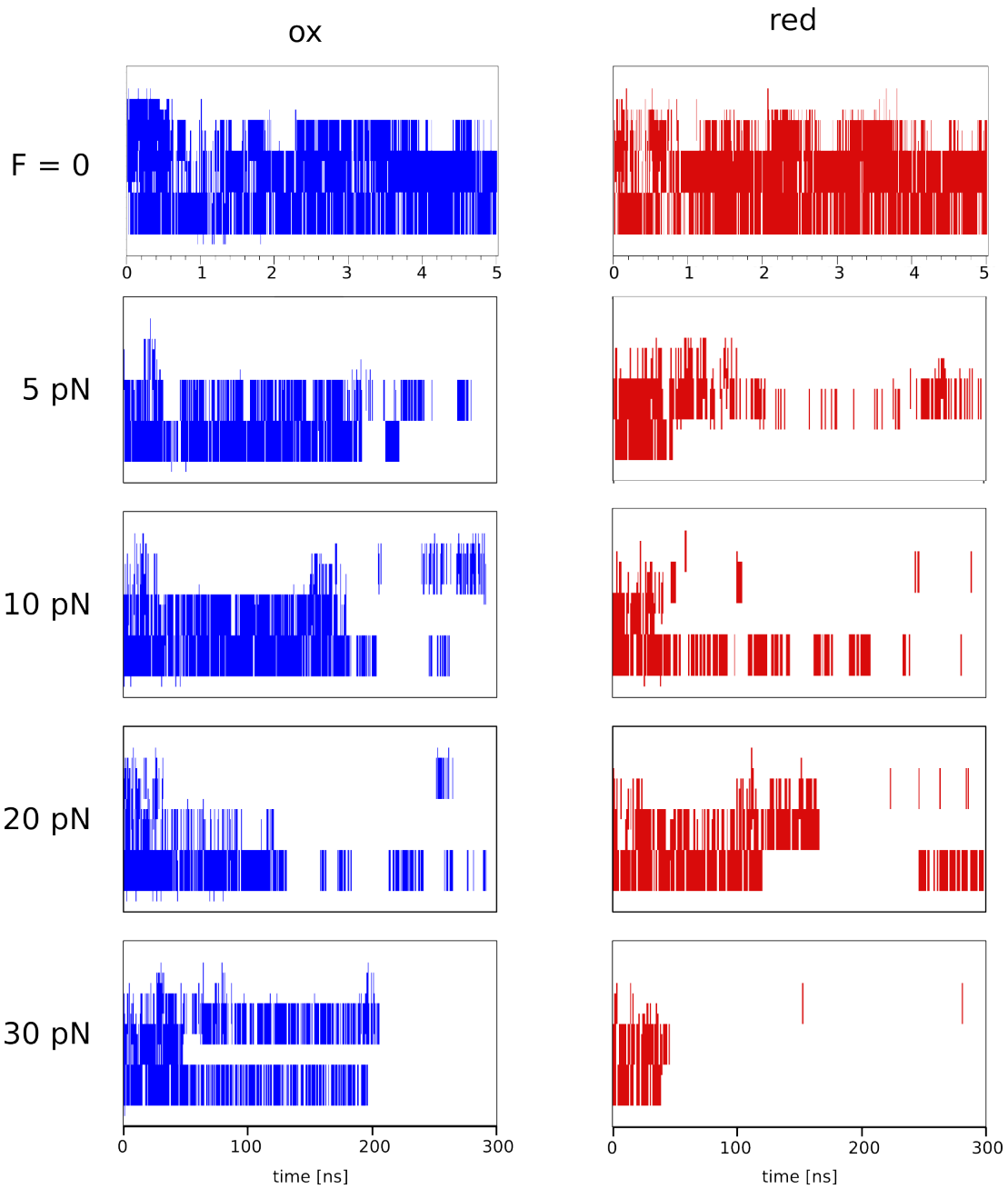

Figure 5.6: **α-Helicity of vWF A2 α6-helix under force** - Using the dssp program (103), we analyzed the un- and refolding of the α6-helix. At forces up to 20 pN, the unfolded helix can partly refold to an α-helix again. At 30 pN no refolding could be observed. We show representative samples for the oxidized (ox) and reduced (red) disulfide bond for $F = 5$, 10 and 20 pN. $F = 0$ and 30 pN have been sampled once.

slightly larger than 2 nm, a length matching the helix length within the A2 domain. Shorter distances derive from coiling that takes place in spite of the small force applied for both helices. The broader distribution of d_{CN} of the reduced state indicates a larger flexibility. At 10 pN, the reduced helix again shows a broader distribution than the oxidized one. Further, it is shifted towards higher end-to-end distances. At $F = 20$ pN, two broad peaks appear for the reduced state. Thus, the reduced helix preferably is in the fully folded or in the unfolded state but not in a semi-stretched state, as found for the oxidized helix. Though very different in their distribution, the resulting average length of the two states is equal. At 30 pN, d_{CN} shows a broad distribution for the oxidized state and a clear peak for the reduced state. Apparently, the reduced state is stretched more easily than the oxidized state.

We conclude that under small mechanical forces, the helix is unfolded more easily in absence of the disulfide bond. This observation is in line with the slightly lower rupture forces found for the unfolding of the reduced A2 domain.

5.4 Simulation Setup

All MD simulations were carried out using the GROMACS 4.5.5 simulation package (48). We used the X-ray structure of the vWF A2 domain (pdb code 3GXB) and controlled the redox state of the vicinal bond through the GROMACS program pdb2gmx. For equilibrium simulations, the protein was set in a box of TIP4P water allowing a distance of 1.2 nm in each direction. Pulling simulations of the A2 domain were performed using a box that was 15 nm in x-direction, along which the protein will be pulled apart. Thereby, we prevent interactions with itself through periodic boundary conditions (PBC). A salt concentration of 0.1 mol/l was chosen to mimic physiological conditions, resulting in 7659 water molecules, 34 sodium and 24 chloride ions in case of the equilibrium simulation. For pulling, the protein domain was surrounded by 19850 water molecules, 48 sodium and 38 chloride ions.

The isolated α6-helix was put in a smaller box, 5.3 nm in each direction, thereby preventing interactions with itself through PBC even if the helix rotates. It was solvated by 4798 water molecules, 10 sodium and 9 chloride ions. Thus for all simulations, the system was neutralized.

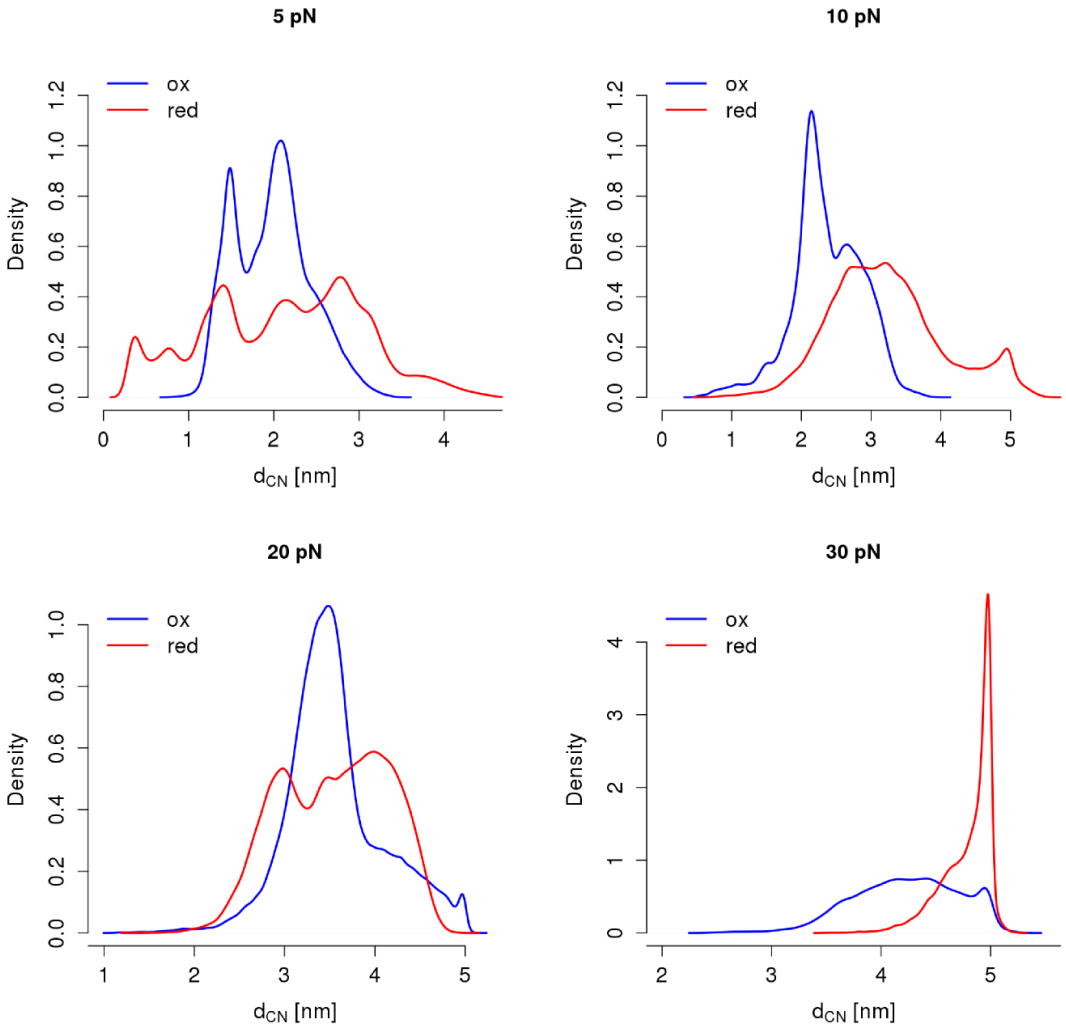

Figure 5.7: **α6-Helix stretching at different forces** - We here show the end-to-end (d_{CN}) distribution of the α6-helix under constant stretching forces of 5, 10, 20 and 30 pN with the vicinal disulfide bond present (ox) and absent (red).

5.4.1 Simulation Details

For all simulations presented in this chapter, we used the GROMACS 4.5.5 (48) software package and the OPLS-AA force field (71). The first step was an energy minimization, using the steepest decent algorithm. Next, the water was equilibrated at 300 K for 1 ns while the motion of the heavy atoms of the protein was restrained with a potential of 100 kJ/mol. Then, we released the position restraints and performed five independent equilibrium simulations for each the oxidized and the reduced state 20 ns in length.

For the pulling simulations, we isolated the equilibrated protein. We chose two starting structures for each the oxidized and the reduced state, all offering identical distances between the C and N termini, d_{CN}, to allow starting conditions as similar as possible for the pulling simulations of both redox state. We rotated the protein such that each of the termini were in different halfs of the simulation box, and solvated the protein as detailed in the simulation setup. We again used the steepest descent algorithm for minimization and equilibrated the water at ambient conditions for 100 ps while using position restraints on all heavy atoms before starting the pulling simulations.

For all simulations, the temperature was kept at 300 K, using the V-rescale algorithm. Protein and solvent were treated in two independent temperature groups, the time step for temperature coupling was chosen as 0.4 ps. We used the Parinello-Rahman barostat (73) to keep a constant pressure of 1 bar, coupling took place every picosecond. Each simulation was started with a random set of velocities. The Lincs constraint (74) was used on all bonds containing a hydrogen atom. Electrostatics beyond 1.3 nm were treated by Particle Mesh Ewald (75) with a grid spacing of 0.12 nm. We used a time step of 2 fs and periodic boundary conditions. Equilibrium simulations of the A2 domain lasted 20 ns.

Pulling simulations of the A2 domain were performed at constant velocity of 1.25 m/s, that corresponds to 1/10 of the speed used by Baldauf *et al.* (16). We used the N and C atoms of the corresponding termini pull groups. The spring constant was chosen as 500 kJ/mol. Pulling of both redox states was performed five times from each two different starting structures, both providing a distance of approximately 1.5 nm between the termini. Force profiles were created from sliding averages over 200 frames of the trajectories deriving from pulling simulations.

For the isolated helices, we used constant force pulling, at 5, 10, 20 and 30 pN. The helices were subjected to the first three forces in five independent simulations, each lasting 300 ns. Force-probe simulations at 30 pN were only performed once for each oxidized and reduced state.

5.5 Discussion and Summary

We here compared the vWF A2 domain in its native state to an equivalent structure with the vicinal disulfide close to the C-terminus opened. Our analysis revealed highly similar stabilities and collective global motions (Figure 2.1.1) under equilibrium conditions. However, mechanical unfolding leads to diverging results depending on the redox state. Force-probed unfolding of the entire domain shows a slightly higher rupture force for the oxidized state, and the isolated α6-helix looses its structure at lower force in the absence of the vicinal disulfide bond. Apparently, the vicinal disulfide bond provides the helix with stability, a result that is in line with speculations put forward just at the discovery of the vicinal disulfide bond (15, 16) and also with observations from thermal unfolding (14). These results suggest that the structure and dynamics of vWF A2 domain may be adapted to exploit redox changes (vicinal disulfide reduction) to exert observed biological activity.

The vWF is the largest soluble vertebrate protein known, a feature leading to difficulties in biosynthesis, storage and secretion (104). Biological spezialization overcomes these challenges. The vWF travels through different storage places - to the endoplasmatic reticulum, where most disulfide bonds are formed, then further to the trans-Golgi network and later to nascent Weibel-Palade bodies. pH-conditions are different in all surroundings, regulating the multimerization of the protein (104). Another feature that is known to be pH-dependent is the redox potential, including the one of disulfide bonds. We expect the vicinal disulfide bond to control unfolding. Such a pH-sensitive bond could function as a redox switch to facilitate unfolding under certain pH-conditions.

6

Discussion and Summary

The goal of this thesis was to explore the impact of mechanical stress on disulfide bonds in proteins. The major questions addressed in this context were how a cystine's redox potential changes when stretched by different forces, how this compares to the impact of changes in the chemical surrounding as induced by point mutations, and finally, how a specific disulfide bond pattern such as a vicinal disulfide between two adjacent cysteines changes the protein's stability against unfolding.

We used QM / MM hybrid calculations (Ch. 3) on a cystine to address the first question. We observed a rise in redox potential even before elongation of the disulfide bond itself sets in. Deformation of the angles and dihedrals enclosing the disulfide bond were found to be responsible for the increasing ease of sulphur-sulphur bond opening under force. Mechanical force alters the redox potential to the same amount as a point mutation in the vicinity of a disulfide bond (compare Figure 3.14). A similar tendency was also found for the engineered protein titin I27 when stretched and unfolded by mechanical force: first the softer degrees of freedom such as dihedrals and angles, then the disulfide bond length respond to the applied force (30).

Having analyzed the impact of an external force, the question arose how internal strain changes a disulfide's redox potential. Such strain exists ubiquitously throughout proteins without external stress being applied. Just like small external stretching forces deform the cysteine and thus change its redox potential, internal strain has been observed to deform cystines. Therefore, we also expect it to tune redox potentials. A simple example for a deformed cystine is the pattern of vicinal disulfide bonds, which form an eight-membered ring with the protein backbone. These will be discussed in de-

tail below. Another example of strained disulfide bonds is the one of a sulphur-sulphur bond crossing antiparallel β-strands in a special conformation, which were classified as -RHStaple by Schmidt *et al.* (9). A -RHStaple is defined as a disulfide bond enclosed by five dihedral angles, of which the outer four have a negative value while the inner one describing the $CSSC$ torsion has a positive value. Such a pattern can be found e.g. in the glycoprotein CD4, and has been predicted to exist also in at least one of the C domains of the von Willebrand factor (vWF) (105, 106). It is typically stiff and under high strain. Zhou *et al.* could extract the force within different disulfide bonds in proteins (106) and the question arose how the redox potentials of these sulphur-sulphur bonds correlate with their strain. Calculating the redox potentials with our QM / MM approach failed due to sampling problems. While a force-dependent relative redox potential of cystine can be calculated from the oxidized state alone (the reduced state has equal energies for all forces), determining the redox potential of disulfide bonds in different protein surroundings requires the energy of the reduced state. Unlike the cystine under stress or the strained disulfide bonds, the reduced state is always very flexible. Our short QM / MM simulations of CD4 or thioredoxin (Trx) in the reduced state, each lasting 20 to 40 ps showed large fluctuations in energy of the reduced state, leading to statistically unsignificant results.

Therefore, we developed another approach to calculate redox potentials that allows more sampling. Free energy calculations (FEC) from a Molecular Mechanics (MM) description of the system have been shown succesful for estimating redox potentials of proteins. The redox states in those proteins differed in the charge of a central metal ion (41) or in the oxidation state of a flavin group (42). In this thesis (Ch. 4), we present a first approach to open a chemical bond, using FEC. Using a single topology approach, we manipulated the force field such that a disulfide bond can be transformed into two thiols. By comparing the oxidized (with disulfide bond) and reduced state (without disulfide bond) to structures derived from the original topology, we assessed the quality of our description.

E. coli and *S. aureus* Trx and some of their mutants served as a first test case of the redox potential calculations. The protein family of oxidoreductases to which Trx belongs offers a suitable data set for this proof-of-principle: Many members of the protein family have been crystallized and their redox potentials have been determined. To date, our FEC approach correctly predicts three out of four relative redox potentials

for *E. coli* Trx. Our structural validation of the oxidized form revealed small inconsistencies for the average $C_\alpha C_\beta S$ angles and for three of the dihedrals, the correction of which we expect to significantly improve the results of calculated redox potentials. These calculations are currently under way.

Point mutations lead to changes in redox potentials, a feature used in biochemical experiments. The redox active group is a $CXXC$ motif, consisting of the two disulfide bridged cysteines C, enclosing two other amino acids X. Therefore, Trx and other members of the oxidoreductase family represent a group of interesing disulfide redox systems with a disulfide bond under different strains. Moreover, even though many studies on point mutants of Trx and their resulting redox potentials exist, no systematic scan has been performed experimentally. We expect our method, once the accuracy could be improved, to allow such a scan, being both cheap and fast as compared to experiments. Such a scan would allow predicting redox potentials for mutated Trxs and other members of the oxidoreductase family. Also, it would provide the means for a systematic analysis of the impact of point mutants on redox potentials in general.

As a biologically highly relevant example of stretched and strained disulfides, we finally analyzed the impact of a vicinal disulfide bond on the unfolding behavior of the vWF A2 domain (Ch. 5). It is strained due to its conformation and additionally subjected to an external force when shear-induced unfolding takes place. Our investigations show equal stability and dynamics of the domain in equilibrium for both the oxidized and reduced state. However, when it comes to force-induced unfolding, the oxidized state requires slightly higher forces than the reduced state. This observation is in line with thermal unfolding experiments by Luken *et al.* (14). Furthermore, we isolated the α-helix that contains the vicinal disulfide bond and stretched it at small forces of up to 30 pN. On average, we observed longer end-to-end distances of the helix' termini for the reduced state. The helix unfolded to a larger extent and refolded muss less as compared to an isolated α-helix from myomesin under equivalent conditions (102). Interestingly, the A2 α6-helix unfolds more easily in absence of the disulfide bond. We conclude that the vicinal disulfide bond contributes to the domain's stability and suggest opening of the sulphur-sulphur bond to regulate its rigidity. pH-dependent studies mimicking the physiological conditions of the vWF in different storage places (endoplasmatic reticulum, trans-Golgi or Weibel-Pallade bodies) could help elucidating this question further.

Vicinal disulfide bonds have been discussed to play a functional role (99). Our observations support this hypothesis. A larger protein survey comparing the occurence, redox potentials and unfolding behavior of proteins with vicinal disulfide bonds are the objective of future studies.

Overall, this thesis could shed light on the mechanochemical coupling in biological systems for the case of disulfide bonds. Our approach can be straightforwardly applied to incidences of strained disulfide bonds and to other biochemical reactions potentially regulated by force such as proteolysis.

References

[1] Jeremy M. Berg, John L. Tymoczko, and Lubert Stryer. *Biochemie*. Spektrum Akademischer Verlag, 2003. 1

[2] Dean P. Jones, Young-Mi Go, Corinna L. Anderson, Thomas R. Ziegler, Joseph M. Kinkade, Jr., and Ward G. Kirlin. **Cysteine/cystine couple is a newly recognized node in the circuitry for biologic redox signaling and control**. *The FASEB Journal*, **11**:1246–1248, 2004. 1, 8

[3] Deborah Fass. **Disulfide Bonding in Protein Biophysics**. *Annual Review of Biophysics*, **41**(1):63–79, 2012. 1, 2

[4] Philip J. Hogg. **Disulfide bonds as switches for protein function**. *Trends in Biochemical Sciences*, **28**:210–214, 2003. 1

[5] Carolyn S. Sevier and Chris A. Kaiser. **Formation and transfer of disulphide bonds in living cells**. *Nat Rev Mol Cell Biol*, **3**(11):836–847, November 2002. 1

[6] Shu Quan, Irmhild Schneider, Jonathan Pan, Annekathrin Von Hacht, and James C A Bardwell. **The CXXC motif is more than a redox rheostat.** *J Biol Chem*, **282**(39):28823–28833, Sep 2007. 2, 8, 50, 51, 53, 54

[7] Hiram F. Gilbert. **Molecular and Cellular Aspects of Thiol-Disulfide Exchange**. *Adv Enzymol Relat Areas Mol Biol.*, **63**:69–172, 1990. 2, 8

[8] Alison R Frand and Chris A Kaiser. **Ero1p Oxidizes Protein Disulfide Isomerase in a Pathway for Disulfide Bond Formation in the Endoplasmic Reticulum**. *Mol Cell*, **4**(4):469–477, October 1999. 2

[9] Bryan Schmidt, Lorraine Ho, and Philip J. Hogg. **Allosteric Disulfide Bonds**. *Biochemistry*, **45**(24):7429–7433, 2006. PMID: 16768438. 2, 88

[10] V. M. Chen and P. J. Hogg. **Allosteric disulfide bonds in thrombosis and thrombolysis**. *Journal of Thrombosis and Haemostasis*, **4**(12):2533–2541, 2006. 2

[11] Oliviero Carugo, Maa emaar, Sotir Zahariev, Ilona Hudky, Zoltn Gspri, Andrs Perczel, and Sndor Pongor. **Vicinal disulfide turns**. *Protein Engineering*, **16**(9):637–639, 2003. 2, 73, 74

[12] Cynthia Czajkowski and Arthur Karlin. **Structure of the Nicotinic Receptor Acetylcholine-binding Site**. *Journal of Biological Chemistry*, **270**(7):3160–3164, 1995. 2, 73

[13] C.C.F. Blake, M. Ghosh, K. Harlos, A. Avezoux, and C. Anthony. **The active site of methanol dehydrogenase contains a disulphide bridge between adjacent cysteine residues**. *Nat Struct Mol Biol*, **1**(2):102–105, February 1994. 3, 73

[14] Brenda M Luken, Luke Y N Winn, Jonas Emsley, David A Lane, and James T B Crawley. **The importance of vicinal cysteines, C1669 and C1670, for von Willebrand factor A2 domain function.** *Blood*, **115**(23):4910–4913, Jun 2010. 3, 74, 85, 89

[15] Qing Zhang, Yan-Feng Zhou, Cheng-Zhong Zhang, Xiaohui Zhang, Chafen Lu, and Timothy A Springer. **Structural specializations of A2, a force-sensing domain in the ultralarge vascular protein von Willebrand factor.** *Proc Natl Acad Sci U S A*, **106**(23):9226–9231, Jun 2009. 3, 73, 74, 75, 85

[16] C. Baldauf, R. Schnepenheim, W. Stacklies, T. Obser, A. Pieconka, S. Schneppenheim, U. Budde, J. Zhou, and F. Gräter. **Shear-induced unfolding activates von Willebrand factor A2 domain for proteolysis**. *Journal of Thrombosis and Haemostasis*, **7**(12):2096–2105, 2009. 3, 73, 74, 77, 84, 85

[17] Yaozu Xiang, Rens de Groot, James T. B. Crawley, and David A. Lane. **Mechanism of von Willebrand factor scissile bond cleavage by a disintegrin and metalloproteinase with a thrombospondin type 1 motif, member 13 (ADAMTS13)**. *Proceedings of the National Academy of Sciences*, **108**(28):11602–11607, 2011. 3

[18] Jordi Ribas-Arino and Dominik Marx. **Covalent Mechanochemistry: Theoretical Concepts and Computational Tools with Applications to Molecular Nanomechanics**. *Chemical Reviews*, **112**(10):5412–5487, 2012. 3

[19] Walter Kauzmann and Henry Eyring. **The Viscous Flow of Large Molecules**. *Journal of the American Chemical Society*, **62**(11):3113–3125, 1940. 3

[20] Charles R. Hickenboth, Jeffrey S. Moore, Scott R. White, Nancy R. Sottos, Jerome Baudry, and Scott R. Wilson. **Biasing reaction pathways with mechanical force**. *Nature*, **446**(7134):423–427, March 2007. 3

[21] R. B. Woodward and Roald Hoffmann. **The Conservation of Orbital Symmetry**. *Angewandte Chemie International Edition in English*, **8**(11):781–853, 1969. 3

[22] Johnathan N. Brantley, Kelly M. Wiggins, and Christopher W. Bielawski. **Unclicking the Click: Mechanically Facilitated 1,3-Dipolar Cycloreversions**. *Science*, **333**(6049):1606–1609, 2011. 4

[23] Arun P Wiita, Raul Perez-Jimenez, Kirstin A Walther, Frauke Gräter, B. J. Berne, Arne Holmgren, Jose M Sanchez-Ruiz, and Julio M Fernandez. **Probing the chemistry of thioredoxin catalysis with force.** *Nature*, **450**(7166):124–127, Nov 2007. 4, 5, 25, 43, 47

[24] Arun P Wiita, Sri Rama Koti Ainavarapu, Hector H Huang, and Julio M Fernandez. **Force-dependent chemical kinetics of disulfide bond reduction observed with single-molecule techniques.** *Proc Natl Acad Sci U S A*, **103**(19):7222–7227, May 2006. 5, 25, 26, 43, 47, 48

REFERENCES

[25] Timothy J Kucharski, Zhen Huang, Qing-Zheng Yang, Yancong Tian, Nicholas C Rubin, Carlos D Concepcion, and Roman Boulatov. **Kinetics of thiol/disulfide exchange correlate weakly with the restoring force in the disulfide moiety.** *Angew Chem Int Ed Engl*, **48**(38):7040–7043, 2009. 5, 47

[26] George I. Bell. **Models for the Specific Adhesion of Cells to Cells**. *Science*, **200**:618–627, 1978. 6, 26, 42, 46, 49

[27] Emily B. Walton, Sunyoung Lee, and Krystyn J. Van Vliet. **Extending Bell's Model: How Force Transducer Stiffness Alters Measured Unbinding Forces and Kinetics of Molecular Complexes**. *Biophys J*, **94**(7):2621–2630, April 2008. 7

[28] O. K. Dudko, A. E. Filippov, J. Klafter, and M. Urbakh. **Beyond the conventional description of dynamic force spectroscopy of adhesion bonds**. *Proceedings of the National Academy of Sciences*, **100**(20):11378–11381, 2003. 7

[29] Gerhard Hummer and Attila Szabo. **Kinetics from Nonequilibrium Single-Molecule Pulling Experiments**. *Biophys J*, **85**(1):5–15, July 2003. 7

[30] Wenjin Li and Frauke Gräter. **Atomistic Evidence of How Force Dynamically Regulates Thiol/Disulfide Exchange**. *J Am Chem Soc*, **132**(47):16790–16795, 2010. 7, 45, 47, 48, 87

[31] Ruma Banerjee, editor. *Redox Biochemistry*. Wiley Interscience, 2007. 7

[32] Claus Jacob, editor. *Redox Signaling and Regulation in Biology and Medicine*. Wiley-VCH, Weinheim, 2009. 7

[33] Moon Sen, Randall Kopper, Laurent Pons, Edathara C. Abraham, A. Wesley Burks, and Gary A. Bannon. **Protein Structure Plays a Critical Role in Peanut Allergen Stability and May Determine Immunodominant IgE-Binding Epitopes**. *The Journal of Immunology*, **169**(2):882–887, 2002. 8

[34] Hiuwan Choi, Khatira Aboulfatova, Henry J. Pownall, Richard Cook, and Jing-fei Dong. **Shear-induced Disulfide Bond Formation Regulates Adhesion Activity of von Willebrand Factor**. *Journal of Biological Chemistry*, **282**(49):35604–35611, 2007. 8

[35] Tiao Yin Lin and Peter S. Kim. **Urea dependence of thiol-disulfide equilibria in thioredoxin: confirmation of the linkage relationship and a sensitive assay for structure**. *Biochemistry*, **28**(12):5282–5287, 1989. 8

[36] Tiao-Yin Lin. **Protein-protein interaction as a powering source of oxidoreductive reactivity**. *Mol. BioSyst.*, **6**(8):1454–1462, 2010. 8

[37] Jochen Blumberger, Leonardo Bernasconi, Ivano Tavernelli, Rodolphe Vuilleumier, and Michiel Sprik. **Electronic Structure and Solvation of Copper and Silver Ions: A Theoretical Picture of a Model Aqueous Redox Reaction**. *Journal of the American Chemical Society*, **126**(12):3928–3938, 2004. PMID: 15038747. 9, 15

[38] Jochen Blumberger. **Free energies for biological electron transfer from QM/MM calculation: method, application and critical assessment**. *Phys. Chem. Chem. Phys.*, **10**:5651–5667, 2008. 9

[39] Thomas F. Hughes and Richard A. Friesner. **Development of Accurate DFT Methods for Computing Redox Potentials of Transition Metal Complexes: Results for Model Complexes and Application to Cytochrome P450**. *Journal of Chemical Theory and Computation*, **8**(2):442–459, 2012. 9

[40] Xiancheng Zeng, Hao Hu, Xiangqian Hu, and Weitao Yang. **Calculating solution redox free energies with ab initio quantum mechanical/molecular mechanical minimum free energy path method**. *J. Chem. Phys.*, **130**:164111–1–164111–8, 2009. 9

[41] Marieke van den Bosch, Marcel Swart, Jaap G. Snijders, Herman J. C. Berendsen, Alan E. Mark, Chris Oostenbrink, Wilfred F. van Gunsteren, and Gerard W. Canters. **Calculation of the Redox Potential of the Protein Azurin and Some Mutants**. *ChemBioChem*, **6**(4):738–746, 2005. 9, 16, 22, 23, 88

[42] Benedict M Sattelle and Michael J Sutcliffe. **Calculating chemically accurate redox potentials for engineered flavoproteins from classical molecular dynamics free energy simulations.** *J Phys Chem A*, **112**(50):13053–13057, Dec 2008. 9, 16, 23, 51, 88

[43] Gaelle Filippini, Florent Goujon, Christine Bonal, and Patrice Malfreyt. **Toward a Prediction of the Redox Properties of Electroactive SAMs: A Free Energy Calculation by Molecular Simulation**. *The Journal of Physical Chemistry B*, **114**(40):12897–12907, 2010. 9

[44] Bernard R. Brooks, Robert E. Bruccoleri, Barry D. Olafson, David J. States, S. Swaminathan, and Martin Karplus. **CHARMM: A program for macromolecular energy, minimization, and dynamics calculations**. *J Comput Chem*, **4**(2):187–217, 1983. 12

[45] F. Jensen. *Computational Chemistry*. John Wiley and Sons Ltd, Sussex, England, 2001. 12, 13

[46] Andrew R. Leach. *Molecular Modelling: Principles and Applications*. Pearson Education Limited, Essex, England, 2001. 13

[47] Andrea Amadei, Antonius B. M. Linssen, and Herman J. C. Berendsen. **Essential dynamics of proteins**. *Proteins: Structure, Function, and Bioinformatics*, **17**(4):412–425, 1993. 13

[48] Berk Hess, Carsten Kutzner, David van der Spoel, and Erik Lindahl. **GROMACS 4: Algorithms for Highly Efficient, Load-Balanced, and Scalable Molecular Simulation**. *J Chem Theory Comput*, **4**(3):435–447, 2008. 15, 29, 30, 55, 82, 84

[49] Martin J. Field, Paul A. Bash, and Martin Karplus. **A combined quantum mechanical and molecular mechanical potential for molecular dynamics simulations**. *Journal of Computational Chemistry*, **11**(6):700–733, 1990. 15

[50] Peter Comba, editor. *Modeling of Molecular Properties*. Wiley VCH, Weinheim, Germany, 2011. 16

[51] E. D. Glendening, A.E. Reed, J.E. Carpenter, and F Weinhold. **NBO, version 3.1, 1995.** 16, 41

[52] Christophe Chipot, Andrew Pohorille, M. Scott Shell, Athanassios Panagiotopouls, Eric Darve, Gerhard Hummer, Nandou Lu, Dellago Christoph Woolf, Thomas B., Ioan Andricioaei, Lawrence R. Pratt, Dilip Asthagiri, Thomas L. Beck, Thomas Simonson, Alan E. Mark, and Vijay S. Pande. *Free Energy Calculations*, **86** of *Springer Series in Chemical Physics*. Springer, Berlin, 2007. 16, 17, 18, 19, 59

[53] Niels Hansen, Joica Dolenc, Matthias Knecht, Serena Riniker, and Wilfred F. van Gunsteren. **Assessment of enveloping distribution sampling to calculate relative free enthalpies of binding for eight netropsinDNA duplex complexes in aqueous solution**. *Journal of Computational Chemistry*, **33**(6):640–651, 2012. 17

[54] Daniel Seeliger, Floris P. Buelens, Maik Goette, Bert L. de Groot, and Helmut Grubmller. **Towards computional specificity screening of DNA-binding proteins**. *Nucleic Acids Research*, **39**:8281–8290, 2011. 19, 23

[55] C. Jarzynski. **Nonequilibrium Equality for Free Energy Differences**. *Phys. Rev. Lett.*, **78**:2690–2693, 1997. 19

[56] Gavin E. Crooks. **Nonequilibrium Measurements of Free Energy Differences for Microscopically Reversible Markovian Systems**. *Journal of Statistical Physics*, **90**:1481–1487, 1998. 20

[57] Gavin E. Crooks. **Entropy production fluctuation theorem and the nonequilibrium work relation for free energy differences**. *Phys Rev E*, **60**:2721–2726, 1999. 20

[58] Maik Goette and Helmut Grubmüller. **Accuracy and convergence of free energy differences calculated from nonequilibrium switching processes**. *Journal of Computational Chemistry*, **30**(3):447–456, 2009. 20, 21, 23, 67, 68

[59] Daniel Seeliger and Bert L. de Groot. **Protein Thermostability Calculations Using Alchemical Free Energy Simulations**. *Biophys J*, **98**(10):2309–2316, May 2010. 23

[60] Sri Rama Koti Ainavarapu, Arun P . Wiita, Lorna Dougan, Einar Uggerud, and Julio M . Fernandez. **Single-Molecule Force Spectroscopy Measurements of Bond Elongation during a Bimolecular Reaction**. *J Am Chem Soc*, **130**(20):6479–6487, 2008. 25, 26, 27, 43, 47

[61] Raul Perez-Jimenez, Jingyuan Li, Pallav Kosuri, Inmaculada Sanchez-Romero, Arun P Wiita, David Rodriguez-Larrea, Ana Chueca, Arne Holmgren, Antonio Miranda-Vizuete, Katja Becker, Seung-Hyun Cho, Jon Beckwith, Eric Gelhaye, Jean P Jacquot, Eric A Gaucher, Eric Gaucher, Jose M Sanchez-Ruiz, Bruce J Berne, and Julio M Fernandez. **Diversity of chemical mechanisms in thioredoxin catalysis revealed by single-molecule force spectroscopy.** *Nat Struct Mol Biol*, **16**(8):890–896, Aug 2009. 25, 26, 47

[62] Sergi Garcia-Manyes, J. Liang, T.-L. Kuo R. Szoszkiewicz, and Julio M. Fernandez. **Force-activated reactivity switch in a bimolecular chemical reaction**. *Nature Chem*, **1**:236 – 242, 2009. 25, 26, 47

[63] C. Houée-Levin and J. Bergès. **Single electron localisation on the cystine/cysteine couple: sulphur or carbon?** *Research Chem Int*, **35**:421–430, 2009. 10.1007/s11164-009-0041-9. 26, 38

[64] Agnieszka Sawicka, Piotr Skurski, and Jack Simons. **Excess Electron Attachment to Disulfide-Bridged l,l-Cystine. An ab Initio Study**. *J Phys Chem A*, **108**(19):4261–4268, 2004. 26, 38

[65] Einar Uggerud. **Electron capture dissociation of the disulfide bond–a quantum chemical model study**. *Int J Mass Spec*, **234**(1-3):45 – 50, 2004. Special Issue in Honour of Alan G. Marshall. 26, 38

[66] Gail A Rickard, Jacqueline Bergès, Chantal Houèe-Levin, and Arvi Rauk. **Ab initio and QM/MM study of electron addition on the disulfide bond in thioredoxin.** *J Phys Chem B*, **112**(18):5774–5787, May 2008. 26, 38

[67] Maria Francesca Iozzi, Trygve Helgaker, and Einar Uggerud. **Influence of external force on properties and reactivity of disulfide bonds.** *J Phys Chem A*, **115**(11):2308–2315, Mar 2011. 26, 48

[68] M. J. Frisch, G. W. Trucks, H. B. Schlegel, G. E. Scuseria, M. A. Robb, J. R. Cheeseman, J. A. Montgomery, Jr., T. Vreven, K. N. Kudin, J. C. Burant, J. M. Millam, S. S. Iyengar, J. Tomasi, V. Barone, B. Mennucci, M. Cossi, G. Scalmani, N. Rega, G. A. Petersson, H. Nakatsuji, M. Hada, M. Ehara, K. Toyota, R. Fukuda, J. Hasegawa, M. Ishida, T. Nakajima, Y. Honda, O. Kitao, H. Nakai, M. Klene, X. Li, J. E. Knox, H. P. Hratchian, J. B. Cross, V. Bakken, C. Adamo, J. Jaramillo, R. Gomperts, R. E. Stratmann, O. Yazyev, A. J. Austin, R. Cammi, C. Pomelli, J. W. Ochterski, P. Y. Ayala, K. Morokuma, G. A. Voth, P. Salvador, J. J. Dannenberg, V. G. Zakrzewski, S. Dapprich, A. D. Daniels, M. C. Strain, O. Farkas, D. K. Malick, A. D. Rabuck, K. Raghavachari, J. B. Foresman, J. V. Ortiz, Q. Cui, A. G. Baboul, S. Clifford, J. Cioslowski, B. B. Stefanov, G. Liu, A. Liashenko, P. Piskorz, I. Komaromi, R. L. Martin, D. J. Fox, T. Keith, M. A. Al-Laham, C. Y. Peng, A. Nanayakkara, M. Challacombe, P. M. W. Gill, B. Johnson, W. Chen, M. W. Wong, C. Gonzalez, and J. A. Pople. **Gaussian 03, Revision C.02**. Gaussian, Inc., Wallingford, CT, 2004. 29, 30

[69] G. Groenhof, M.F. Lensink, J.G. Snijders, H.J.C. Berendsen, Function A.E. Mark. Proteins: Structure, and Genetics. **Signal Transduction in the Photoactive Yellow Protein. I: Photon Absorption and the Isomerization of the Chromophore.** *Proteins*, **48**:202–211, 2002. 29, 30

[70] W. L. Jorgensen, J. Chandrasekhar, J. D. Madura, and M. L. Impey, R. W.and Klein. **Comparison of simple potential functions for simulating liquid water**. *J Chem Phys*, **79**(2):926–935, 1983. 29, 55

[71] William L. Jorgensen, David S. Maxwell, and Julian Tirado-Rives. **Development and Testing of the OPLS All-Atom Force Field on Conformational Energetics and Properties of Organic Liquids**. *J Am Chem Soc*, **118**(45):11225–11236, 1996. 29, 84

REFERENCES

[72] H. J. C. Berendsen, J. P. M. Postma, W. F. van Gunsteren, A. DiNola, and J. R. Haak. **Molecular dynamics with coupling to an external bath**. *J. Chem. Phys.*, **81**:3684–3690, 1984. 29, 31

[73] M. Parrinello and A. Rahman. **Polymorphic transitions in single crystals: A new molecular dynamics method.** *J. Appl. Phys.*, **52**:7182–7190, 1981. 29, 84

[74] B Hess, H Bekker, H J C Berendsen, and J G E M Fraaije. **LINCS: A Linear Constraint Solver for molecular simulations**. *J. Comput. Chem*, **18**(12):1463–1472, 1997. 29, 31, 84

[75] U. Essmann, L. Perera, M. L. Berkowitz, T. Darden, H. Lee, and L. G. Pedersen. **A smooth particle mesh Ewald method**. *J Chem Phys*, **103**:8577–8592, 1995. 29, 56, 84

[76] S. Nosé. **A molecular dynamics method for simulations in the canonical ensemble.** *Mol. Phys.*, **52**:255–268, 1984. 29

[77] W. G. Hoover. **Canonical dynamics: equilibrium phase-space distributions**. *Phys. Rev. A*, **31**:1695–1697, 1985. 29

[78] C. Moller and M. S. Plesset. **Note on an Approximation Treatment for Many-Electron Systems**. *Phys. Rev.*, **46**:618–622, 1934. 30

[79] J. Bergès, G. Rickards, A. Rauk, and C. Houée-Levin. **QM/MM study of electron addition on protein disulfide bonds**. *Chem Phys Lett*, **421**:63–67, April 2006. 30, 48

[80] Moshe Faraggi, Michael H. Klapper, and Leon M. Dorfman. **Fast reaction kinetics of one-electron transfer in proteins. The histidyl radical. Mode of electron migration**. *J. Phys. Chem.*, **82**:508–512, 1978. 39

[81] Stephen P. Mezyk and David A. Armstrong. **Disulfide anion radical equilibria: effects of -NH3+, -CO2-, -NHC(O)- and -CH3 groups**. *J. Chem. Soc., Perkin Trans. 2*, pages 1411–1420, 1999. 39

[82] C. El Hanine Lmoumène, D. Conte, J.-P. Jacquot, and C. Houée-Levin. **Redox Properties of Protein Disulfide Bond in Oxidized Thioredoxin and Lysozyme: A Pulse Radiolysis Study**. *Biochem*, **39**(31):9295–9301, 2000. 40

[83] M. J. Frisch, G. W. Trucks, H. B. Schlegel, G. E. Scuseria, M. A. Robb, J. R. Cheeseman, G. Scalmani, V. Barone, B. Mennucci, G. A. Petersson, H. Nakatsuji, M. Caricato, X. Li, H. P. Hratchian, A. F. Izmaylov, J. Bloino, G. Zheng, J. L. Sonnenberg, M. Hada, M. Ehara, K. Toyota, R. Fukuda, J. Hasegawa, M. Ishida, T. Nakajima, Y. Honda, O. Kitao, H. Nakai, T. Vreven, Jr. J. A. Montgomery, J. E. Peralta, F. Ogliaro, M. Bearpark, E. Brothers J. J. Heyd, K. N. Kudin, V. N. Staroverov, R. Kobayashi, J. Normand, K. Raghavachari, A. Rendell, J. C. Burant, S. S. Iyengar, J. Tomasi, M. Cossi, N. Rega, J. M. Millam, M. Klene, J. E. Knox, J. B. Cross, V. Bakken, C. Adamo, J. Jaramillo, R. Gomperts, R. E. Stratmann, O. Yazyev, A. J. Austin, R. Cammi, C. Pomelli, J. W. Ochterski, R. L. Martin, K. Morokuma, V. G. Zakrzewski, G. A. Voth, P. Salvador, J. J. Dannenberg, S. Dapprich, A. D. Daniels, O. Farkas, J. B. Foresman, J. V. Ortiz, J. Cioslowski, and D. J. Fox. **Gaussian 09, Revision A.02**. Gaussian, Inc., Wallingford CT, 2009. 41

[84] Olga K. Dudko, Gerhard Hummer, and Attila Szabo. **Intrinsic Rates and Activation Free Energies from Single-Molecule Pulling Experiments**. *Phys Rev Lett*, **96**(10):108101–1 – 108101–4, Mar 2006. 46, 49

[85] Oleg Prezhdo Yuriy Pereverzev. **Deformation Model for Thioredoxin Catalysis of Disulfide Bond Dissociation by Force**. *Cellular and Molecular Bioengineering*, **2**:255 – 263, 2009. 48

[86] Goedele Roos, Abel Garcia-Pino, Karolien Van Belle, Elke Brosens, Khadija Wahni, Guy Vandenbussche, Lode Wyns, Remy Loris, and Joris Messens. **The conserved active site proline determines the reducing power of Staphylococcus aureus thioredoxin.** *J Mol Biol*, **368**(3):800–811, May 2007. 49, 50, 55, 71

[87] W. W. Cleland. **Dithiothreitol, a new protective reagent for SH groups.** *Biochemistry*, **3**:480–482, Apr 1964. 50

[88] M. Rief, M. Gautel, F. Oesterhelt, J. M. Fernandez, and H. E. Gaub. **Reversible unfolding of individual titin immunoglobulin domains by AFM.** *Science*, **276**(5315):1109–1112, May 1997. 49

[89] P. P. Lehenkari and M. A. Horton. **Single integrin molecule adhesion forces in intact cells measured by atomic force microscopy.** *Biochem Biophys Res Commun*, **259**(3):645–650, Jun 1999. 49

[90] Hayden Huang, Roger D. Kamm, and Richard T. Lee. **Cell mechanics and mechanotransduction: pathways, probes, and physiology**. *American Journal of Physiology - Cell Physiology*, **287**(1):C1–C11, 2004. 49

[91] M. S. Formaneck, G. Li, Zhang, X., and Q. Cui. **Calculation Accurate Redox Potentials in Enzymes with a Combined QM/MM Free Energy Perturbation Approach**. *J Theoret Comp Chem*, **1**(1):53–67, 2002. 51

[92] Martina Huber-Wunderlich and Rudi Glockshuber. **A single dipeptide sequence modulates the redox properties of a whole enzyme family**. *Folding and Design*, **3**(3):161 – 171, 1998. 54

[93] Mei-Fen Jeng, A.Patricia Campbell, Tadhg Begley, Arne Holmgren, David A Case, Peter E Wright, and H.Jane Dyson. **High-resolution solution structures of oxidized and reduced Escherichia coli thioredoxin**. *Structure*, **2**(9):853 – 868, 1994. 55

[94] Giovanni Bussi, Davide Donadio, and Michele Parrinello. **Canonical sampling through velocity rescaling**. *J Chem Phys*, **126**:014101–1 – 014101–7, 2007. 55

[95] Berk Hess. **P-LINCS: A Parallel Linear Constraint Solver for Molecular Simulation**. *Journal of Chemical Theory and Computation*, **4**(1):116–122, 2008. 56

[96] T. Darden, D. York, and L. Pedersen. **Particle mesh Ewald: An N-log(N) method for Ewald sums in large systems.** *J. Chem. Phys.*, **98**:10089–10092, 1993. 56

[97] Marcel Swart, Piet Th. van Duijnen, and Jaap G. Snijders. **A charge analysis derived from an atomic multipole expansion**. *Journal of Computational Chemistry*, **22**(1):79–88, 2001. 63

[98] C. Jarzynski. **Rare events and the convergence of exponentially averaged work values**. *Physical Review E*, **73**:46105, 2006. 66

[99] Erik L. Ruggles, P. Bruce Deker, and Robert J. Hondal. **Synthesis, redox properties, and conformational analysis of vicinal disulfide ring mimics**. *Tetrahedron*, **65**(7):1257 – 1267, 2009. 73, 90

[100] Xiu-hong Wang, Mark Connor, Ross Smith, Mark W. Maciejewski, Merlin E.H. Howden, Graham M. Nicholson, Macdonald J. Christie, and Glenn F. King. **Discovery and characterization of a family of insecticidal neurotoxins with a rare vicinal disulfide bridge**. *Nat Struct Mol Biol*, **7**(6):505–513, June 2000. 73

[101] Felix Berkemeier, Morten Bertz, Senbo Xiao, Nikos Pinotsis, Matthias Wilmanns, Frauke Gräter, and Matthias Rief. **Fast-folding -helices as reversible strain absorbers in the muscle protein myomesin**. *Proceedings of the National Academy of Sciences*, **108**(34):14139–14144, 2011. 78

[102] Senbo Xiao and Frauke Gräter. **Myomesin Uses α-helices as Rapidly Refolding Elastomers to Maintain Structural Stability of the Sarcomere**. *Unpublished results*. 78, 89

[103] W. Kabsch and C. Sander. **Dictionary of protein secondary structure: pattern recognition of hydrogen-bonded and geometrical features.** *Biopolymers. PMID: 6667333; UI: 84128824.*, **22**:2577–2637, 1983. 78, 81

[104] Yan-Feng Zhou, Edward T. Eng, Jieqing Zhu, Chafen Lu, Thomas Walz, and Timothy A. Springer. **Sequence and structure relationships within von Willebrand factor**. *Blood*, **120**(2):449–458, 2012. 85

[105] Philipp. J. Hogg. **Contribution of allosteric disulfide bonds to regulation of hemostasis**. *Journal of Thrombosis and Haemostasis*, **7**:13–16, 2009. 88

[106] Beifei Zhou, Ilona B. Baldus, and Frauke Gräter. **Prestress in Protein of Disulfide Bonds Tunes Their Stabilities**. *Unpublished results*. 88

Eidesstattliche Erklärung

Die vorliegende Arbeit wurde in der Zeit von April 2009 bis September 2012 am Max-Planck-Institut für Metallforschung und am Heidelberger Institut für Theoretische Studien gGmbH unter Betreuung von Dr. Frauke Gräter und Prof. Dr. Peter Comba vom Anorganisch-Chemischen Institut der Ruprecht-Karls-Universität Heidelberg angefertigt. Ein Teil der Arbeit wurde im Rahmen eines Forschungsaufenthaltes von Juli bis September 2009 am CAS-MPG Partner Institute and Key Laboratory for Computational Biology (PICB), Shanghai, China, angefertigt.

Ein Teil der Arbeit wurde im Biophysical Journal veröffentlicht.

Erklärung gemäß § 8 (3) b) und c) der Prüfungsordnung:

Ich erkläre hiermit an Eides statt, dass ich die vorliegende Arbeit selbst verfasst und mich dabei keiner anderen als der von mir ausdrücklich bezeichneten Quellen und Hilfen bedient habe.

Ich erkläre hiermit, dass ich an keiner anderen Stelle ein Prüfungsverfahren beantragt bzw. die Dissertation in dieser oder anderer Form bereits anderweitig als Prüfungsarbeit verwendet oder einer anderen Fakultät als Dissertation vorgelegt habe.

Heidelberg,